

National Chiao Tung University

Department of Materials Science and Engineering

PhD Thesis

**Synthesis of Low Band-Gap Polymers and
Metallo-Polymers for Bulk Heterojunction Solar Cells**

低能隙高分子及金屬高分子材料於總體異質接面太陽
能電池之合成與應用

Harihara Padhy (哈瑞)

Advisor: Hong-Cheu Lin, Ph.D. (林宏洲 教授)

October, 2010

**Synthesis of Low Band-Gap Polymers and
Metallo-Polymers for Bulk Heterojunction Solar Cells**
低能隙高分子及金屬高分子材料於總體異質接面太陽
能電池之合成與應用

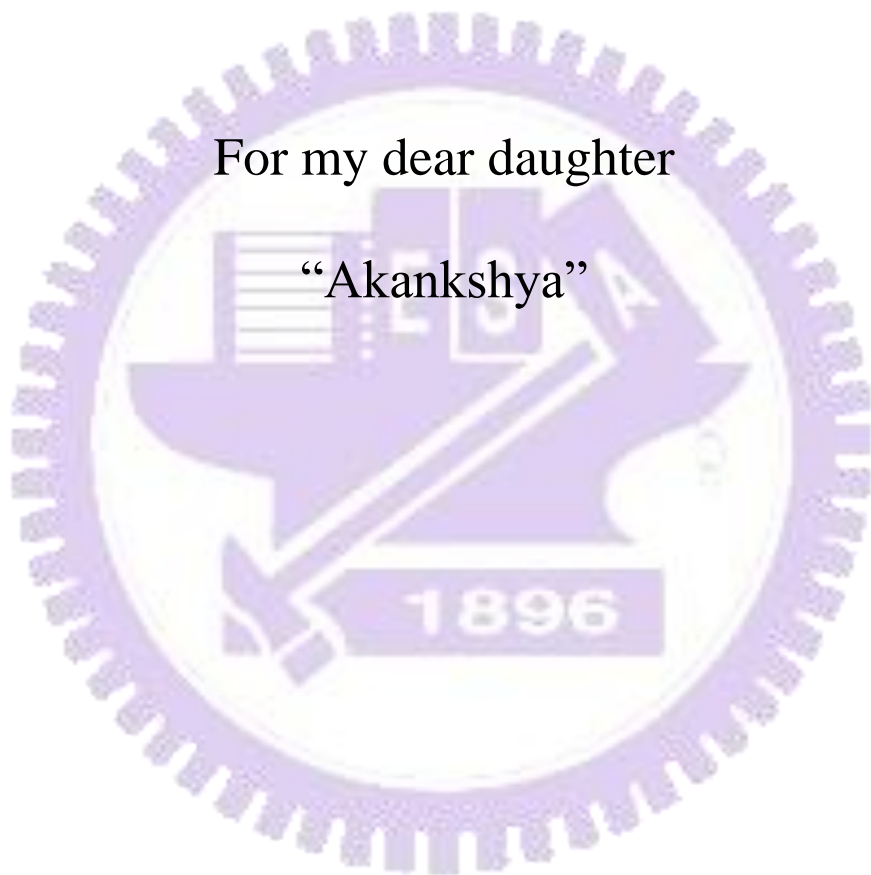
Student: Harihara Padhy (哈瑞)

Advisor: Hong-Cheu Lin, Ph.D. (林宏洲 教授)



A Thesis submitted to
Department of Materials Science and Engineering
College of Engineering
National Chiao Tung University
In partial fulfillment of the requirement for the degree of
Doctor of Philosophy
In materials science and engineering

October, 2010



For my dear daughter

“Akankshya”

“If we did all the things we are capable of doing, we would astound ourselves.”

Thomas A. Edison

Abstract

The main objective of this dissertation is to study the performance of polymer bulk heterojunction solar cell involving conjugated donor-acceptor polymers/metallo-polymers as electron donors. In the introduction of this thesis, we gave an explanation on the historical evolution of polymer solar cells, and summarized the literature in the recent years.

In the second chapter, we describe the design, synthesis, and polymer solar cells (PSC) fabrication of a series of soluble donor-acceptor conjugated polymers comprising of phenothiazine donor and various benzodiazole acceptors (i.e., benzothiadiazole, benzoselenodiazole, and benzoxadiazole) sandwiched between hexyl-thiophene. These low band-gap (LBG) polymers demonstrated broad absorption in the region of 300-750 nm with optical band gaps of 1.80-1.93 eV. Both highest occupied molecular orbital (HOMO) (-5.38 to -5.47 eV) and lowest unoccupied molecular orbital (LUMO) (-3.47 to -3.60 eV) energy levels of the LBG polymers were within the desirable range of ideal energy levels. The best performance of the PSC device was obtained by using one of the polymers containing benzothiadiazole acceptor at the core and [6,6]-phenyl-C₇₁-butyric acid methyl ester (PC₇₁BM) in the weight ratio of 1:4, and a PCE value of 1.20%, an open-circuit voltage (V_{oc}) value of 0.75 V, a short-circuit current (J_{sc}) value of 4.60 mA/cm², and a fill factor (FF) value of 35.0% were achieved.

In the third chapter, we describe the design, synthesis, and characterization of β -cyano-thiophenevinylene-substituted polymers containing cyclopentadithiophene and dithienosilole units. The effects of the bridged atoms (C and Si) and cyano-vinylene groups on their thermal, optical, electrochemical, charge transporting,

and photovoltaic properties were investigated. Both LBG polymers had broad absorption spectra with ideal HOMO (ca. -5.30 eV) and LUMO (ca. -3.60 eV) levels and possessed hole mobilities as high as $9.82 \times 10^{-4} \text{ cm}^2/\text{Vs}$. The PSC device based on one of the polymers containing dithienosilole moiety with PC₇₁BM (1:2 w/w) exhibited a best power conversion efficiency of 2.25% under AM 1.5, 100 mW/cm².

In the fourth chapter, synthesis, and characterization of a series of π -conjugated bis-terpyridyl ligands bearing various benzodiazole cores and their corresponding main-chain Ru^{II} metallo-polymers were described. The effects of electron donor and acceptor interactions on their thermal, optical, electrochemical, and photovoltaic properties were investigated. Due to the broad sensitization areas of the metallo-polymers, their BHJ solar cell devices containing [6,6]-phenyl C₆₁ butyric acid methyl ester (PC₆₁BM) as an electron acceptor exhibited a high short-circuit current (J_{sc}). An optimum PVC device based on the blended polymer with PCBM in 1:1 (w/w) achieved the maximum power conversion efficiency (PCE) value up to 0.45 %, with $V_{oc} = 0.61 \text{ V}$, $J_{sc} = 2.18 \text{ mA/cm}^2$, and $\text{FF} = 34.1 \%$ (under AM 1.5 G 100 mW/cm²), which demonstrated a novel family of conjugated polyelectrolytes with the highest PCE value comparable with BHJ solar cells fabricated from ionic polythiophene and C₆₀.

摘要

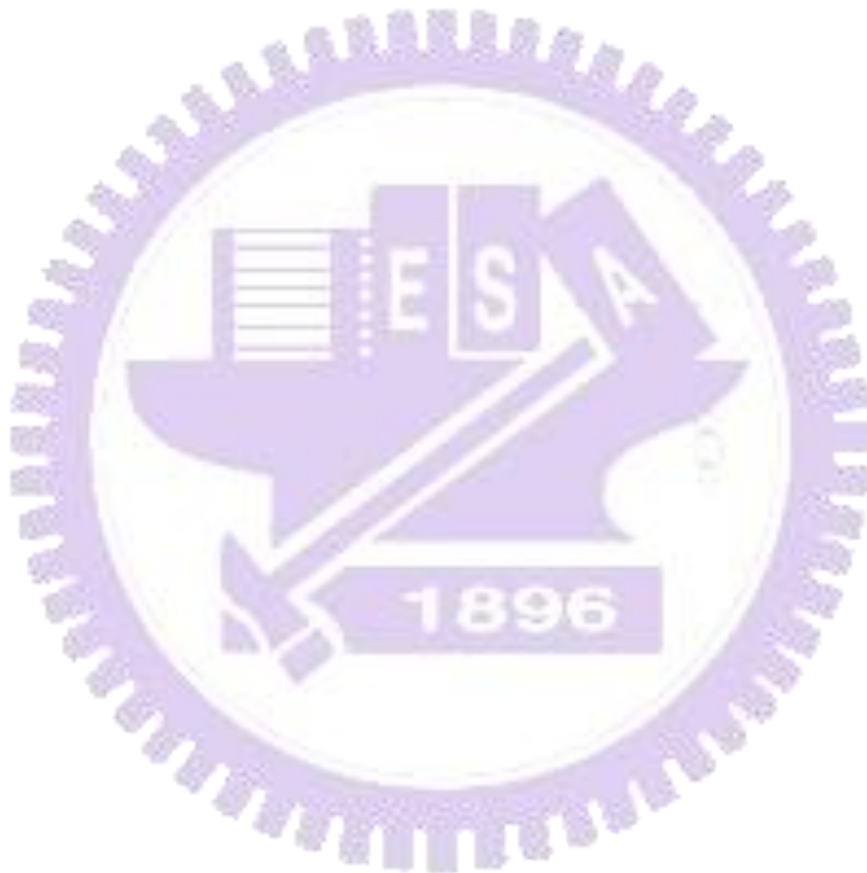
本論文的主要目的是研究具有電子予體及受體的聚合物及含金屬聚合物，在異質結太陽能電池中的性質研究。論文首先介紹，聚合物太陽能電池的發展歷程，並做個總結。

在第二章中，描述了一系列聚合物設計概念、合成方法及應用在聚合物太陽能電池 (PSC) 中的效果，這些聚合物主要是由可溶性的phenothiazine做為電子予體，和各種 benzodiazole (如:benzothiadiazole, benzoselenodiazole和benzoxadiazole) 做為電子受體，以及夾在中間的hexyl-thiophene所組成。這些低能隙 (LBG型) 聚合物具有廣泛的吸收範圍(300-750 nm)，光學能隙在1.80-1.93 eV之間，且 HOMO (-5.38至-5.47 eV) 和LUMO (-3.47至-3.60 eV) 能階均在LBG聚合物的理想範圍內。在PSC裝置應用中，以benzothiadiazole為分子內電子受體的聚合物，以重量比1:4混合PC71BM ([6,6]-phenyl-C₇₁-butyric acid methyl ester)時，所得光電轉換效率1.20%，為所有聚合物中最佳，其開路電壓0.75 V、短路電流值4.60 mA/cm²時、填充因子35.0%。

在第三章中，我們描述一系列含cyclopentadithiophene和dithienosilole的 β -cyano-thiophenevinylene-substituted聚合物的設計概念，合成方法和性質分析。並探討橋接原子 (C和Si) 和cyano-vinylene基團在熱，光，電化學，電荷傳輸和光伏效應等性質上造成的影響。此類LBG聚合物具有廣闊的吸收光譜和理想的 HOMO (約 -5.30 eV) 和LUMO (約 -3.60 eV) 的能階，並具有相當高的hole mobility (9.82×10^{-4} cm²/Vs)。PSC裝置應用中，一含有dithienosilole之聚合物，混合 PC₇₁BM (1:2 w/w) 表現出最佳的功率轉換效率為 2.25%，光源為 AM 1.5 下，100 mW/cm²。

在第四章中，描述合成一系列以benzodiazole為核心的bisterpyridine，利用螯合金屬原子形成的含 Ru^{II}聚合物。並探討聚合物中電子予體和受體的相互作用，

以及熱，光，電和光伏效應等性質。由於其廣泛的吸收光譜範圍金屬，嘗試應用於BHJ太陽能電池設備中。混合PC₆₁BM (1:1 w/w) 作為電子受體表現出高短路電流 (J_{sc})。所得的最大光電轉換效率(PCE)高達 0.45%，開路電壓 = 0.61 eV，短路電流 = 2.18 mA/cm²，FF = 34.1% (AM 1.5，100 mW/cm²)。因此證明這種新穎的共軛高分子電解質，相較普遍的polythioene，同樣可在B H J 裝置中，作為供應電子的主動層。



Acknowledgements

First and foremost I want to thank my advisor Prof. Hong-Cheu Lin. It has been an honor to be his first foreign Ph.D. student. I appreciate all his contributions of time, patience, motivation, immense knowledge ideas, and funding to make my Ph.D. experience productive and stimulating. The joy and enthusiasm he has for his research was contagious and motivational for me, even during tough times in the Ph.D. pursuit. I could not have imagined having a better advisor and mentor for my Ph.D study.

I owe my deepest gratitude also to Dr. Chih-Wei Chu and his group members for their support in a number of ways including device fabrications and characterizations. My thanks and appreciation goes to my thesis committee members, for their encouragement, insightful comments, and suggestions. I owe my deepest gratitude to Prof Kung-Hwa Wei (Chairman), and all professor and secretaries of Department of Materials Science and Engineering, NCTU for their support.

The members of our group have contributed immensely to my personal and professional time at NCTU. The group has been a source of friendships as well as good advice and collaboration. I am especially grateful to all group members including Rajan, Hsuan-Chih, Duryodhan, Wei-Hong, Dhananjaya, Yen-Hsing, Hsiao-Ping, Muthya, Rudrakanta, Ashutosh, Ramesh, Murali, Raju, I-Hung, Han, Chong-Lun, Chung-Ji, Ming-shaw, Shin-Chieh, Chia-Lin, Kuan-Ying and Li-Han. I would like to show my gratitude to Dr. Kartik for introducing me with my advisor and also for his valuable help during my tough time.

I would like to thank prof. Sangram Mudali (Director), Prof. Ajit Panda (Dean), Prof. Arun Padhy and all my collogues at National Institute of Science and Technology, Berhampur, Orissa, India for their encouragement and help in many directions.

Last but not least, I would like to thank my family for all their love and encouragement. For my parents who raised me with a love of science and supported me in all my pursuits. And most of all for my loving, supportive, encouraging, and patient wife Manoswini Nayak and daughter Akankshya whose faithful support during Ph.D. is so appreciated. Thank you.

Table of Contents

Abstract	I
摘要	III
Acknowledgements.....	V
List of Figures and Schemes	IX
List of Tables	XIII
Chapter 1. Introduction	1
1.1 History of Photovoltaic Cells.....	1
1.2 General Principle of Polymer Solar Cells.....	3
1.2.1 Organic Solar Cells on the Basis of Mechanistic Principles.....	3
1.2.2 Characterization of Solar Cell Device	6
1.2.3 Organic Photovoltaic Device Architectures.....	9
1.2.4 Comparison Between Organic and Inorganic Solar Cell.....	12
1.3 Literature Survey of Polymer Solar Cell Materials	13
1.3.1 Design Considerations for Low Band Gap Polymers	14
1.3.2 Polymer Solar Cell Materials.....	17
1.3.3 P3HT Containing Polymer Solar Cells	18
1.3.4 Other Low Band-Gap Containing Polymer Solar Cells.....	19
1.3.5 Conjugated Polyelectrolytes for Solar Cells	25
1.3.6 Characterization of Active Materials for Polymer Solar Cells.	26
1.4 Motivation.....	27
Chapter 2. Synthesis and Applications of Low-Bandgap Conjugated Polymers Containing Phenothiazine Donor and Various Benzodiazole Acceptors for Polymer Solar Cells	31

2.1 Introduction.....	31
2.2 Experimental Section.....	34
2.2.1 Materials	34
2.2.2 Measurements and Characterization.....	34
2.2.3 Device Fabrication of Polymer Solar Cells.	35
2.2.4 Synthesis of Monomers and Polymers.....	36
2.3 Results and Discussions.....	42
2.3.1 Synthesis and Structural Characterization	42
2.3.2 Optical Properties.....	47
2.3.3 Electrochemical Properties	50
2.3.4 Photovoltaic Properties	53
2.4 Conclusion	58
Chapter 3. Cyclopentadithiophene- and Dithienosilole-Based Polymers Containing Cyano-Vinylene Groups for Photovoltaic Applications....	60
3.1 Introduction.....	60
3.2 Experimental Section.....	62
3.2.1 Materials	62
3.2.2 Measurements and Characterization.....	62
3.2.3 Fabrication of Polymer Solar Cells.....	63
3.2.4 Fabrication of Hole- and Electron-only Devices	64
3.2.5 Synthesis of Monomers and Polymers.....	65
3.3 Results and Discussion	70
3.3.1 Synthesis and Structural Characterization	70
3.3.2 Optical properties.....	73
3.3.3 Electrochemical properties.....	75

3.3.4 Photovoltaic properties	77
3.4 Conclusion	79
Chapter 4. Synthesis and Applications of Main-Chain RuII Metallo-Polymers Containing Bis-terpyridyl Ligands with Various Benzodiazole Cores for Solar Cells.....	81
4.1 Introduction.....	81
4.2 Experimental Section	84
4.2.1 Materials	84
4.2.2 Measurements and Characterization	85
4.2.3 Device fabrication of polymer solar cells	86
4.2.4 Synthesis of Monomers and Polymers.....	87
4.3 Results and Discussion	92
4.3.1 Synthesis and Structural Characterization	92
4.3.2 UV-Visible Titration.....	96
4.3.3 Optical Properties.....	97
4.3.4 Electrochemical Properties	102
4.3.5 Photovoltaic Properties	105
4.4 Conclusions.....	108
Chapter 5. Conclusion.....	109
References	111

List of Figures and Schemes

Figure 1.1	Terrestrial cell efficiencies measured under the global AM1.5 spectrum.	2
Figure 1.2	Schematic device structure for bulk heterojunction solar cells.....	3
Figure 1.3	General mechanism for photoenergy conversion in excitonic solar cells.....	4
Figure 1.4	Current (voltage) characteristics of a typical organic diode shown together with the metal-insulator-metal (MIM) picture for the characteristic points. (a) Short circuit condition. (b) Open circuit condition. (c) Forward bias. (d) Reverse bias.	8
Figure 1.5	Four device architectures of conjugated polymer-based photovoltaic cells: (a) single-layer PV cell; (b) bilayer PV cell; (c) disordered bulk heterojunction; (d) ordered bulk heterojunction.....	9
Figure 1.6	Absorption coefficients of films of commonly used materials in comparison with the standard AM 1.5 terrestrial solar spectrum.	13
Figure 1.7	Resonance structures in benzo-bis-thiadiazole.	15
Figure 1.8	Alternating donor–acceptor units lower the effective band gap by orbital mixing.	15
Figure 1.9	Example of organic semiconductors used in polymer solar cells.	17
Figure 1.10	Nonexhaustive survey of reports focusing on photovoltaic devices based on P3HT:PCBM blends.....	19
Figure 1.11	Chemical Structures of Benzothiadiazole-Containing Polymers.....	20

Figure 1.12	General structure of the fluorene copolymers with a variety of acceptors. General structure of the fluorene copolymers with a variety of acceptors.	21
Figure 1.13	General structure of the phenothiazine containing copolymers.	22
Figure 1.14	Structure of the carbazole copolymers with a variety of acceptors.....	22
Figure 1.15	Structure of the diketopyrrolopyrrole containing copolymers with a variety of donors.....	23
Figure 1.16	Structure of the polymers containing donating moieties from the 2,2'-bithiophene unit covalently bridged with an atom at 3,3'-position.	24
Figure 1.17	Chemical structure of PBDTTT-E, PBDTTT-C and PBDTTT-CF...	24
Figure 1.18	Structure of the conjugated polyelectrolytes used in solar cells.	25
Figure 1.19	Nonexhaustive list of investigation techniques required for an extended characterization of active materials for polymer solar cells.....	26
Figure 2.1	Synthetic Routes of Monomers.....	41
Figure 2.2	Synthetic Routes of Polymers (PP6DHTBT, PP6DHTBSe, and PP6DHTBX).	42
Figure 2.3	¹ H NMR spectra of polymers in CDCl ₃	43
Figure 2.4	TGA thermograms of polymers.	44
Figure 2.5	Normalised UV-vis spectra of polymers in (a) dilute chlorobenzene solutions and (b) solid films, respectively.....	46
Figure 2.6	Cyclic voltammograms of polymers	49
Figure 2.7	Current-voltage curves of polymer solar cells using polymer:PCBM blends under the illumination of AM 1.5G, 100 mW/cm ²	52

Figure 2.8	(a) Absorbance spectra of PP6DHTBT:PC ₇₁ BM thin films measured from the solar cell devices by using an ITO/PEDOT substrate as a reference. (b) External quantum efficiency (EQE) of PP6DHTBT:PC ₇₁ BM solar cells.	55
Figure 2.9	AFM images of PP6DHTBT: PC ₇₁ BM blend films. (a) 1:1 (w/w), (b) 1:3 (w/w), and (c) 1:4 (w/w) ratios.	56
Figure 3.1	Synthetic route for monomers and polymers.	70
Figure 3.2	TGA measurements of polymers at a heating rate of 10°C/min.	71
Figure 3.3	Normalized absorption spectra of polymers in dilute chloroform solutions (10 ⁻⁶ M) and solid films.	72
Figure 3.4	Cyclic voltammograms of polymers in solid films at a scan rate of 100 mV/s.	74
Figure 3.5	(a) Current-voltage curves of polymer solar cells using polymer:PCBM blends under the illumination of AM 1.5G, 100 mW/cm ² . (b) EQE curves of the PSC devices based on polymers/PC ₆₁ BM (1:1, w/w). ..	76
Figure 3.6	AFM images of (a) CPDT-CN: PC ₆₁ BM 1:1 (w/w) and (b) DTS-CN: PC ₆₁ BM 1:1 (w/w).	79
Figure 4.1	Synthetic Route for Bis-terpyridyl Ligands (M1-M3) and Ru ^{II} -containing Metallo-Polymers (P1-P3).....	91
Figure 4.2	¹ H NMR spectra (aromatic region) of bis-terpyridyl ligands M1-M3 (in CDCl ₃) and metallo-polymers P1-P3 (in DMSO-d ₆).	93
Figure 4.3	TGA thermograms of bis-terpyridyl ligands (M1-M3) and metallo-polymers (P1-P3) at a heating rate of 10°C/min under nitrogen.	94

Figure 4.4	UV-vis absorption spectra acquired upon the titration of (a) M1, (b) M2, and (c) M3 (in 2:8 v/v CH ₃ CN:CHCl ₃) with Zn(OAc) ₂ (in EtOH). The insets show the normalized absorption at 325 nm as a function of Zn ²⁺ :M2-M3, respectively.....	95
Figure 4.5	Normalized UV-vis spectra of bis-terpyridyl ligands (M1-M3) and metallo-polymers (P1-P3). In (a) dilute (10 ⁻⁶ M) solutions and (b) solid films, respectively.	99
Figure 4.6	Cyclic voltammograms of bis-terpyridyl ligands (M1-M3) and metallo-polymers (P1-P3) at a scan rate of 100 mV/s.	101
Figure 4.7	Current-voltage curves of BHJ solar cells using blended films of M1-M3 or P1-P3:PCBM (1:1 w/w) under the illumination of AM 1.5G, 100 mW/cm ²	104
Figure 4.8	EQE curves of the PSC devices based on polymers P1-P3: PCBM (1:1 wt%).	106

List of Tables

Table 2.1	Molecular Weights and Thermal Properties of Polymers	44
Table 2.2	Optical Properties of Polymers	45
Table 2.3	Electrochemical Properties of Polymers	49
Table 2.4	Photovoltaic Properties of Polymer Solar Cell Devices with the Configuration of ITO/PEDOT:PSS/Polymer:PCBM/Ca/Al	52
Table 2.5	Annealing Effects on Polymer Solar Cell Device Containing PP6DHTBT:PC ₇₁ BM (1:4 wt%)	58
Table 3.1	Molecular Weights and Thermal Properties of Polymers	72
Table 3.2	Optical and electrochemical properties of Polymers.....	74
Table 3.3	Photovoltaic properties of PSC devices with the configuration of ITO/PEDOT:PSS/Polymer:PCBM/Ca/Al.....	78
Table 4.1	Optical, Thermal, and Viscosity Properties of Bis-terpyridyl Ligands (M1-M3) and Metallo-Polymers (P1-P3).....	97
Table 4.2	Electrochemical Properties of Bis-terpyridyl Ligands (M1-M3) and Metallo-Polymers (P1-P3).....	101
Table 4.3	Photovoltaic Properties of BHJ Solar Cell Device with a Configuration of ITO/PEDOT:PSS/Compound:PCBM/Ca/Al	104

Chapter 1.

Introduction

1.1 History of Photovoltaic Cells

The predictable exhaustion of fossil energy resources and the increasing pressure generated by environmental concerns and climate change have triggered an intensification of research on the most clean sustainable energy sources, in particular on the photovoltaic conversion of solar energy. The 'photovoltaic effect' is the mechanism in which a solar cell converts photons from the solar light into electricity. While the photovoltaic effect was first observed in 1839 in an electrochemical process by French physicist Alexander-Edmond Becquerel,¹ the first well-performing solid-state solar cell was built by Charles Fritts in 1883. He coated the semiconductor Selenium with an very thin layer of gold to form a junction that had an efficiency of 1%.² Modern generation of solar cells was born in 1953 when at Bell Laboratories (New Jersey, USA) the first silicon solar cell was developed with a power conversion efficiency of 6%.³ After that, many different technologies and materials were developed in order to improve the performance of the device and lower their production cost. In order to achieve this goal, organic materials provide us with a variety of possibilities. Especially semiconducting polymers combine the favorable opto-electronic properties of organic materials, such as high absorption coefficients, with the excellent solution processability onto a flexible substrate using simple and cheaper methods such as spin coating and inkjet printing.⁴

Classification ^a	Effic. ^b (%)	Area ^c (cm ²)	V _{oc} (V)	J _{sc} (mA/cm ²)	FF (%)	Test centre (and date)
Cells (silicon)						
Si (MCZ crystalline)	24.7 ± 0.5	4.0 (da)	0.704	42.0	83.5	Sandia (7/99) ^d
Si (moderate area)	23.9 ± 0.5	22.1 (da)	0.704	41.9	81.0	Sandia (8/96) ^d
Si (large crystalline)	23.0 ± 0.6	100.4 (t)	0.729	39.6	80.0	AIST (2/09)
Si (large crystalline)	22.0 ± 0.7	147.4 (t)	0.677	40.3	80.6	FhG-ISE (3/06) ^d
Si (large multicrystalline)	19.3 ± 0.5	217.7 (t)	0.651	38.8	76.4	AIST (7/09)
Cells (other)						
GaInP/GaAs/GaInAs (tandem)	35.8 ± 1.5	0.880 (ap)	3.012	13.9	85.3	AIST (9/09)
CIGS (thin film)	20.1 ± 0.6	0.503 (t)	0.720	36.3	76.8	FhG-ISE (4/10)
a-Si/nc-Si/nc-Si (tandem)	12.5 ± 0.7 ^e	0.27 (da)	2.010	9.11	68.4	NREL (3/09)
Dye-sensitized	11.2 ± 0.3 ^f	0.219 (ap)	0.736	21.0	72.2	AIST (3/06) ^d
Organic	7.9 ± 0.3 ^{fg}	0.0441 (ap)	0.756	14.7	70.9	NREL (11/09)

^a CIGS = CuInGaSe₂.

^b Effic. = efficiency.

^c (ap) = aperture area; (t) = total area; (da) = designated illumination area.

^d Recalibrated from original measurement.

^e Light soaked under 100 mW/cm² white light at 50°C for 1000 h.

^f Stability not investigated.

^g Light soaked under simulated AM1.5 for about 140 h prior to shipment to NREL.

Figure 1.1 Terrestrial cell efficiencies measured under the global AM1.5 spectrum.⁵

The current status of solar cells is shown Figure 1.1. In more than 20 years since the seminal work of Tang,⁶ organic solar cells have undergone a gradual evolution that has led to energy conversion efficiencies of about 7.9%. Solution-processed organic solar cells were first reported in 1995,⁷ where, the best efficiency reported at that time barely reached values higher than 1%, but now could be achieved easily efficiencies beyond 5% today. To attain efficiencies approaching 10 % for the commercialization in large area, much effort is required to understand the fundamental electronic interactions as well as the complex interplay of device architecture, morphology, processing, and the fundamental electronic processes.

1.2 General Principle of Polymer Solar Cells

1.2.1 Organic Solar Cells on the Basis of Mechanistic Principles

The architecture of a typical Organic Solar Cells is sketched in Figure 1.2. The core of the cell is the photoactive layer, which is generally composed by a p-type electron-donor compound (D) and an n-type electron-acceptor compound (A). Both A and D are organic π -conjugated materials, and either one or the other (or both) is a polymer. The photoactive layer, typically around 100–200 nm in thickness, is interposed between the electrodes; additional layers of electron or hole transporting materials can be present.

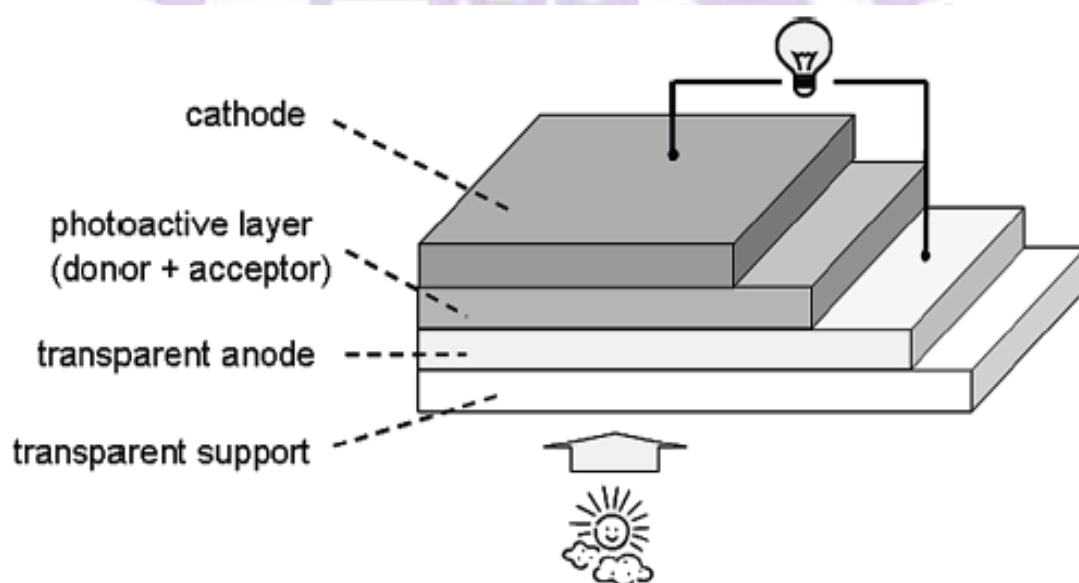


Figure 1.2 Schematic device structure for bulk heterojunction solar cells.⁸

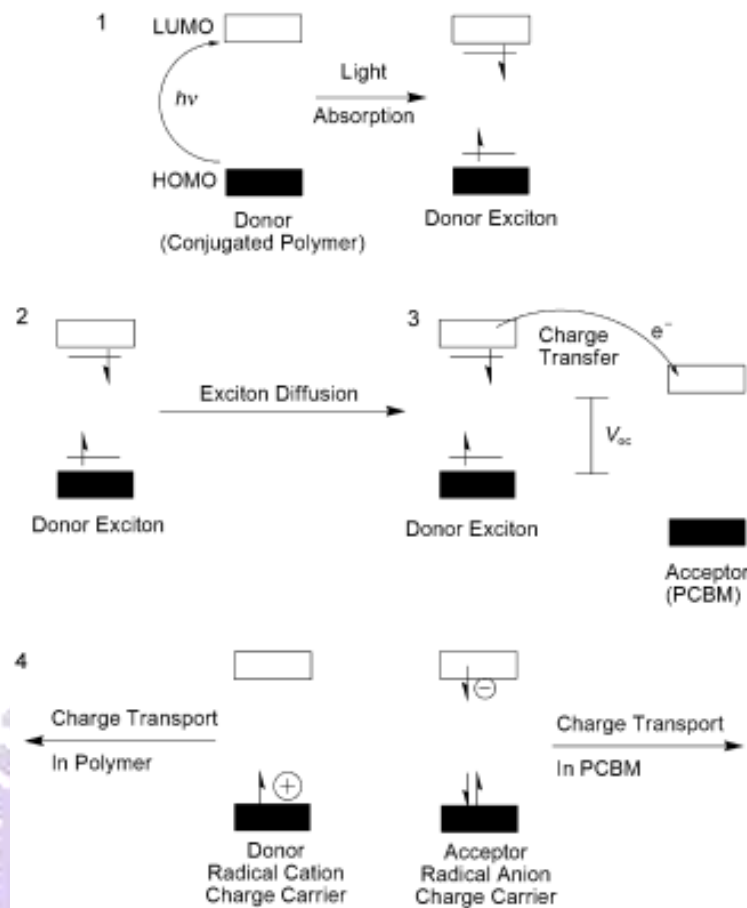


Figure 1.3 General mechanism for photoenergy conversion in excitonic solar cells.⁹

Figure 1.3 illustrates the mechanism by which light energy is converted into electrical energy in the devices. The energy conversion process has four fundamental steps in the commonly accepted mechanism:¹⁰

1. *Absorption of light and generation of excitons:* Photoexcitation of the absorber material(s) causes the promotion of electrons from the ground state, approximated by the highest occupied molecular orbital (HOMO), to the excited state, approximated by the lowest unoccupied molecular orbital (LUMO). These photoexcitation depends upon the value of the optical absorption coefficient and on the thickness of the donor material. Then the excitons are generated which, consists of an electron and a hole paired by an energy that is smaller than the energy gap between the limits of the permitted bands (LUMO and HOMO bands,

respectively). The difference between two energies is called exciton binding energy which, is around 0.1-0.2 eV in organic materials. The occupation of these excited states, the LUMO by the electron, and the HOMO by the hole, is termed as a nonrecombined excitons.

2. *Diffusion of the excitons:* Excitons produced within a diffusion length from the D/A interface will have the chance to reach it before decaying, radiatively or not. Diffusion takes place as long as recombination process do not takes place. Forster (long range) or Dexter (between the adjacent molecules) transfers can takes place between an excited molecule.
3. *Dissociation of the excitons:* If the offsets of the energy levels of the D and the A materials are higher than the exciton binding energy, excitons dissociate at the D/A interface. Excitons photogenerated in the donor side will dissociate by transferring the electron to the LUMO level of the acceptor and retaining the positive charge, while those created in the other side will transfer the hole to the HOMO of the donor while retaining the negative charge. This step leads to the formation of free charge carriers.
4. *Charge transport and charge collection:* The charge carriers diffuse to the electrodes through the respective materials (electrons in the acceptor and holes in the donor). The charges reach the electrodes and are collected. For this to occur most efficiently, the following conditions must be satisfied:

$$(E_F)_{\text{cathode}} < (E_{\text{LUMO}})_{\text{acceptor}} \text{ and } (E_F)_{\text{anode}} < (E_{\text{LUMO}})_{\text{donor}}.$$

In each of the above steps several phenomena can take place that decrease the efficiency of the global process, so that only a limited portion of the photons reaching the cell are able to generate “useful” charge carriers. Thus, the optimization of each step is fundamental to extract as much energy as possible from the device.

1.2.2 Characterization of Solar Cell Device

Solar cells are further characterised by measuring the current-voltage $I(V)$ curve under illumination of a light source that mimics the sun spectrum. A typical current-voltage $I(V)$ curve of a polymer solar cell is shown in Figure 1.4. Since organic semiconductors show very low intrinsic carrier concentration, the metal-insulator-metal (MIM) model seems to be best suited to explain this characteristic. The characteristic points used to characterise a solar cell are labelled in Figure 1.4. In addition, for each of these points, the energy diagram for a single-layer cell with an indium tin oxide (ITO) anode and aluminium cathode is displayed.

- (a) The current delivered by a solar cell under zero bias is called short circuit current (I_{sc}). In this case, exciton dissociation and charge transport is driven by the so-called built-in potential. This can be determined by the product of photoinduced charge carrier density and the charge carrier mobility within the organic semiconductors:

$$I_{sc} = ne\mu E$$

Where, n is the density of charge carriers, e is the elementary charge, μ is the mobility, and E is the electrical field. Therefore, for improving the short circuit current, high mobility/low band gap materials are essential. In the MIM picture, this potential is equal to the difference in work function (Φ) of the hole- and electron-collecting electrodes. For polymer solar cells, the transparent ITO electrode is often chosen ($\Phi_{ITO} = 4.7$ eV) in combination with a low work function material ($\Phi_{Ca} = 2.87$ eV, $\Phi_{Mg} = 3.66$ eV, $\Phi_{Al} = 4.24$ eV) as counter-electrode to achieve a high internal field.

The external quantum efficiency (EQE) is simply the number of electrons collected under short circuit conditions per the number of incident photons.

$$\text{EQE} = \frac{1240 I_{sc}}{\lambda P_{in}}$$

- (b) The voltage where the current equals zero is called open circuit voltage (V_{oc}). In the MIM picture this situation is described by the case where the band is flat, since the applied voltage equals the difference in the work function of the electrodes. (Note that diffusion effects are neglected in this simplified picture)
- (c) When $V > V_{oc}$, the diode is biased in the forward direction. Electrons are now injected from the low work function electrode into the LUMO and holes from the high work function electrode into the HOMO of the organic layer, respectively.
- (d) When $V < 0$, the diode is driven under a reverse biased condition the solar cells works as a photodiode. The field is higher than in (a) which often leads to enhanced charge generation and/or collection efficiency.

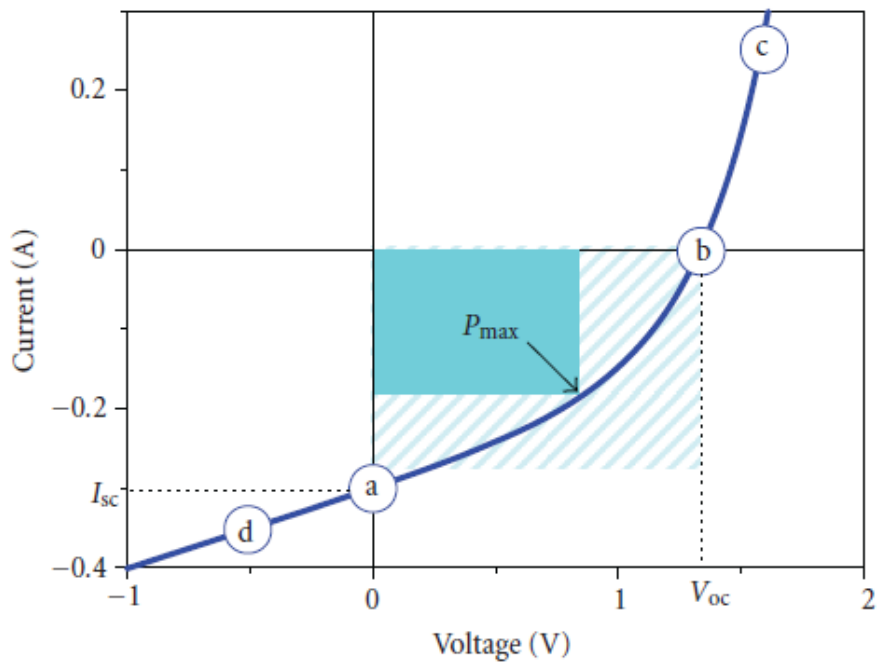
The point where the electrical power $P = I \times V$ reaches the maximum value represents the condition where the solar cell can deliver its maximum power to an external load. It is called the maximum power point. The ratio of this maximum electrical power P_{max} to the product of the short circuit current and the open circuit voltage is termed the fill factor (FF).

$$\text{FF} = \frac{P_{max}}{V_{oc} \times I_{sc}}$$

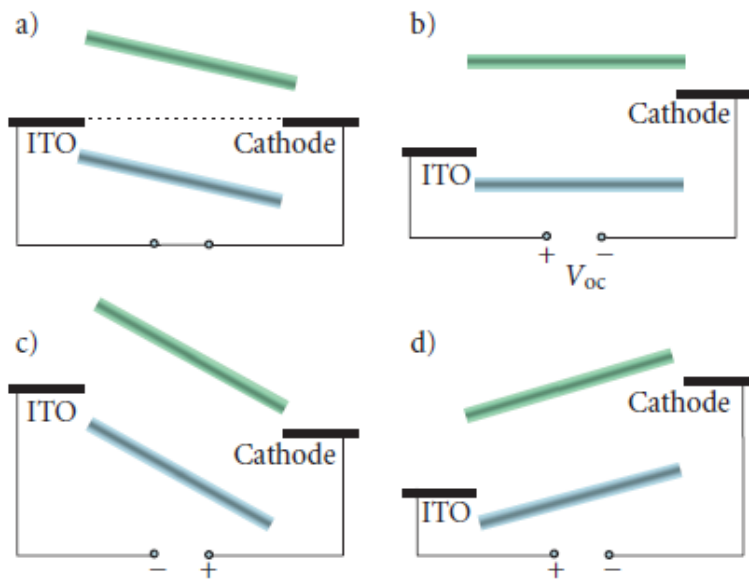
Ideally, the fill factor should be unity, but losses due to transport and recombination result in values between 0.2–0.7 for organic photovoltaic devices.

The photovoltaic power conversion efficiency (η) is then calculated for an incident light power P_{in} :

$$\eta = \frac{V_{oc} \times I_{sc} \times \text{FF}}{P_{in}}$$



(a)



(b)

Figure 1.4 Current (voltage) characteristics of a typical organic diode shown together with the metal-insulator-metal (MIM) picture for the characteristic points. (a) Short circuit condition. (b) Open circuit condition. (c) Forward bias. (d) Reverse bias.¹¹

1.2.3 Organic Photovoltaic Device Architectures

The organic cells reported in the literature can be categorized by their device architecture as having single layer, bilayer, disordered bulk heterojunction; or ordered bulk heterojunction structure (Figure 1.5)

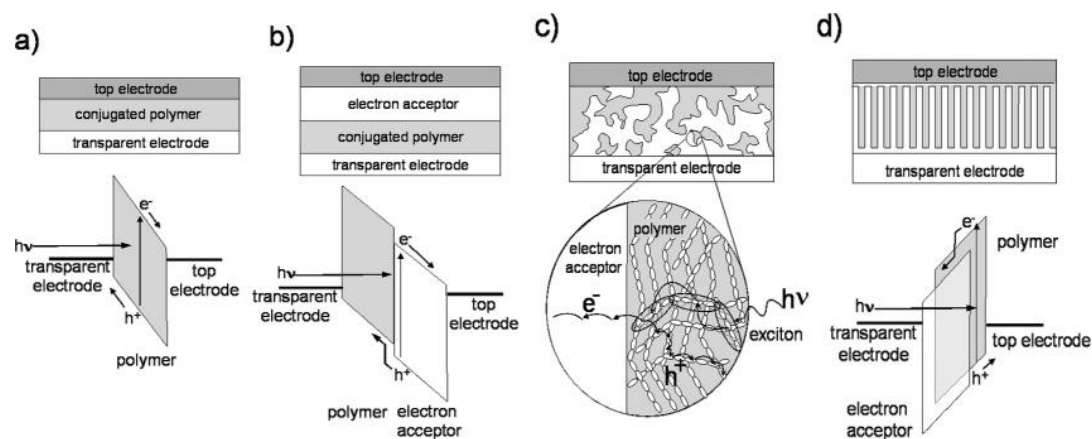


Figure 1.5 Four device architectures of conjugated polymer-based photovoltaic cells: (a) single-layer PV cell; (b) bilayer PV cell; (c) disordered bulk heterojunction; (d) ordered bulk heterojunction.¹²

(a) *Single-layer PV cell*: Although it is possible to generate a built-in field in an inorganic semiconductor through the controlled placement of n- and p-type dopant atoms, it is difficult to controllably dope most conjugated polymers. As a result of this, conjugated polymers are usually made as pure as is practically possible and can effectively be considered to be intrinsic semiconductors. Generating built-in electric fields within a film in the dark requires sandwiching the polymer between electrodes with varying work functions or incorporating interfaces with a second semiconductor into the device structure.¹³ In single-layer conjugated polymer PV cells, the sign and magnitude of V_{oc} could at least be partially attributed to an electrode work-function difference. Although single-layer PV cells tend to produce a reasonable V_{oc} , their photocurrent is

typically very low.¹⁴

- (b) *Bilayer PV cell*: C. W. Tang in 1985 discovered that, by making two-layer PV cells with organic semiconductors that have offset energy bands, the external quantum efficiency of PV cells could be improved to 15% at the wavelength of maximum absorption.⁵ The improved efficiency resulted from exciton dissociation at the interface between the two semiconductors. Excitons generated within a few nanometers of the heterojunction could diffuse to the interface and undergo forward electron or hole transfer. This process of forward charge transfer led to the spatial separation of the electron and hole, thereby preventing direct recombination and allowing the transport of electrons to one electrode and holes to the other. Because there were essentially no minority free carriers in the undoped semiconductors, there was little chance of carrier recombination once the charges moved away from the interface, despite the long transit times to the electrodes. Sariciftci et al. first applied this two-layer technique to a conjugated polymer PV cell by evaporating C₆₀ on top of a spin-cast MEH-PPV layer.¹⁵ However, in the organic PV cell, the excitons in these materials need to be generated near the interface for dissociation to occur before recombination. The exciton diffusion length in several different conjugated polymers has subsequently been measured to be 4–20 nm.¹⁶ Because the exciton diffusion length in a conjugated polymer is typically less than the absorption length of the material (~100 nm), the EQE of a bilayer device made with a conjugated polymer and another semiconductor is ultimately limited by the number of photons that can be absorbed within an exciton diffusion length of the interface.
- (c) *Disordered bulk heterojunction*: To address the problem of limited exciton diffusion length in conjugated polymers, Yu et al.¹⁷ and Halls et al.¹⁸

independently intermixed two conjugated polymers with offset energy levels so that all excitons would be formed near an interface. They observed that the photoluminescence from each of the polymers was quenched. This implied that the excitons generated on one polymer within the film reached an interface with the other polymer and dissociated before recombining. This device structure, called a bulk heterojunction, provided a route by which nearly all photogenerated excitons in the film could be split into free carriers.

(d) *Ordered bulk heterojunction:* In all of the bulk heterojunction devices that we have described above, the conjugated polymer and electron acceptor have been randomly interspersed throughout the film. The randomly distributed interface between the two semiconductors can lead to incomplete PL quenching in the conjugated polymer in regions of the polymer that are more than an exciton diffusion length away from an acceptor. For these reasons, some have sought to create well-ordered conjugated polymer–electron acceptor films. In an ideal device structure, every exciton formed on the conjugated polymer will be within a diffusion length of an electron acceptor, although quantitative modeling has pointed out that some light emission will still occur in the polymer even if this is the case.¹⁹ Polymeric bulk heterojunction devices, whose photoactive layer is composed of a blend of bicontinuous and interpenetrating donor and acceptor, can maximize interfacial area between the donor and the acceptor. In addition, these devices can be processed in solution, such as spin-coating or roll-to-roll printing, thereby contributing several attractive advantages such as low-cost, lightweight, and flexible devices.

1.2.4 Comparison Between Organic and Inorganic Solar Cell

The mechanism underneath the operation of a polymer (or an organic) solar cell exhibits, of course, many similarities with that of inorganic cells, but also some distinctions, arising from a few important different characteristics of the materials involved:

- (1) While inorganic semiconductors exhibit a band structure, organic semiconductors possess discrete energy levels (molecular orbitals). Nevertheless, the term “bandgap” is often improperly used for organic semiconductors.
- (2) In solar cells based on inorganic semiconductors such as silicon, the absorbed photons lead to the direct creation of free charge carriers. In contrast, in organic semiconductors based on π -conjugated systems because of the low dielectric constant of these materials, light absorption leads to the creation of excitons, strongly Coulombically bound electron-hole pairs. In organic heterojunctions, the driving force for exciton dissociation is provided by the energy offset between the molecular orbitals of the donor and acceptor. Exciton dissociation into free charge carriers thus represents a key process that imposes one of the major limitations to the power conversion efficiency of organic solar cells.
- (3) When a bound hole-electron pair (exciton) is generated in an inorganic semiconductor, its immediate dissociation is observed. Excitons in organic semiconductors are tightly bound (binding energy of around 0.3–0.5 eV) and dissociation must be promoted in some way avoiding radiative recombination.
- (4) Compared to inorganics, charge carrier mobilities in organic semiconductors are very low.
- (5) Light absorption coefficients of organic materials are much higher than those of inorganics.

1.3 Literature Survey of Polymer Solar Cell Materials

In a typical polymeric BHJ PVC, the photoactive blend layer, sandwiched between an indium tin oxide (ITO) positive electrode and a metal negative electrode, may be composed of a low band gap conjugated polymer donor and a soluble nanosized acceptor.⁹⁻¹² A fullerene derivative, [6,6]- phenyl-C₆₁-butyric acid methyl ester (PCBM), showing better solubility than C₆₀ in common solvents, is a widely utilized acceptor. As a component in the active layer, a conjugated polymer donor serves as the main absorber to solar photon flux, as well as the hole transporting phase.^{9,20} Thus a low band gap feature to match the solar spectrum (Figure 1.6) and fast hole mobility are basic requirements to design an ideal polymer donor.

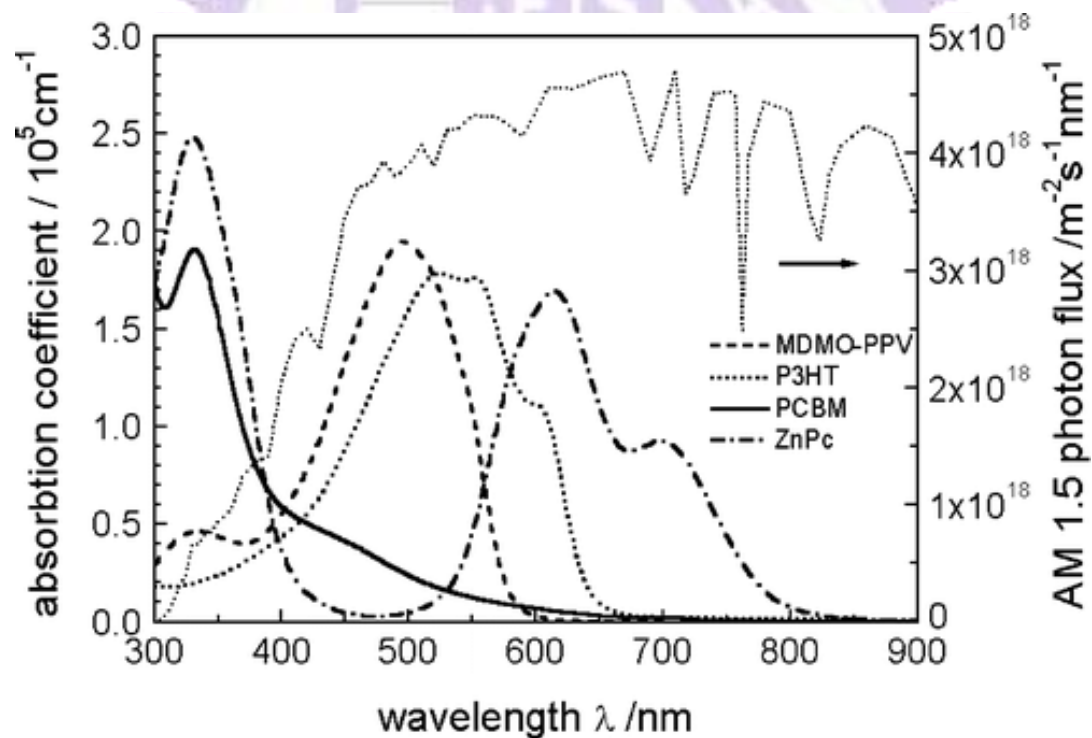


Figure 1.6 Absorption coefficients of films of commonly used materials in comparison with the standard AM 1.5 terrestrial solar spectrum.²¹

1.3.1 Design Considerations for Low Band Gap Polymers

In recent days, interests in the design and synthesis of conjugated polymers have been increased for the applications of electronic and photonic devices. It remains a key challenge to synthesize ideal low band gap (LBG) polymers with high intrinsic conductivities to develop their potential applications in highly efficient bulk-heterojunction (BHJ) solar cells. Concerning the band gaps of LBG polymers, the following factors should be taken into the account: intra-chain charge transfers, bond-length alternation, aromaticity, substituents effects, intermolecular interactions, and π -conjugation length etc.²²⁻²³

The low band gap copolymers reported are often based on thiophene but other electron rich aromatic units such as pyrrole are also found. Identical for these copolymers are the alternation between electron donor (electron rich) and electron acceptor (electron deficient) units. The high energy level for the HOMO of the donor and the low energy level for the LUMO of the acceptor results in a lower band gap due to an intra-chain charge transfer from donor to acceptor.²³ Planarity along the aromatic backbone results in a low band gap, due to a high degree of delocalization of the π -electrons. The alternation between single and double bonds along the polymer chain has a tendency to increase the band gap. A reduction of the difference in bond length alternation is achieved by the alternation of donor and acceptor units along the conjugated polymer chain thus lowering the band gap. As described interactions between acceptor and donor enhance double bond character between the repeating units, this stabilizes the quinoid form of e.g. benzo-bis(thiadiazole) (Figure 1.7) formed within the polymer backbone, and hence a reduction in band gap is achieved.²⁴

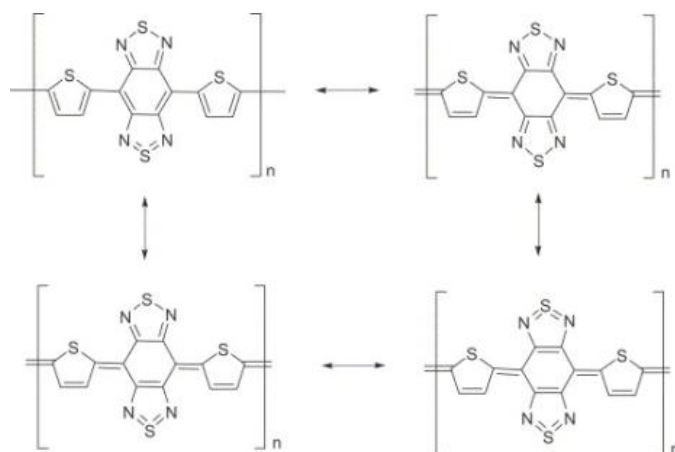


Figure 1.7 Resonance structures in benzo-bis-thiadiazole.²⁵

If the HOMO level of the donor and the LUMO level of the acceptor are close in energy it results in a low band gap as shown in (Figure 1.8). Therefore, to achieve a lower band gap the strength of the donor and the acceptor must be increased. This is efficiently achieved by using electron withdrawing groups such as CN, NO₂, quinoxalines, pyrazines or thiadiazole on the acceptor and electron donating groups such as thiophene or pyrrole on the donor.²⁴

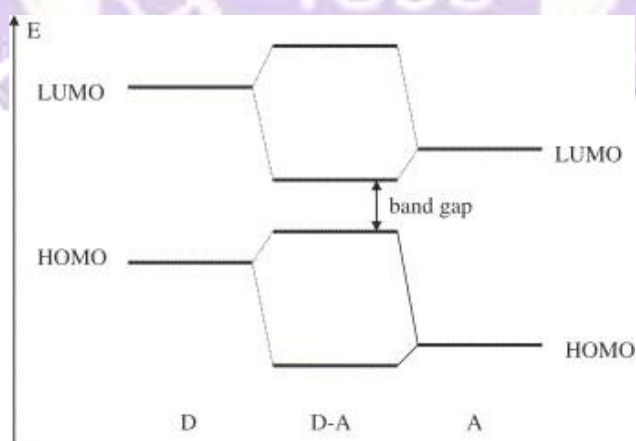


Figure 1.8 Alternating donor–acceptor units lower the effective band gap by orbital mixing.²⁵

In order to increase the power conversion efficiency (PCE) in BHJ solar cells, some important characteristics of LBG polymers need to be dealt, such as: (i) a more favorable overlap of the absorption spectrum of the active layer with the solar emission²⁶ – Many classes of LBG polymers with the absorption edges extended into the near-infrared regions have been synthesized and investigated.²⁷ (ii) a better charge carrier mobility²⁸ – This can be improved by optimization of intra-chain ordering (co-planarity and conjugation length) and inter-chain stacking, which often can be increased upon annealing the BHJ solar cell devices.²⁹ (iii) an optimized relative positions of the energy levels of the electron donors and acceptors³⁰ – The maximization of the open circuit voltage (V_{oc}) is correlated to have more efficient charge separation between electron-donor polymers and electron-acceptor PCBM. For this purpose, the donor polymer should exhibit a band gap between 1.2 and 1.9 eV, which corresponds to a HOMO energy level between -5.8 and -5.2 eV and LUMO energy level between -4.0 and -3.8 eV.³¹ In order to achieve higher efficiencies of BHJ solar cell devices, the difference of the LUMO levels between donor polymer and acceptor PCBM needs to be at least 0.3 eV.³² Otherwise, the driving force for charge separation will be decreased, and also V_{oc} will be reduced by raising the HOMO level of the donor polymer. Therefore, in order to synthesize LBG polymers, the design rules described above suggest that the optimization of HOMO and LUMO levels of LBG polymers is the most promising strategy to develop BHJ solar cells with high efficiencies. However, it is difficult to synthesize the LBG polymers with all three properties like broad absorption spectra, high carrier mobilities, and appropriate molecular energy levels.

1.3.2 Polymer Solar Cell Materials

Generally, organic materials having delocalized π electrons, absorbing sunlight, creating photo generated charge carriers and transporting these charge carriers can be used for fabrication of polymer solar cells. These materials are classified to the electron donors and the electron acceptors.

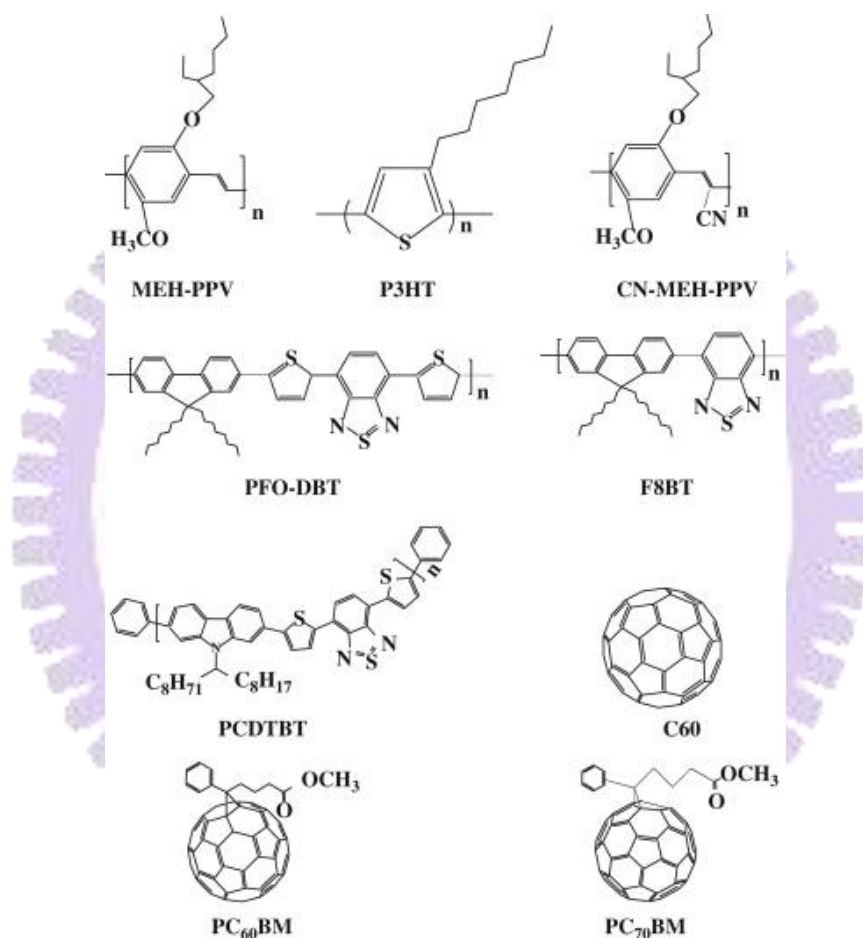


Figure 1.9 Example of organic semiconductors used in polymer solar cells.³³

Most of semiconducting polymers are hole-conductors. This kind of semiconducting polymers was named as the electron donor polymers. Figure 1.9 shows some representative semiconducting polymers. Four important representatives of electron donor polymers are MEH-PPV, P3HT, PFO-DBT and PCDTBT. The

electron acceptor polymers like CN-MEH-PPV, F8TB, and small molecules, C₆₀ and soluble derivatives of C₆₀ and C₇₀, namely PC₆₀BM and PC₇₀BM, are also shown in Figure 1.8. Fullerenes are considered to be the best electron acceptors so far. This is because: (i) ultrafast (50 fs) photo induced charge transfer was happened between the donor polymers and fullerenes; (ii) fullerenes exhibited high mobility, for example, PC₆₀BM shown electron mobility up to 1 cm² V⁻¹ s⁻¹ measured by field effect transistors; (iii) fullerenes shown a better phase segregation in the blend film.³⁴

Dialkoxy-substituted poly(para-phenylene vinylene)s (PPVs), for example, poly[2-methoxy-5-(2-ethyl-hexyloxy)- 1,4-phenylene vinylene] (MEH-PPV) and poly[2-methoxy-5-(3',7'-dimethyloctyloxy)-1,4-phenylene vinylene] (MDMOPPV) show strong absorption in the visible light band. Notable PCE values of 2-3% have been reproducibly achieved.³⁵⁻³⁶

1.3.3 P3HT Containing Polymer Solar Cells

During the last five years, research efforts have focused on poly(alkyl-thiophenes), and in particular on P3HT. In 2002, the first encouraging results for P3HT:PCBM solar cells with a weight ratio of 1:3 were published.³⁷ At that time, the short-circuit current density was the largest ever observed in an organic solar cell (8.7 mA cm⁻²), and resulted from an EQE that showed a maximum of 76% at 550 nm. Many optimization methods, such as using different solvents to fabricate the active layer, thermally annealing the active layer or the device, film forming speed, additives to the active layer, optical spacer, anode or cathode interfacial layer, and tandem structure, have been extensively carried out with P3HT as donors and have demonstrated significant improvements in the photovoltaic performance of BHJ PVCs.³⁷⁻⁴⁷ (Figure 1.10)

Year	P3HT Provider	M_w [g mol ⁻¹]	Ratio to PCBM (weight)	Layer thickness [nm]	Solvent	Annealing time [min]	Annealing Temp. [°C]	Max EQE [%]	V_{oc} [V]	FF	J_{sc} [mA cm ⁻²]	Eff [%]	Light intensity [mW cm ⁻²]
2002	–	–	1: 3	350	–	–	–	76	0.58	0.55	8.7	2.8	100
2003	–	–	–	110	DCB	4	75	70	0.55	0.6	8.5	3.5	80
2004	Rieke	–	1: 2	350	CB	4	75	65	0.54	0.37	15.2	3.1	100
2005	Rieke	100 000	1: 1	70	DCB	60	120	58	0.615	0.61	7.2	2.7	100
2005	Merck	11 600	1: 1	–	CB	15	140	58	0.61	0.53	9.4	3.0	100
2005	–	–	1: 1	63	DCB	10	110	–	0.61	0.62	10.6	4.0	100
2005	Rieke	–	1: 1	220	DCB	10	110	63	0.61	0.67	10.6	4.4	100
2005	Aldrich	87 000	1: 0.8	–	CB	5	155	–	0.65	0.54	11.1	4.9	80
2005	Rieke	–	1: 0.8	–	CB	30	150	–	0.63	0.68	9.5	5.0	80
2006	Merck	21 100	1: 1	175	CB	120	140	70	0.6	0.52	12	4.4	85
2006	–	–	1: 0.8	–	CB	10	150	88	0.61	0.66	11.1	5.0	90
2006	Rieke	–	1: 1	320	DCB	10	110	82	0.56	0.48	11.2	3.0	100
2008	Rieke	–	1: 1	220	DCB	10	120	87	0.64	0.69	11.3	5.0	100

Figure 1.10 Nonexhaustive survey of reports focusing on photovoltaic devices based on P3HT:PCBM blends.³¹

Despite the promising efficiencies obtained for the P3HT:PCBM devices, this system has several drawbacks: P3HT:PCBM based solar cells generate a low open circuit voltage of only 0.65–0.70 V. This low open circuit voltage is one of the major loss mechanisms in this system, taking into account that only photons with energies exceeding the optical band gap of P3HT of 1.9 eV are absorbed. The absorbance coefficient of PCBM in the visible region is relatively low, such that the photoresponse of the P3HT:PCBM devices is mainly due to the P3HT absorption alone. As these devices are limited by their photocurrent generation and intrinsic absorption properties, further increase of PCE is rather difficult. Therefore, an alternative approach to get a higher efficiency is to use LBG donor-acceptor polymeric materials, as their electronic and optoelectronic properties can be tuned through intra-molecular charge transfers.

1.3.4 Other Low Band-Gap Containing Polymer Solar Cells

Despite the advances of PVC performance with the classic MEH-PPV, MDMO-PPV, and P3HT as the BHJ donor phase reaching PCE up to 5%, further significant enhancement of PCE is necessary in order to meet the requirements for

large scale commercialization as a renewable energy source. One of the routes for such improvements is the design of new polymer donors that have extended absorption edge to match solar terrestrial radiation, higher carrier mobility, and better energy alignment with acceptors to reach high open circuit voltage. These studies have paved the pathway toward better understanding of the nature of BHJ solar cells, and some of them might be promising candidates for future commercial applications.

One of the most widely used strategies to make narrow band gap donor polymers is the synthesis of an alternating copolymer from electron-rich (donor) and electron-deficient (acceptor) units in their backbone. One of the such acceptor heterocycle, 2,1,3-benzothiadiazole has been utilized to construct some n-type semiconducting polymers in cooperation with varieties of electron-donating (D) units to show outstanding photovoltaic performances.²⁷ (Figure 1.11)

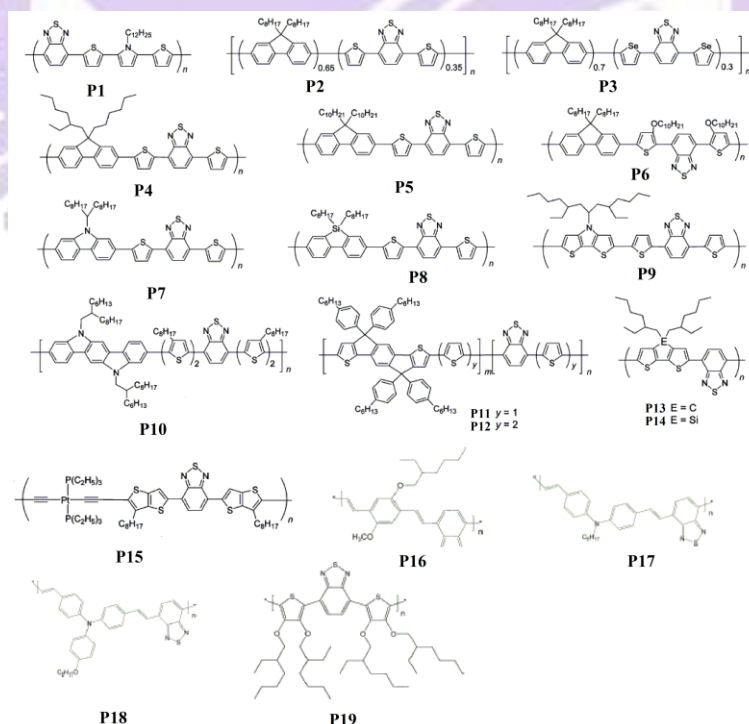


Figure 1.11 Chemical Structures of Benzothiadiazole-Containing Polymers

Copolymers of a dialkylated fluorene unit with a donor-acceptor-donor (DAD) group have been researched quite extensively in the past years. The fluorene unit provides a group which has a broad energy gap, which is stable and exhibits a high hole mobility, resulting in high values for Voc and moderate to good fill factors. The performance of solar cells fabricated with these materials is, depending on the material and conditions used, moderate to excellent with some cell achieving efficiencies of 2.8%.⁴⁸⁻⁵¹ (figure 1.12)

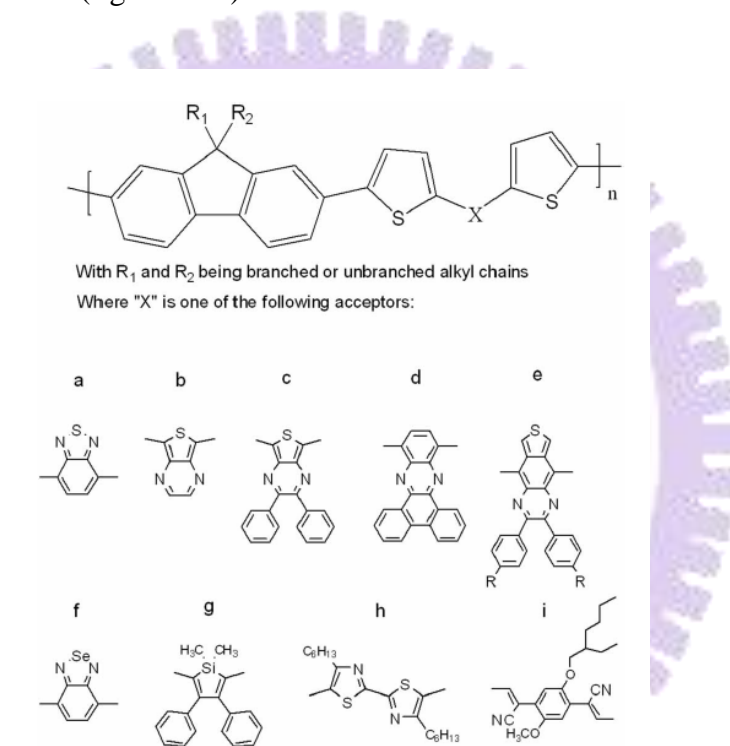


Figure 1.12 General structure of the fluorene copolymers with a variety of acceptors. General structure of the fluorene copolymers with a variety of acceptors.

The phenothiazine moiety with its electron-rich sulfur and a nitrogen heteroatom incorporated into the donor-acceptor conjugated polymer can potentially serve as the donor segment in BHJ solar cells and improve their hole-transporting abilities.⁵²⁻⁵⁵ (figure 1.13)

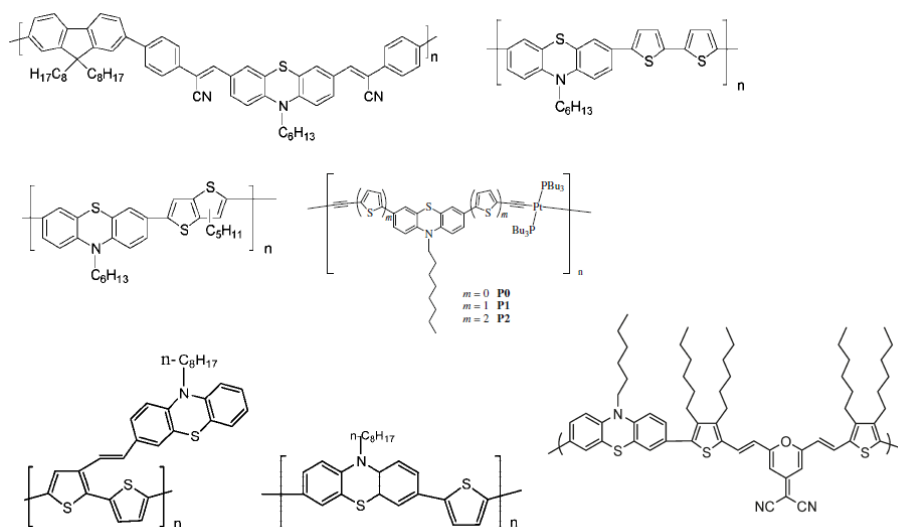


Figure 1.13 General structure of the phenothiazine containing copolymers.

One of the important developments in the solar cell materials are the conjugated polymers containing an alkylated carbazole. These polymers can be regarded as a relative of the family of dialkylated polyfluorene polymers containing a donor-acceptor-donor group (Figure 1.14). The main reasons for using a carbazole unit over a fluorene unit is that they are reported to have better hole transporting properties with respect to the fluorene unit, while maintaining the stability. Efficiencies up to 5.6% have been reported matching the performance of P3HT based solar cells leading to V_{oc} values of 0.97 V.⁵⁶

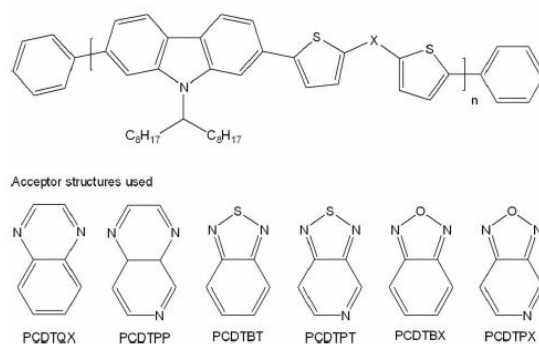


Figure 1.14 Structure of the carbazole copolymers with a variety of acceptors.

Low bandgap diketopyrrolopyrrole based copolymers have been recently synthesized by alternating electron-rich and electron-deficient units. These polymers (Figure 1.15) have proved to exhibit excellent ambipolar charge transport properties (hole and electron mobilities up to $0.1 \text{ cm}^2 \text{ V}^{-1} \text{ s}^{-1}$) and the power conversion efficiency (PCE) goes up to 4.0%.⁵⁷⁻⁵⁸

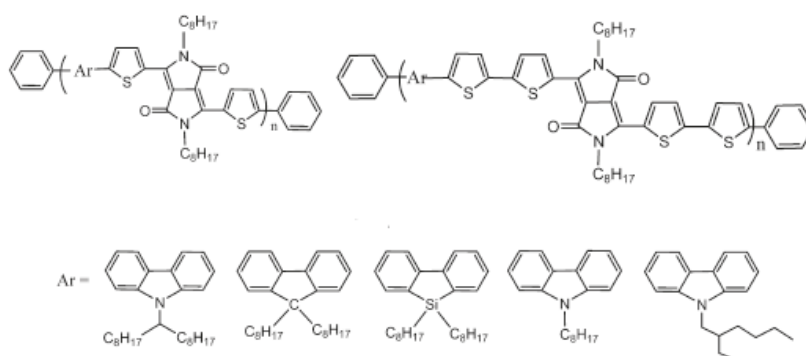


Figure 1.15 Structure of the diketopyrrolopyrrole containing copolymers with a variety of donors.

LBG polymers containing electron donating moieties from the 2,2'-bithiophene unit covalently bridged with an atom, such as C, N, S, and Si at 3,3'-position, have attracted considerable research attentions. The bridging atoms at 3,3'-position of donor moieties play an important role for LBG polymers in terms of solubility, planarity, band gap, and interchain packing, as well as for the performance of the BHJ solar cells.⁵⁹ As compared with polythiophene and polyfluorene derivatives, LBG polymers based on these donor moieties showed relatively high conductivities due to more extensive π -conjugation lengths, narrow band gaps, high planarities, and strong intermolecular π - π interactions of donor units.⁶⁰

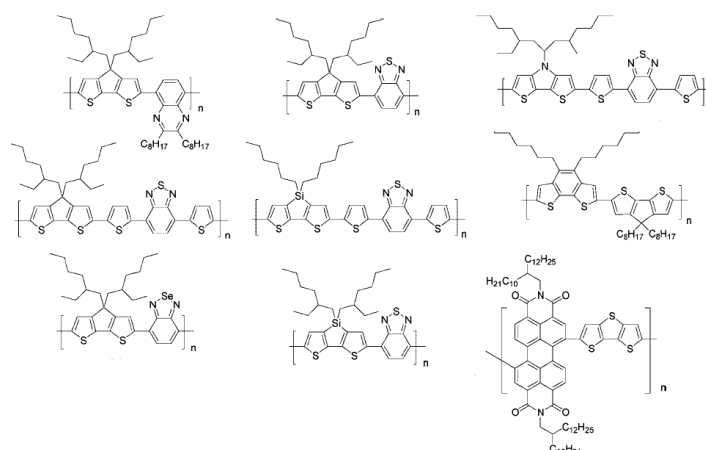


Figure 1.16 Structure of the polymers containing donating moieties from the 2,2'-bithiophene unit covalently bridged with an atom at 3,3'-position.

Following the development of the bulk heterojunction structure, recent years have seen a dramatic improvement in the efficiency of polymer solar cells. Maximizing the open-circuit voltage in a low-bandgap polymer is one of the critical factors towards enabling high-efficiency solar cells. Study of the relation between open-circuit voltage and the energy levels of the donor/acceptor in bulk heterojunction polymer solar cells has stimulated interest in modifying the open-circuit voltage by tuning the energy levels of polymers. Recently, by tuning the open-circuit voltage of polymer solar cells based on the structure of a low-bandgap polymer, PBDTTT (Figure 1.17), yielded power conversion efficiency as high as 7.7%, as certified by the National Renewable Energy Laboratory.⁶¹

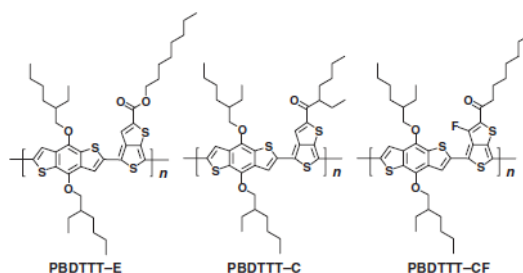


Figure 1.17 Chemical structure of PBDTTT-E, PBDTTT-C and PBDTTT-CF.

1.3.5 Conjugated Polyelectrolytes for Solar Cells

Motivations for examining the potential incorporation of conjugated polyelectrolytes into solar cell development include their easy processability, their ability to be used in layer by layer (LBL) processing, and the fact that their applications in a variety of chemical and sensory schemes have shown that they are efficiently quenched by electron acceptors. Due to the success in solar cells by increasing the donor/ acceptor interfacial area, it is not surprising that the LBL approach, and its multilayer heterostructure, has been of great interest. Some of such conjugated polyelectrolytes utilized in the polymer solar cells are depicted in figure 1.18

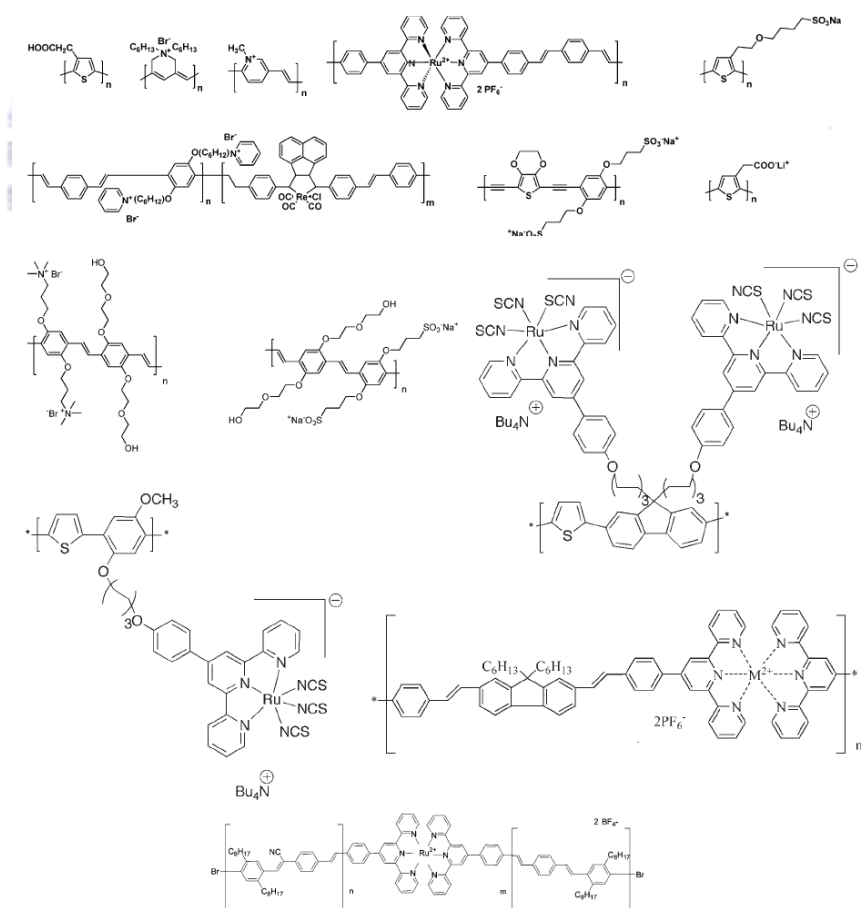


Figure 1.18 Structure of the conjugated polyelectrolytes used in solar cells.⁶²⁻⁶⁷

1.3.6 Characterization of Active Materials for Polymer Solar Cells.

The molecular design of D/A pairs for high efficiency PSC has to meet a lot of optoelectronic requirements, other than an excellent processability from solution, very high chemical purity, etc. To this end, an extensive characterization of the newly synthesized materials is required, involving multidisciplinary expertise (Figure 1.19), to assess their potentials as promising donors or acceptors for polymer solar cells. Chemists are making a great effort in the direction of energy level engineering and a variety of fullerene derivatives and p-type conjugated polymers (vide infra) have been proposed as functional materials toward high efficiency PSC.

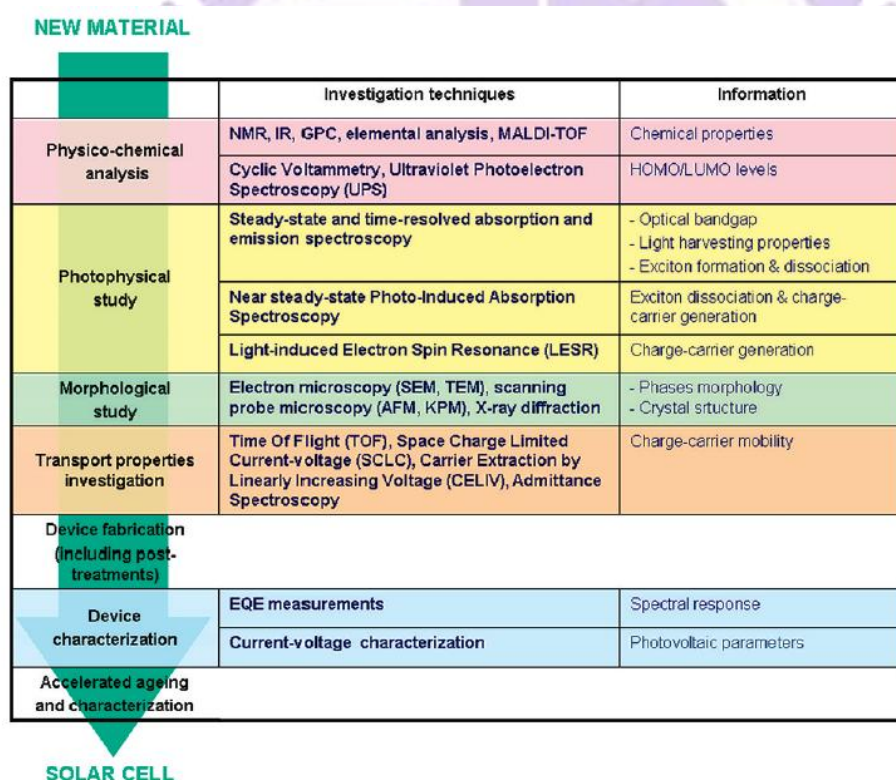


Figure 1.19 Nonexhaustive list of investigation techniques required for an extended characterization of active materials for polymer solar cells.⁶⁸

1.4 Motivation

The main objective of this dissertation is to construct the donor-acceptor polymer or metallo-polymer architectures by incorporating various donors and acceptors and to study their performance in polymer bulk heterojunction solar cells as electron donors with fullerene derivatives as electron acceptors. Addition of electron-withdrawing imine nitrogen to a conjugated polymer backbone generally enhances its electron-accepting properties and makes it susceptible to n-doping. Benzodiazole units are, in that sense, typical examples of such units containing imine nitrogen,⁵⁶ which have been widely used electron acceptors for the synthesis of D-A polymers. For example, copolymers of benzodiazole with variety of donors such as, fluorene,⁴⁹ silafluorene,⁸⁶ carbazole,⁵⁶ dithienosilole,⁸⁷ dithienocyclopentadiene,²⁶ and dithieno[3,2-b:2',3'-d]pyrroles⁸⁸ were synthesized and applied to PSCs, yielding PCE values in the range of 0.18-5.4%. Recently, many LBG copolymers have been synthesized by sandwiching acceptors in the midst of two thiophene units to alleviate the severe steric hindrance between the electron donors and acceptors, resulting in more planar structures to facilitate inter-chain associations and improve the hole mobilities of the LBG polymers. Among all heterocyclic donors, phenothiazine contains both electron-rich sulfur and nitrogen heteroatoms. The electron-rich nature of phenothiazine contributes for the efficient electron donor and hole transporting materials in polymers. In order to have better photophysical, electrochemical, and photovoltaic properties in the polymers, we incorporated of phenothiazine donor units with various benzodiazole acceptors (such as benzothiadiazole, benzoselenodiazole, and benzoxadiazole units) sandwiched between two hexyl thiophene units to form alternating conjugated donor-acceptor polymers. These polymers were synthesized by palladium(0)-catalysed Suzuki coupling reactions. The effects of donor-acceptor

strengths on the electronic and optoelectronic properties of the LBG polymers were also investigated. In addition, the PSC devices fabricated by polymer/PC₆₁BM or polymer/PC₇₁BM blends sandwiched between a transparent anode (ITO/PEDOT:PSS) and a cathode (Ca) were explored.

LBG polymers containing electron donating moieties from 2,2'-bithiophene unit covalently bridged with an atom, such as C, N, S, and Si, at 3,3'-position have attracted considerable research attentions. The bridging atoms at 3,3'-position of donor moieties play an important role for LBG polymers in terms of solubility, planarity, band gap, and interchain packing, as well as for the performance of the bulk heterojunction (BHJ) solar cells.⁵⁹ As compared with polythiophene and polyfluorene derivatives, LBG polymers based on these donor moieties showed relatively high conductivities due to more extensive π -conjugation lengths, narrow band gaps, high planarities, and strong intermolecular π - π interactions of donor units.¹⁰⁵⁻¹⁰⁶ Again, To obtain the broad absorption bands with high absorptivities, electron-donating groups and/or electron-withdrawing groups are substituted on the main-chains of the conjugated polymers to raise the HOMO levels and/or to reduce the LUMO levels of the polymers.¹⁰⁷⁻¹⁰⁸ Hence, introduction of electron-withdrawing cyano-vinylene groups to polymer backbones to lower the LUMO levels,¹⁰⁹ tune their electro-optical properties,¹¹⁰ and enhance the electrochemical stabilities of the polymers¹¹¹ are desirable for optoelectronic device applications. Moreover, LBG polymers containing electron-accepting cyano-vinylene groups were proven to possess higher hole mobilities,¹¹² and were applied as photovoltaic materials in BHJ solar cells.¹¹³⁻¹¹⁶ However, the PCE values of these photovoltaic cells are still low at present. All these research results inspire further development in exploring cyclopentadithiophene- and dithienosilole- derivatives with cyano-vinylene cgroups for the better photophysical,

electrochemical, and photovoltaic properties. Based on this concept, soluble cyclopentadithiophene- and dithienosilole-based LBG D-A polymers (**CPDT-CN**, **DTS-CN**) containing β -cyano-thiophenevinylene groups are designed and synthesized. The effects of the bridged atoms on the optical, electrochemical, charge transporting and photovoltaic properties of the polymers are compared and reported also in this study.

Nowadays, some terpyridyl Ru(II) complexes have attracted researchers to use in the applications of photovoltaic cells (PVC).^{62-65,147-150} The insertion of ruthenium metals into conjugated backbones has several advantages, such as to facilitate the charge generation by extending its absorption range due to its characteristic long-lived metal to ligand charge transfer (MLCT) transition¹³⁶ and to exhibit a reversible Ru^{II,III} redox process along with some ligand-centered redox processes. Motivations for examining the potential incorporation of such conjugated polyelectrolytes into solar cell development include the easy processability, layer-by-layer (LBL) processing capability, and also due to efficiently quenched by electron acceptors. But PCE values of these devices were limited either by the low open-circuit voltage (V_{oc}) or low short circuit current (J_{sc}). Due to relatively high HOMO levels and less sensitization ranges in all reported polymers, there were inefficient photocurrents generated which probably affected their PCE values. One of the feasible solutions to conquer these problems, i.e. to get a higher V_{oc} value and a more favorable overlap of the absorption spectra from both active layer and solar emission, is to introduce electron donor-acceptor structures to the cores of bis-terpyridyl ligands. The incorporation of the thiophene donor units with benzodiazole acceptor units at the cores of bis-terpyridyl ligands in Ru^{II}-containing metallo-polymers to have better photophysical, electrochemical,

and photovoltaic properties are very intriguing us. So, we design, synthesis, properties, and device applications of Ru^{II}-containing metallo-polymers containing donor-acceptor (D-A) bis-terpyridyl ligands bearing different benzodiazole acceptors, including benzothiadiazole, benzoselenodiazole, and benzoxadiazole cores sandwiched between symmetrical thiophene and terpyridyl units. The effects of their donor-acceptor strengths on the electronic and optoelectronic properties were also investigated. In addition, the PVC devices fabricated by these bis-terpyridyl ligands and metallo-polymers with [6,6]-phenyl-C₆₁-butyric acid methyl ester (PCBM) inserted between a transparent anode (ITO/PEDOT:PSS) and a cathode (Ca) were explored.



Chapter 2.

Synthesis and Applications of Low-Bandgap Conjugated Polymers Containing Phenothiazine Donor and Various Benzodiazole Acceptors for Polymer Solar Cells

2.1 Introduction

In spite of poor long-term stability, polymer solar cell (PSC) devices based on conjugated polymers as electron donors and fullerene derivatives as electron acceptors are of broad interests because of the advantages of low cost, light-weight flexible devices, tunable electronic properties, and ease of processing for the conversion of solar energy to electricity.^{9-10,21,69} Although poly(3-hexylthiophene) (P3HT) is proven to be one of the most efficient donor materials ever tested in PSCs for giving the power conversion efficiency (PCE) up to 5%,³⁷⁻⁴⁷ further enhanced PCE values are limited due to both lower photocurrent generation and intrinsic absorption properties. In order to conquer these problems, low-bandgap (LBG) polymers composed of electron-rich (donor) and electron-deficient (acceptor) units have been utilized recently in PSCs with fullerene derivatives, such as [6,6]-phenyl-C₆₁-butyric acid methyl ester (PC₆₁BM) or [6, 6]-phenyl-C₇₁-butyric acid methyl ester (PC₇₁BM), yielding a power conversion efficiency (PCE) value up to 7.7%.^{61,70-74} Polymer solar cells consisting of such donor-acceptor (D-A) LBG polymers have attracted more attention owing to their tunable optical, electrochemical, electronic, and photovoltaic properties.²³⁻²⁴ Incorporation of wide ranges of donors and acceptors into LBG polymers can manipulate the electronic structures, i.e., the highest occupied molecular orbital (HOMO) and lowest unoccupied molecular orbital (LUMO) levels through the partial intramolecular charge transfer (ICT) in the D-A systems.⁷⁵⁻⁷⁶ By optimizing materials and device structures, photovoltaic parameters, such as the short-circuit

current (J_{sc}) and open-circuit voltage (V_{oc}), can be further improved to obtain higher PCE values in the PSCs. In solar cell devices, J_{sc} is determined by the creation and subsequent dissociation of excitons at the polymer/acceptor interface followed by transport of free charge carriers towards the collecting electrodes,⁷⁷ V_{oc} is primarily determined by the effective band gap of the bulk hetero-junction (BHJ) film.⁷⁸ For this purpose, the electron donor polymer should exhibit a band gap between 1.2 and 1.9 eV, which corresponds to a HOMO energy level between -5.8 and -5.2 eV and a LUMO energy level between -4.0 and -3.8 eV.³¹ Again, if the energy difference between the LUMO levels of polymer and acceptor is less than 0.3 eV,³² the driving force for charge separation will be reduced, and V_{oc} can be reduced by raising the HOMO level. Consequently, it is of great importance to match the energy levels of the polymer and acceptor carefully to develop BHJ solar cells with high efficiencies.

Among all heterocyclic compounds, phenothiazine contains both electron-rich sulfur and nitrogen heteroatoms. The electron-rich nature of phenothiazine contributes for the efficient electron donor and hole transporting materials in polymers and organic molecules for photo-induced charge separation and it has been also proven as a superior electron donor for reductive quenching.⁷⁹ Due to their unique electro-optical properties, these materials are potential candidates for diverse applications for light-emitting diodes,⁸⁰⁻⁸¹ solar cells, chemiluminescence devices,⁸²⁻⁸³ and organic field effect transistors.⁸⁴ Phenothiazine ring hampers stacking aggregation and intermolecular excimer formation in the main chain of the polymer due to its non-planar structure.⁸⁵ However, till now only a limited number of phenothiazine-based polymers for photovoltaic devices have been explored.⁵²⁻⁵⁵

Addition of electron-withdrawing imine nitrogen to a conjugated polymer backbone generally enhances its electron-accepting properties and makes it susceptible

to n-doping (reduction). Benzodiazole units are, in that sense, typical examples of such units containing imine nitrogen.⁵⁶ 2,1,3-Benzothiadiazole is a widely used electron acceptor for the synthesis of D-A polymers. For example, copolymers of benzothiadiazole with fluorene,⁴⁹ silafluorene,⁸⁶ carbazole,⁵⁶ dithienosilole,⁸⁷ dithienocyclopentadiene,²⁶ and dithieno[3,2-*b*:2',3'-*d*]pyrroles⁸⁸ were synthesized and applied to PSCs, yielding PCE values in the range of 0.18-5.4%. Recently, many photovoltaic papers have reported LBG copolymers made of electron donors and acceptors sandwiched between two thiophene units.^{26,49,56,87-88} Incorporation of acceptor units in the midst of two thiophene units, alleviate the severe steric hindrance between the electron donors and acceptors, resulting in more planar structures to facilitate inter-chain associations and improve the hole mobilities of the LBG polymers. Despite of these advantages, addition of thiophene units could induce solubility problems and yield low molecular weights in polymers.⁸⁹ To utilize the aforementioned merits of thiophene units, structural modifications, such as incorporation of alkyl or alkoxy chains on the 3- and/or 4-position of thienyl units⁹⁰ or addition of supplementary alkylated thiophene units,⁹¹ have been outfitted to acquire higher molecular weights and better solubilities than the original polymers without any soluble side-chains.

In order to have better photophysical, electrochemical, and photovoltaic properties in the resulting LBG polymers, the incorporation of phenothiazine donor units with various acceptor units are very intriguing and thus to motivate this study. Herein, we report the design, synthesis, properties, and device applications of phenothiazine-based alternating conjugated donor-acceptor polymers, in which the acceptor benzodiazole units include benzothiadiazole, benzoselenodiazole, and benzoxadiazole sandwiched between two hexyl thiophene units. These polymers were

synthesized by palladium(0)-catalysed Suzuki coupling reactions. The effects of donor-acceptor strengths on the electronic and optoelectronic properties of the LBG polymers were also investigated. In addition, the PSC devices fabricated by polymer/PC₆₁BM or polymer/PC₇₁BM blends sandwiched between a transparent anode (ITO/PEDOT:PSS) and a cathode (Ca) were explored.

2.2 Experimental Section

2.2.1 Materials

All chemicals and solvents were reagent grades and purchased from Aldrich, ACROS, Fluka, TCI, TEDIA, and Lancaster Chemical Co. Toluene, tetrahydrofuran, and diethyl ether were distilled over sodium/benzophenone to keep anhydrous before use. Chloroform (CHCl₃) was purified by refluxing with calcium hydride and then distilled. If not otherwise specified, the other solvents were degassed by nitrogen 1 h prior to use.

2.2.2 Measurements and Characterization

¹H NMR and ¹³C NMR spectra were recorded on a Varian Unity 300 MHz spectrometer using CDCl₃ solvent. Elemental analyses were performed on a HERAEUS CHN-OS RAPID elemental analyzer. Thermogravimetric Analyses (TGA) were conducted with a TA Instruments Q500 at a heating rate of 10 °C/min under nitrogen. The molecular weights of polymers were measured by gel permeation chromatography (GPC) using Waters 1515 separation module (concentration = 1 mg/mL in THF; flow rate = 1 mL/min), and polystyrene was used as a standard with THF as an eluant. UV-visible absorption spectra were recorded in dilute chlorobenzene solutions (10⁻⁵ M) as well as on solid films (spin-coated with a spin rate ca. 1000 rpm for 60 s on glass substrates from chlorobenzene solutions with a

concentration of 10 mg/mL) on a HP G1103A. Cyclic voltammetry (CV) measurements were performed using a BAS 100 electrochemical analyzer with a standard three-electrode electrochemical cell in a 0.1 M solution of tetrabutylammonium hexafluorophosphate ((TBA)PF₆) in acetonitrile at room temperature with a scanning rate of 100 mV/s. During the CV measurements, the solutions were purged with nitrogen for 30 s. In each case, a carbon working electrode coated with a thin layer of polymers, a platinum wire as the counter electrode, and a silver wire as the quasi-reference electrode were used, and Ag/AgCl (3 M KCl) electrode was served as a reference electrode for all potentials quoted herein. The redox couple of ferrocene/ferrocenium ion (Fc/Fc⁺) was used as an external standard. The onset potentials were determined from the intersections of two tangents drawn at the rising currents and background currents of the cyclic voltammetry (CV) measurements. Surface morphology images of thin films (on glass substrates) were obtained using atomic force microscopy (AFM, Digital instrument NS 3a controller with D3100 stage).

2.2.3 Device Fabrication of Polymer Solar Cells.

The polymer solar cells in this study were composed of an active layer of blended polymers (Polymer: PCBM) in solid films, which was sandwiched between a transparent indium tin oxide (ITO) anode and a metal cathode (Ca). Prior to the device fabrication, ITO-coated glass substrates (1.5×1.5 cm²) were ultrasonically cleaned in detergent, deionized water, acetone, and isopropyl alcohol. After routine solvent cleaning, the substrates were treated with UV ozone for 15 min. Then a modified ITO surface was obtained by spin-coating a layer of poly(ethylene dioxythiophene): polystyrenesulfonate (PEDOT:PSS) (~30 nm). After baking at 130 °C for one hour, the substrates were transferred to a nitrogen-filled glovebox.

Then, on the top of PEDOT:PSS layer, an active layer was prepared by spin coating from blended solutions of polymers:PC₆₁BM (with 1:1 w/w) and **PP6DHTBT**:PC₇₁BM (with 1:1, 1:3, and 1:4 w/w) subsequently with a spin rate ca. 1500 rpm for 60 s, and the thickness of the active layer was typically ca. 80 nm. Initially, the blended solutions were prepared by dissolving both polymers and PCBM in 1,2-dichlorobenzene (20 mg/mL), followed by continuous stirring for 12 h at 50 °C. In the slow-growth approach, blended polymers in solid films were kept in the liquid phase after spin-coating by using the solvent with a high boiling point. Finally, a calcium layer (30 nm) and a subsequent aluminum layer (100 nm) were thermally evaporated through a shadow mask at a pressure below 6×10^{-6} Torr. The active area of the device was 0.12 cm². All PSC devices were prepared and measured under ambient conditions. The solar cell testing was done inside a glove box under simulated AM 1.5G irradiation (100 mW/cm²) using a Xenon lamp based solar simulator (Thermal Oriel 1000W). The light intensity was calibrated by a mono-silicon photodiode with KG-5 color filter (Hamamatsu, Inc.). The external quantum efficiency (EQE) action spectrum was obtained at short-circuit condition. The light source was a 450 W Xe lamp (Oriel Instrument, model 6266) equipped with a water-based IR filter (Oriel Instrument, model 6123NS). The light output from the monochromator (Oriel Instrument, model 74100) was focused onto the photovoltaic cell under test.

2.2.4 Synthesis of Monomers and Polymers

General Synthetic Procedures for 4a-4c

In a 100 mL flame-dried two-neck flask fitted with a condenser, 1.00 eq of dibromoarene (**3a-3c**), 2.2 eq of 2-(4-hexylthiophen-2-yl)-4,4,5,5-tetramethyl-

1,3,2-dioxaborolane (**2**), and 0.03 eq. of tetrakis(triphenylphosphine)palladium was added. The mixture was degassed and purged nitrogen. Afterward, 40 mL of anhydrous toluene and 2 M aqueous potassium carbonate solution (8 mL) was added. The reaction mixture was heated to 90 °C with vigorous stirring until reaction completion by TLC analyses (~ 24 h). The mixture was poured into water (100 mL) and extracted with methylene chloride. The organic layer was washed thrice with water, once with brine and dried over magnesium sulfate. The solvent was evaporated and the residue was purified by column chromatography on silica gel with hexane/ethyl acetate = 20/1 to give the products. Their chemical characterization analyses are shown as follows:

4,7-bis(4-hexylthiophen-2-yl)-2,1,3-benzothiadiazole (4a) Orange needles (yield: 88%); mp 75-77 °C. ¹H NMR (ppm, CDCl₃): δ 7.97 (dd, 2H), 7.82 (d, *J*=1.8 Hz, 2H), 7.04 (dd, 2H), 2.66 (t, *J*=7.5 Hz, 4H), 1.70 (m, 4H), 1.25-1.53 (m, 12H), 0.90 (t, *J*=6.7 Hz, 6H). ¹³C NMR (ppm, CDCl₃): δ 153.02, 139.75, 128.42, 127.90, 127.21, 126.38, 126.15, 31.68, 29.70, 29.65, 29.03, 22.67, 14.14.

4,7-bis(4-hexylthiophen-2-yl)-2,1,3-benzoselenadiazole (4b) Purple solid (yield: 87%); mp 82-83 °C. ¹H NMR (ppm, CDCl₃): δ 7.87 (d, *J*= 1.2 Hz, 2H), 7.71 (s, 2H), 7.04 (d, *J*=1.5 Hz, 2H), 2.68 (t, *J*=7.8 Hz, 4H), 1.68 (m, 4H), 1.20-1.43 (m, 12H), 0.90 (t, *J*=6.9 Hz, 6H). ¹³C NMR (ppm, CDCl₃): δ 158.19, 143.98, 139.29, 128.87, 127.42, 125.75, 121.83, 31.68, 30.56, 30.45, 29.04, 22.62, 14.10.

4,7-bis(4-hexylthiophen-2-yl)-2,1,3-benzoxadiazole (4c) Yellow solid (yield: 92%); mp 78-79 °C. ¹H NMR (ppm, CDCl₃): δ 7.95 (d, *J*= 1.2 Hz, 2H), 7.57 (s, 2H), 7.02 (d, *J*=1.2 Hz, 2H), 2.67 (t, *J*=7.6 Hz, 4H), 1.70 (m, 4H), 1.20-1.43 (m, 12H), 0.89

(t, $J=7.2$ Hz, 6H). ^{13}C NMR (ppm, CDCl_3): δ 148.081, 145.28, 137.77, 30.40, 126.32, 122.31, 121.88, 31.90, 30.83, 30.65, 29.24, 22.85, 14.34.

General Bromination Procedures for 5a-5c

In a 100 mL flask, 1.00 eq of 4,7-di(4-hexyl-2-thienyl)-arene (**4a-4c**) was added into THF under nitrogen flow. After solids were dissolved completely, 2.10 eq *N*-bromosuccinimide (NBS) was added in portion wise. The reaction mixtures were stirred at a room temperature for 5 h. Subsequently, hexane was added into the mixture, and the white precipitate formed was filtered off. In addition, the filtrate was extracted with ethyl acetate, and the organic layer was washed with brine followed by being dried over anhydrous sodium sulfate. After that, the residue was purified by column chromatography on silica gel with hexane/methylene chloride = 1/2 to give the products. Their chemical characterization analyses are shown as follows:

4,7-Bis(5-bromo-4-hexyl-2-thienyl)-2,1,3-benzothiadiazole (5a) Red solid (yield: 94%); mp 101-103 °C. ^1H NMR (ppm, CDCl_3): δ 7.75 (s, 2H), 7.71 (s, 2H), 2.63 (t, $J=7.2$ Hz, 4H), 1.67 (m, 4H), 1.33-1.40 (m, 12H), 0.89 (t, $J=7.1$ Hz, 6H). ^{13}C NMR (ppm, CDCl_3): δ 152.19, 143.01, 138.46, 128.03, 125.25, 124.80, 111.59, 31.62, 29.74, 29.67, 28.96, 22.64, 14.11. Element Anal. Calcd for $\text{C}_{26}\text{H}_{30}\text{Br}_2\text{N}_2\text{S}_3$: C, 49.84%; H, 4.83%; N, 4.47%; Found: C, 49.62%; H, 5.02%; N, 4.62%. EIMS (m/z): calcd for $\text{C}_{26}\text{H}_{30}\text{Br}_2\text{N}_2\text{S}_3$, 626.53; found, 626.

4,7-Bis(5-bromo-4-hexyl-2-thienyl)-2,1,3-benzoselenadiazole (5b) Purple solid (yield: 96%); mp 92-94 °C. ^1H NMR (ppm, CDCl_3): δ 7.65 (s, 2H), 7.64 (s, 2H), 2.62 (t, $J=7.2$ Hz, 4H), 1.67 (m, 4H), 1.33-1.42 (m, 12H), 0.90 (t, $J=6.9$ Hz, 6H). (ppm, CDCl_3): δ 157.71, 142.62, 138.73, 127.63, 126.75, 124.93, 112.19, 31.62, 29.74, 29.67, 28.96, 22.64, 14.11. Element Anal. Calcd for $\text{C}_{26}\text{H}_{30}\text{Br}_2\text{N}_2\text{S}_2\text{Se}$: C, 46.37%; H,

4.49%; N, 4.16. Found: C, 46.78%; H, 5.14%; N, 4.33%. EIMS (m/z): calcd for $C_{26}H_{30}Br_2N_2S_3$, 673.43; found, 674.

4,7-Bis(5-bromo-4-hexyl-2-thienyl)-2,1,3-benzoxadiazole (5c) Orange solid (yield: 93%); mp 108-110 °C. 1H NMR (ppm, $CDCl_3$): δ 7.77 (s, 2H), 7.38 (s, 2H), 2.60 (t, $J=7.2$ Hz, 4H), 1.62 (m, 4H), 1.33-1.42 (m, 12H), 0.90 (t, $J=6.9$ Hz, 6H). ^{13}C NMR (ppm, $CDCl_3$): δ 147.42, 143.88, 137.08, 129.71, 125.68, 121.35, 111.56, 31.59, 29.66, 29.64, 28.94, 22.60, 14.10. Element Anal. Calcd for $C_{26}H_{30}Br_2N_2OS_2$: C, 51.15%; H, 4.95%; N, 4.59%. Found: C, 51.30%; H, 5.52%; N, 4.27%. EIMS (m/z): calcd for $C_{26}H_{30}Br_2N_2S_3$, 610.47; found, 610.

10-hexyl-3,7-bis(4,4,5,5-tetramethyl-1,3,2-dioxaborolan-2-yl)-10H-phenothiazine (7) A solution of 3,7-dibromo-10-hexyl-10H-phenothiazine (4.41 g, 10 mmol) in anhydrous tetrahydrofuran (100 mL) was cooled to -78 °C under nitrogen and stirred at this temperature for 5 min in the flame-dried two-neck round-bottom flask. *n*-Butyl lithium (8.4 mL of 2.5 M solution in hexane, 21 mmol) was added dropwise, using a syringe, and the mixture was stirred at -78 °C, warmed to 0 °C for 15 min, and cooled again at -78 °C for 15 min. 2-Isopropoxy-4,4,5,5-tetramethyl-1,3,2-dioxaborolane (6.13 mL, 30 mmol) was added rapidly to the solution, and the resulting mixture was warmed to room temperature and stirred overnight. The mixture was poured into water and extracted with ether. The organic extracts were washed with brine and dried over magnesium sulfate. The solvent was removed by rotary evaporation, and the residue was recrystallized from acetone to obtain 3.96 g (74%) of the title product as a slight yellow solid ; mp 212-214 °C. 1H NMR (ppm, $CDCl_3$): δ 7.54 (m, 4H), 6.80 (d, $J = 7.8$ Hz, 2H), 3.84 (t, $J = 6.9$ Hz, 2H), 1.78 (m, 2H), 1.4 (m, 2H), 1.32 (s, 24H), 1.25 (m, 4H), 0.86 (t, $J = 7.2$ Hz, 3H). ^{13}C NMR (ppm, $CDCl_3$): δ 147.47, 134.23, 133.97, 124.15, 114.90, 83.91, 47.71, 31.62, 26.89, 26.72, 25.06, 22.78, 14.21.

Element Anal. Calcd for C₃₀H₄₃B₂NO₄S: C, 67.31%; H, 8.10%, N, 2.62%. Found: C, 66.47%; H, 7.73% N, 2.93%. EIMS (m/z): calcd for C₃₀H₄₃B₂NO₄S, 535.35; found, 536.

General Polymerization Procedure

All polymerization steps were carried out through the palladium(0)-catalyzed Suzuki coupling reactions. In a 50 mL flame dried two-neck flask, 1 eq of 10-hexyl-3,7-bis(4,4,5,5-tetramethyl-1,3,2-dioxaborolan-2-yl)-10H-phenothiazine (**7**), 1 eq of bis(bromo-4-hexyl-2-thienyl) arene (**5a-5c**), and Pd(PPh₃)₄ (1.5 mol %) were dissolved in a mixture of toluene ([monomer] = 0.5 M) and aqueous 2 M Na₂CO₃ (2:3). The solution was first put under a nitrogen atmosphere and vigorously stirred at 90-95 °C for 4-5 days. After reaction completion, an excess of bromobenzene was added to the reaction then one hour later, excess of phenylboronic acid was added and the reaction refluxed overnight to complete the end-capping reaction. The polymer was purified by precipitation in methanol/water (10:1), filtered through 0.45 μm nylon filter and washed on Soxhlet apparatus using hexane, acetone and chloroform. The chloroform fraction was reduced to 40-50 mL under reduced pressure, precipitated in methanol/water (10:1, 500 mL), filtered through 0.45 μm nylon filter and finally air-dried overnight.

Poly[(10-hexyl-10H-phenothiazine-3,7-ylene)-alt-(4,7-bis(4-hexylthien-2-yl)-2,1,3-benzothiadiazole)2',2''-diyl] (PP6DHTBT) Dark orange solid (yield: 71%).
¹H NMR (ppm, CDCl₃): δ 8.02 (br, 2H), 7.84 (br, 2H), 7.32 (br, 4H), 6.93 (br, 2H), 3.92 (br, 2H), 2.74 (br, 4H), 1.88 (br, 2H), 1.72 (br, 4H), 1.50 (br, 4H), 1.18-1.40 (br, 14H), 0.81-0.90 (br, 9H). Anal. Calcd C, 70.45%; H, 6.85%, N, 5.60%. Found: C, 69.78%; H, 6.97% N, 5.42%.

Poly[(10-hexyl-10*H*-phenothiazine-3,7-ylene)-alt-(4,7-bis(4-hexylthien-2-yl)-2,1,3- benzoselenadiazole)2',2''-diyl] (PP6DHTBSe) Dark black solid (yield: 76%).
¹H NMR (ppm, CDCl₃): δ 7.92 (br, 2H), 7.77 (br, 2H), 7.32 (br, 4H), 6.94 (br, 2H), 3.92 (br, 2H), 2.74 (br, 4H), 1.88 (br, 2H), 1.71 (br, 4H), 1.50 (br, 4H), 1.18-1.40 (br, 14H), 0.81-0.90 (br, 9H). Anal. Calcd C, 66.30%; H, 6.45%, N, 5.27%. Found: C, 64.49%; H, 6.38% N, 4.94%.

Poly[(10-hexyl-10*H*-phenothiazine-3,7-ylene)-alt-(4,7-bis(4-hexylthien-2-yl)-2,1,3- benzoxadiazole)2',2''-diyl] (PP6DHTBX) Dark solid (yield: 69%). ¹H NMR (ppm, CDCl₃): δ 8.00 (br, 2H), 7.53 (br, 2H), 7.30 (br, 4H), 6.91 (br, 2H), 3.89 (br, 2H), 2.69 (br, 4H), 1.88 (br, 2H), 1.69 (br, 4H), 1.48 (br, 4H), 1.18-1.40 (br, 14H), 0.81-0.90 (br, 9H). Anal. Calcd C, 71.99%; H, 7.00%, N, 5.72%. Found: C, 72.00%; H, 6.84% N, 5.75%.

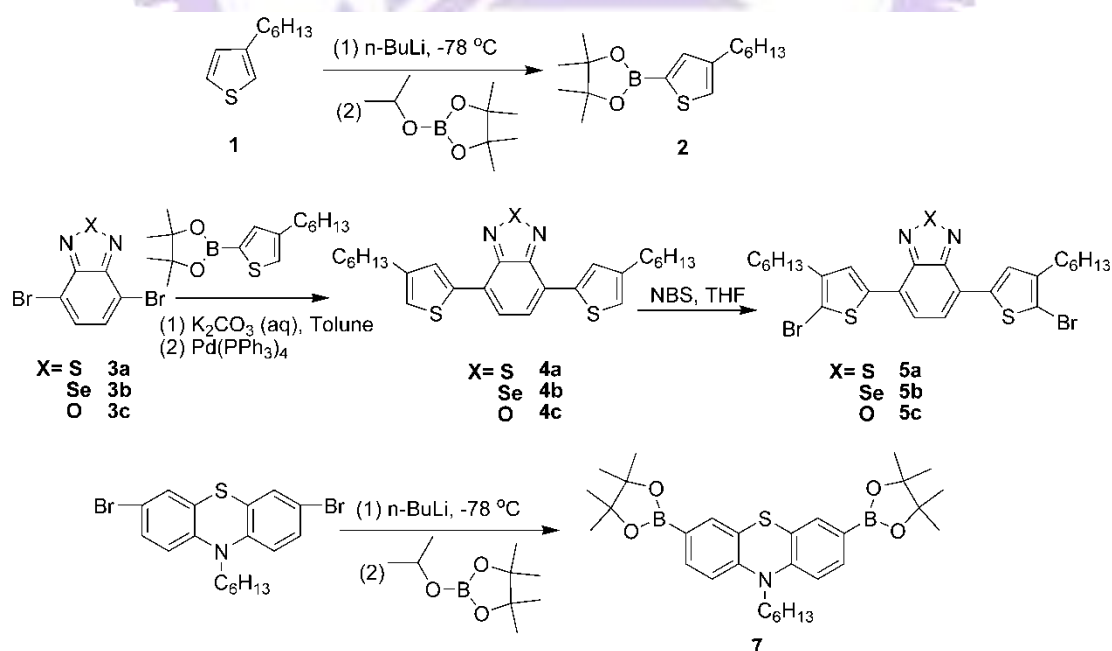


Figure 2.1 Synthetic Routes of Monomers (**5a-5c** and **7**).

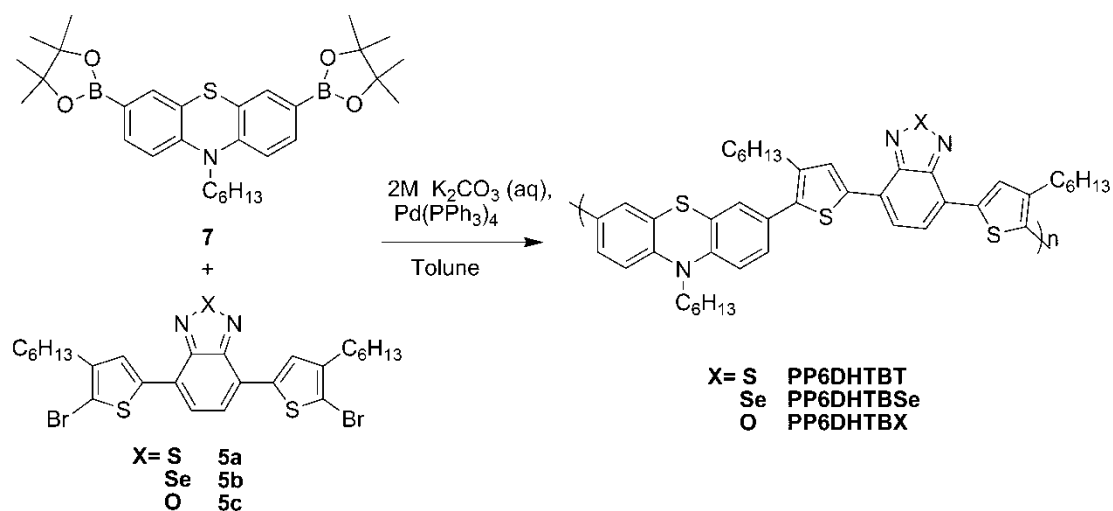


Figure 2.2 Synthetic Routes of Polymers (**PP6DHTBT**, **PP6DHTBSe**, and **PP6DHTBX**).

2.3 Results and Discussions

2.3.1 Synthesis and Structural Characterization

The general synthetic routes of monomers **5a-5c** and **7** are shown in Figure 2.1. Synthesis of 2-(4-hexylthiophen-2-yl)-4,4,5,5-tetramethyl-1,3,2-dioxaborolane (**2**), 4,7-dibromo-2,1,3-benzothiadiazole (**3a**), 4,7-dibromo-2,1,3-benzoselenadiazole (**3b**), and 4,7-dibromo-2,1,3-benzoxadiazole (**3c**) were prepared by following the literature procedures.^{56,92} Hexyl-thiophene units were added to both sides of each acceptor units through the Suzuki coupling reaction between 2-(4-hexylthiophen-2-yl)-4,4,5,5-tetramethyl-1,3,2-dioxaborolane (**2**) and dibromo arenes (**3a-3c**) in presence of a catalyst $\text{Pd(PPh}_3)_4$. Next, these compounds were brominated with NBS to produce monomers **5a-5c**. The diboronate ester monomer (**7**) was prepared according to the literature method,⁵⁴ i.e., alkylation of phenothiazine with 1-bromohexane, followed by bromination with molecular bromine, then lithiation of dibromo compound with *n*-Buli and quenching with 2-isopropoxy-4,4,5,5-tetramethyl-1,3,2-dioxaborolane produced monomer **7**.

Monomers (**5a-5c** and **7**) were satisfactorily characterized by ^1H NMR, ^{13}C NMR, MS spectroscopy, and elemental analyses. As shown in Figure 2.2, three alternating polymers **PP6DHTBT**, **PP6DHTBSe**, and **PP6DHTBX** were prepared with the well-known Suzuki polymerization between the diboronic ester of phenothiazine (**7**) and the dibromide monomers (**5a-5c**). The obtained polymers were further purified by washing on Soxhlet apparatus using hexane, acetone, and chloroform. The chloroform fraction was reduced to 40-50 mL under reduced pressure, precipitated in methanol, filtered through 0.45 μm nylon filters and finally dried under reduced pressure at room temperature. After purification and drying, all polymers were obtained as fibrous solids in overall good yields (69-76%). The chemical structures of the polymers were confirmed with ^1H NMR and elemental analysis. The ^1H NMR spectra of polymers are demonstrated in Figure 2.3, where the broadening signals of ^1H NMR spectra in both aromatic and aliphatic regions were observed as a result of polymerization. The polymers exhibited good solubilities in common organic solvents, such as THF, chloroform, toluene, and chlorobenzene at room temperature.

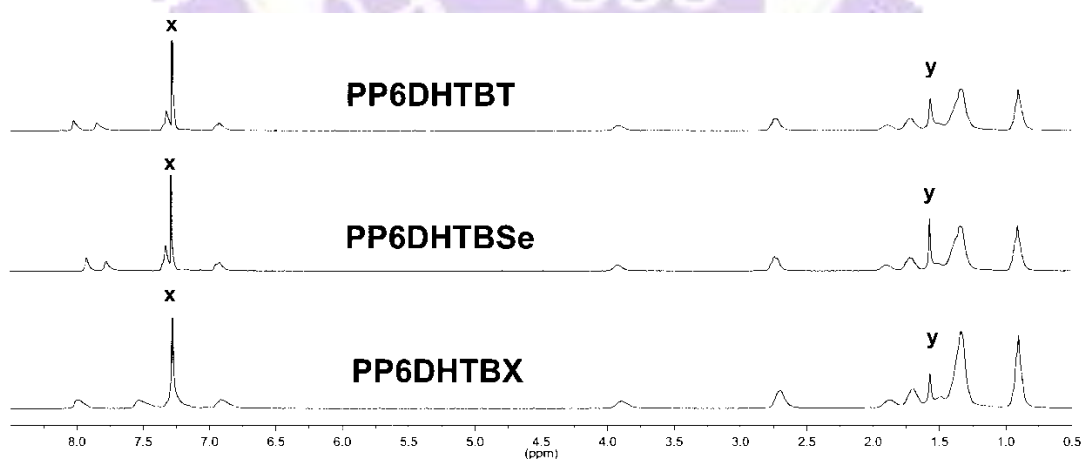


Figure 2.3 ^1H NMR spectra of polymers in CDCl_3 . Labels of x and y are CDCl_3 and H_2O , respectively.

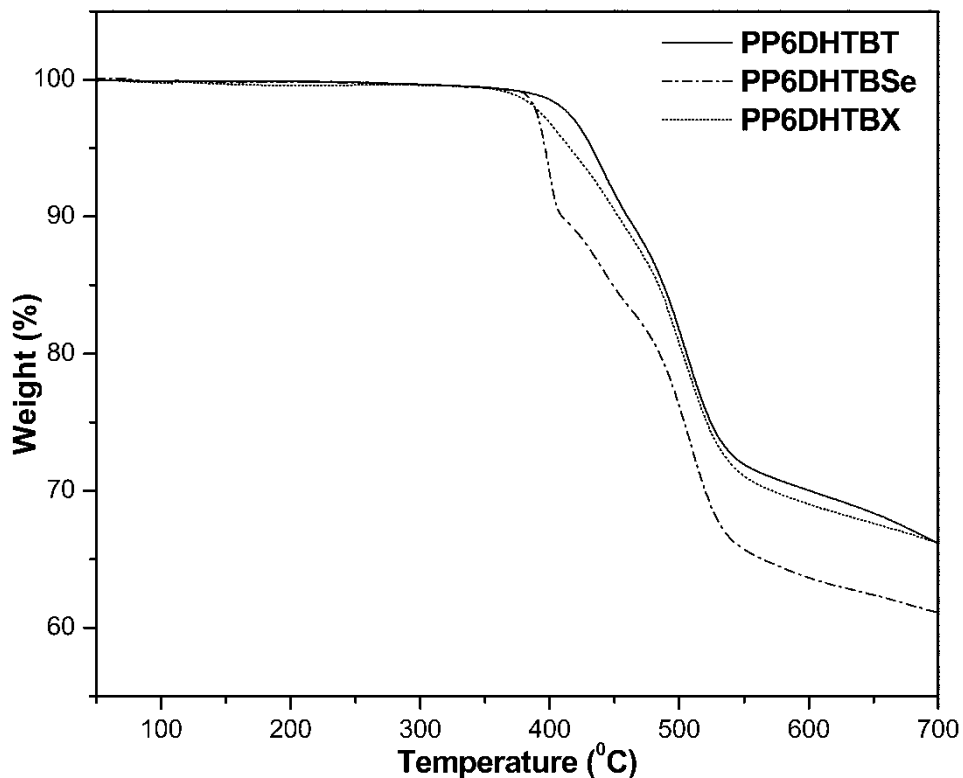


Figure 2.4 TGA thermograms of polymers.

Table 2.1 Molecular Weights and Thermal Properties of Polymers

Polymer	Yield (%)	M_n^a ($\times 10^4$)	M_w^a ($\times 10^4$)	PDI (M_w/M_n)	T_d^b (°C)
PP6DHTBT	71	4.07	7.54	1.85	434
PP6DHTBSe	76	5.13	10.17	1.98	401
PP6DHTBX	79	3.85	6.45	1.67	417

^aMolecular weights and polydispersity index (PDI) values were measured by GPC, using THF as an eluent, polystyrene as a standard. M_n , number average molecular weight. M_w , weight average molecular weight. ^bTemperature (°C) at 5% weight loss measured by TGA at a heating rate of 10 °C/min under nitrogen.

The molecular weights of the polymers were determined by gel permeation chromatography (GPC) against monodisperse polystyrene standards in THF are summarized in Table 2.1. These results show that reasonable molecular weights were obtained in these polymers, which had number-average molecular weights (M_n) ranging 38,500-51,300 and weight-average molecular weights (M_w) ranging 64,500-101,700, respectively, with polydispersity indices ($PDI = M_w/M_n$) ranging 1.67-1.98. The thermal properties of the polymers determined by thermogravimetric analysis (TGA) are shown in Figure 2.4 and summarized in Table 2.1. The TGA thermograms of the polymers revealed (5% weight loss) decomposition temperatures (T_d) in the range of 401-434 °C, indicative of excellent thermal stabilities.

Table 2.2 Optical Properties of Polymers

Polymer	Solution ^a			Solid Film ^b		
	$\lambda_{\max,abs}$	λ_{edge}	E_g^{opt}	$\lambda_{\max,abs}$	λ_{edge}	E_g^{opt}
	(nm)	(nm)	(eV) ^c	(nm)	(nm)	(eV) ^c
PP6DHTBT	337,515	607	2.04	347,552	642	1.93
PP6DHTBSe	349,552	656	1.89	358,582	689	1.80
PP6DHTBX	330,522	610	2.03	341,553	652	1.90

^aIn chlorobenzene dilute solution; ^bSpin coated from chlorobenzene solution; ^cThe optical bandgap was obtained from the equation $E_g = 1240/\lambda_{edge}$

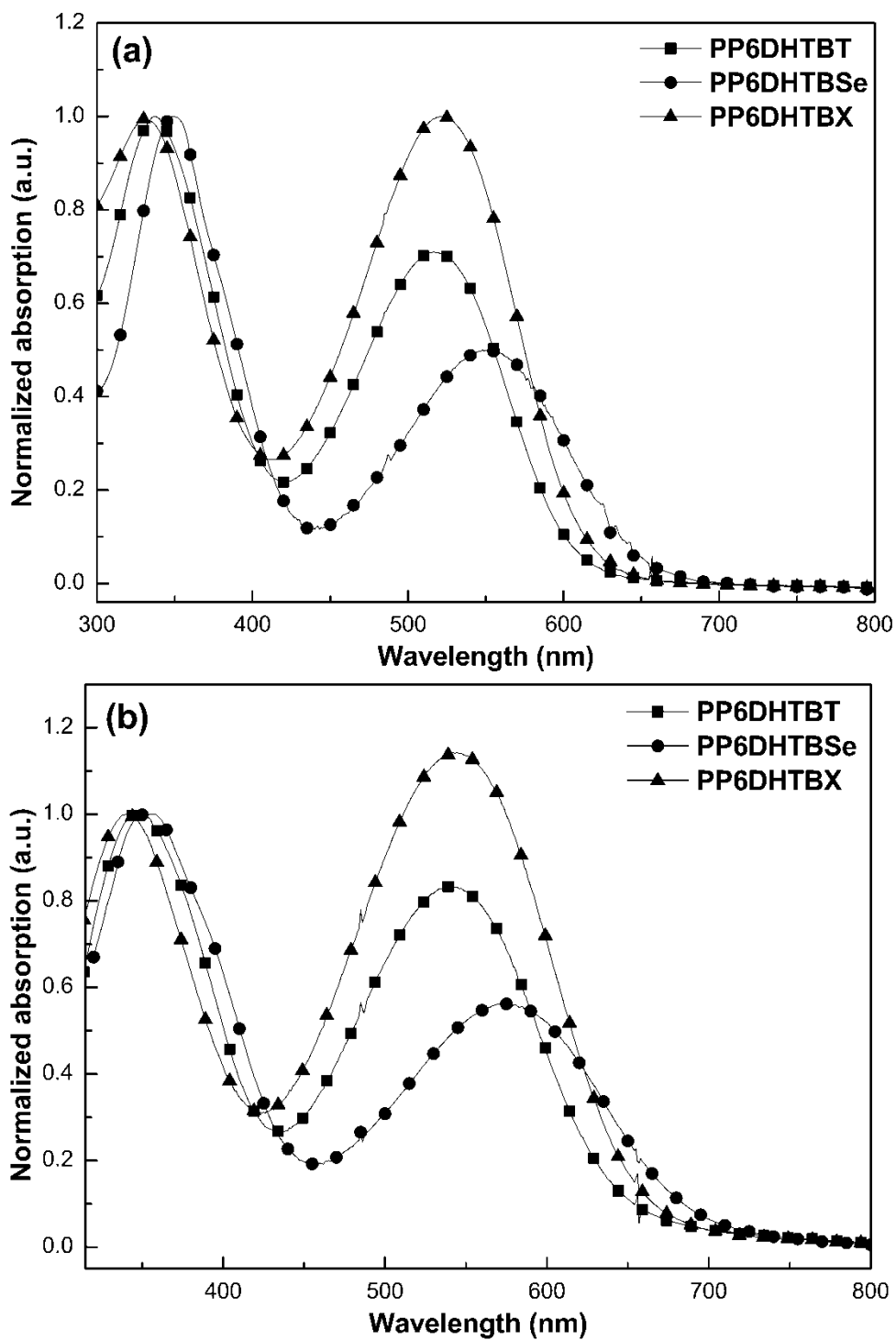


Figure 2.5 Normalised UV-vis spectra of polymers in (a) dilute chlorobenzene solutions and (b) solid films, respectively.

2.3.2 Optical Properties

The normalized UV-vis absorption of the synthesized polymers in dilute chlorobenzene solutions (concentration 10^{-5} M) and solid films are shown in Figure 2.5, and the main optical properties are listed in Table 2.2. The absorption spectra of polymers, i.e., **PP6DHTBT**, **PP6DHTBSe**, and **PP6DHTBX**, exhibited two distinct broad absorption peaks. The short-wavelength absorption peaks have been attributed to a delocalized π - π^* transition in the polymer chains and long-wavelength absorption peaks attributed to a localized transition between the donor-acceptor (D-A) charge transfer states in polymer segments. The high energy transition bands situated at 300-400 nm are consistent with the reported phenothiazine homopolymers⁹³ or phenothiazine containing copolymers.⁸⁰ The low energy peaks appeared at 500-600 nm, with tailing the absorption around 700 nm are due to the intramolecular charge transfer (ICT) happening inside these phenothiazine based D-A conjugated polymers. The maximum absorption wavelengths ($\lambda_{\text{max,abs}}$) for **PP6DHTBT**, **PP6DHTBSe**, and **PP6DHTBX** in solutions were located at 515, 552, and 522 nm, respectively, while those in solid films at 552, 582, and 553 nm, respectively. As illustrated in Table 2.2, the optical band gaps ($E_{\text{g}}^{\text{opt}}$) of **PP6DHTBT**, **PP6DHTBSe**, and **PP6DHTBX** in solid films, which were estimated from the absorption edges of UV-vis spectra, were 1.93, 1.80 and 1.90 eV, respectively. Compared with UV-vis absorption spectra in solutions, all polymers in solid films had a red shift (30-37 nm), this could be attributed to the interchain associations and aggregations in solids. The maximum absorption wavelength ($\lambda_{\text{max,abs}} = 552$ nm) of **PP6DHTBT** in solid film was red-shifted compared with that (540 nm) of its analogue F8TBT (phenothiazine units replaced with fluorene units).⁹⁴ Though **PP6DHTBSe** bearing alkyl chains at 4-position of thiophene units revealed $\lambda_{\text{max,abs}} = 582$ nm in solid film, which also red

shifted to its fluorene-based polymer analogue bearing alkyl-chain free thiophenes, PFO-DBTSe (ca. 570 nm).⁹⁵ Since the side-chain functionalization usually cause steric hindrance to affect the coplanarity of the conjugated backbone, side-chain functionalized polymer has a blue shift in the absorption spectra compared with its side-chain free polymer analogue. It suggests that the phenothiazine unit possesses stronger electron-donating capability (stronger degree of delocalization and the stronger ICT) than the fluorene unit, thus to improve the effective conjugation length along the phenothiazine-based polymer backbone.⁵⁴ Due to the presence of Selenium (Se) atom, which has larger size and is more electron rich than both S and O atoms, **PP6DHTBSe** had a more red-shifted absorption wavelength ($\lambda_{\text{max,abs}}$) compared with the other two polymers (**PP6DHTBT** and **PP6DHTBX**). Similar results were reported for the polymers containing benzoselenadiazole units,⁹⁶ where the presence of imine nitrogens in benzodiazole units can stabilize the quinoid resonance structures by the most electron rich Se atom.

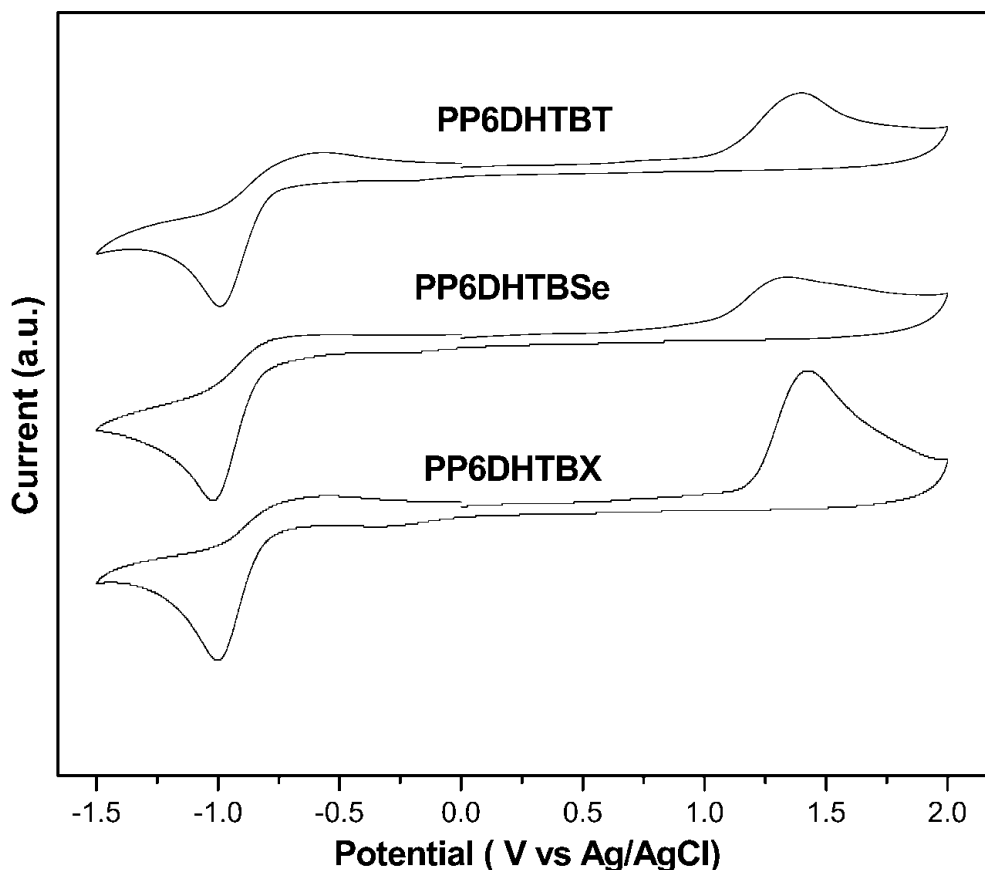


Figure 2.6 Cyclic voltammograms of polymers

Table 2.3 Electrochemical Properties of Polymers^a

Polymer	Oxidation potential (V vs. Ag/Ag ⁺)		Reduction Potential (V vs. Ag/Ag ⁺)		Energy Level ^d (eV)		Band Gap (eV)	
	E _{ox/onset} ^b	E _{ox/o} ^c	E _{red/onset} ^b	E _{red/o} ^c	HOMO	LUMO	E _g ^{ec}	E _g ^{opt}
PP6DHTBT	1.07	1.36	-0.88	-0.97	-5.42	-3.47	1.95	1.93
PP6DHTBSe	1.03	1.31	-0.80	-1.01	-5.38	-3.55	1.83	1.80
PP6DHTBX	1.12	1.40	-0.75	-0.99	-5.47	-3.60	1.87	1.90

^aReduction and oxidation potentials measured by cyclic voltammetry in solid films;

^bOnset oxidation and reduction potentials; ^cFormal oxidation and reduction potentials;

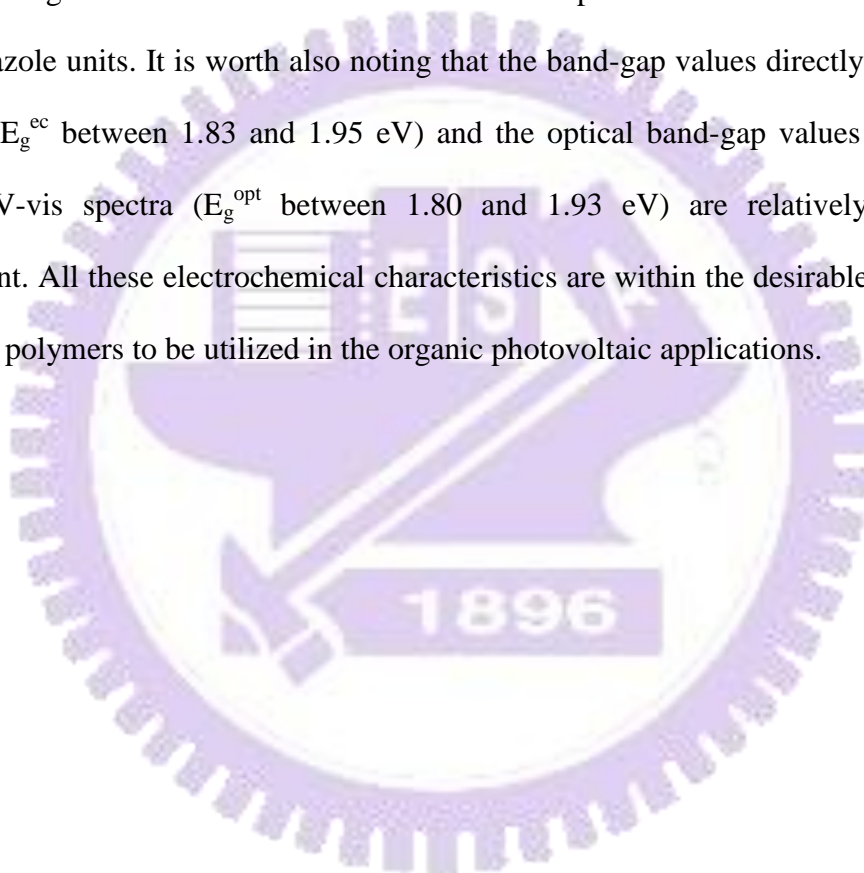
^dE_{HOMO}/E_{LUMO} = [-(E_{onset} - 0.45) - 4.8] eV, where 0.45 V is the value for ferrocene vs. Ag/Ag⁺ and 4.8 eV is the energy level of ferrocene below the vacuum.

2.3.3 Electrochemical Properties

The energy band structures, i.e., highest occupied molecular orbital (HOMO) and lowest unoccupied molecular orbital (LUMO) levels, of the polymers were investigated by cyclic voltammetry (CV) measurements to understand the charge injection processes of these polymers in their PSC devices. The cyclic voltammograms of the polymers in solid films are displayed in Figure 2.6 and the related CV data (formal potentials, onset potentials, HOMO and LUMO levels, and band gaps) are summarized in Table 2.3. Ag/AgCl was served as a reference electrode and it was calibrated by ferrocene ($E_{1/2}(\text{FC}/\text{FC}^+) = 0.45$ eV versus Ag/AgCl). The HOMO and LUMO energy levels were estimated by the oxidation and reduction potentials from the reference energy level of ferrocene (4.8 eV below the vacuum level) according to the following equation:⁹⁷ $E_{\text{HOMO}}/E_{\text{LUMO}} = [-(E_{\text{onset}} - E_{\text{onset}(\text{FC}/\text{FC}^+ \text{ vs. Ag/Ag}^+)}) - 4.8]$ eV where 4.8 eV is the energy level of ferrocene below the vacuum level and $E_{\text{onset}(\text{FC}/\text{FC}^+ \text{ vs. Ag/Ag}^+)} = 0.45$ eV. All polymers exhibited one quasi-reversible p-doping/dedoping (oxidation/rereduction) process at positive potentials and one quasi-reversible or reversible n-doping/dedoping (reduction/reoxidation) process at negative potentials, which are good signs of high structural stability in the charged state.

The HOMO levels were in the range of -5.38 to -5.47 eV, which were estimated from the onset oxidation potentials ($E_{\text{ox/onset}}$) of polymers (1.03 - 1.12 V). The LUMO levels were in the range of -3.47 to -3.60 eV, which were estimated from the onset reduction potentials ($E_{\text{red/onset}}$) of polymers (-0.75 to -0.88 V). As all HOMO levels were below the air oxidation threshold (ca. -5.27 eV or 0.57 V vs. SCE),²⁹ the polymers should show good air stabilities. More importantly, the introduction of phenothiazine unit in the **PP6DHTBT** polymer backbone decreases the energy band

gap in contrast to its fluorene analogue F8TBT,⁹⁴ which may be due to the presence of electron-rich sulfur and nitrogen heteroatoms of the phenothiazine unit that renders the resulting conjugated backbone more electron-rich.⁵⁴ On the other hand, the LUMO energy levels are clearly affected by the electron-deficient centers of the benzodiazole comonomers, stronger electron-deficient units resulting in lower LUMO energy levels. It has been found that the band gaps of these polymers were affected due to stronger ICT interactions between the donor phenothiazine unit and acceptor benzodiazole units. It is worth also noting that the band-gap values directly measured by CV (E_g^{cc} between 1.83 and 1.95 eV) and the optical band-gap values estimated from UV-vis spectra (E_g^{opt} between 1.80 and 1.93 eV) are relatively in good agreement. All these electrochemical characteristics are within the desirable range for the ideal polymers to be utilized in the organic photovoltaic applications.



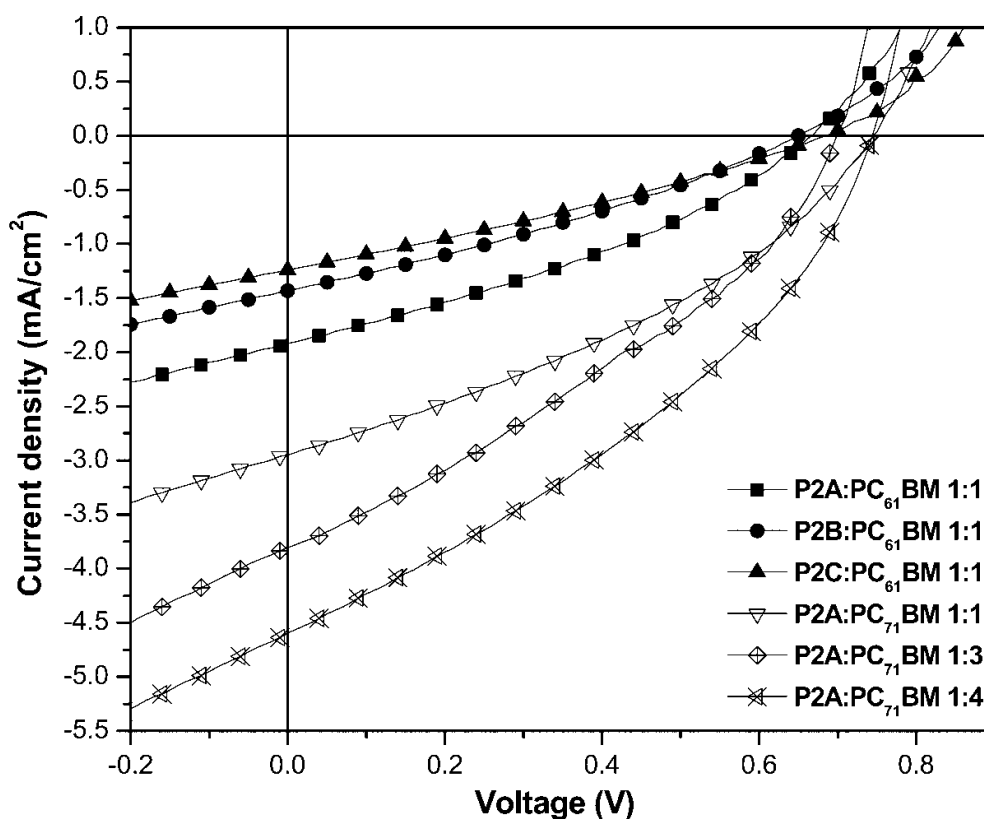


Figure 2.7 Current-voltage curves of polymer solar cells using polymer:PCBM blends under the illumination of AM 1.5G, 100 mW/cm².

Table 2.4 Photovoltaic Properties of Polymer Solar Cell Devices with the Configuration of ITO/PEDOT:PSS/Polymer:PCBM/Ca/Al^a

Polymer	Polymer/PCBM (w/w)	V_{oc} (V)	J_{sc} (mA/cm ²)	FF (%)	PCE (%)
PP6DHTBT	1:1 (C61)	0.67	1.92	32.1	0.41
PP6DHTBSe	1:1 (C61)	0.65	1.43	30.5	0.28
PP6DHTBX	1:1 (C61)	0.69	1.24	29.1	0.25
PP6DHTBT	1:1 (C71)	0.73	2.95	34.0	0.74
PP6DHTBT	1:3 (C71)	0.73	3.80	33.1	0.88
PP6DHTBT	1:4 (C71)	0.75	4.60	35.0	1.20

^a Measured under AM 1.5 irradiation, 100 mW/cm².

2.3.4 Photovoltaic Properties

To investigate the potential use of polymers **PP6DHTBT**, **PP6DHTBSe**, and **PP6DHTBX** in PSCs, the bulk hetero-junction (BHJ) solar cell devices comprising of these polymers as electron donors and fullerene derivatives (PC₆₁BM or PC₇₁BM) as an electron acceptor in their active layer were fabricated with a structure of ITO/PEDOT:PSS (30 nm) /polymer:PCBM blend (~80 nm)/Ca(30 nm)/Al(100 nm). The blended solutions were prepared with polymers and PC₆₁BM in a weight ratio of 1:1 (w/w) initially, and later the active layer compositions were modified with various weight ratios for the previous optimum polymer with PC₇₁BM. The current density (J) versus voltage (V) curves of the PSCs are shown in Figure 2.7; the open circuit voltage (V_{oc}), short circuit current density (J_{sc}), fill factor (FF), and the PCE values of the devices are summarized in Table 2.4. In BHJ solar cell devices, V_{oc} is determined by the difference between HOMO level of the electron donor polymer and LUMO level of the electron acceptor material (PCBM).⁷⁸ Due to negligible differences in HOMO levels of all polymers ((-5.38)-(-5.47) eV), there were minor variations in V_{oc} values (0.69-0.65 V). With the similar V_{oc} values and fill factor (29.1-32.1 %) in the devices containing the polymers blended with PC₆₁BM in a weight ratio of 1:1 (w/w), it was evident that due to the major variations of the J_{sc} values (1.92, 1.43, and 1.24 mA/cm²) in polymers **PP6DHTBT**, **PP6DHTBSe**, and **PP6DHTBX**, they are crucially affected to have the power conversion efficiency (PCE) values of 0.41, 0.28, and 0.25, respectively. Among these PSC devices containing polymers, the best performance was the PSC device containing **PP6DHTBT**:PC₆₁BM (1:1 w/w) with a highest PCE value of 0.41%, $V_{oc} = 0.67$ V, $J_{sc} = 1.92$ mA/cm², and FF = 32.1%.

Since the best performance of PSC device was observed in the previous optimum polymer blend **PP6DHTBT**:PC₆₁BM (1:1 wt%) as an active layer, the PSC devices as

a function of polymer blends **PP6DHTBT**:PC₇₁BM in various weight compositions (1:1, 1:3, and 1:4 w/w) were fabricated owing to a broader absorption and a higher absorption coefficient of PC₇₁BM than PC₆₁BM.⁹ The absorption spectra of the polymer blends **PP6DHTBT**:PC₇₁BM (1:1, 1:3, and 1:4 w/w) prepared under the same conditions as the process of device fabrication are demonstrated in Figure 2.8(a). The current-voltage characteristics of these devices are also shown in Figure 2.7 and their related photovoltaic properties are illustrated in Table 2.4. The optimum photovoltaic performance with the maximum PCE value of 1.20 % ($V_{oc} = 0.75$ V, $J_{sc} = 4.60$ mA/cm², and FF = 35.0 %) was obtained in the PSC device having a weight ratio of **PP6DHTBT**:PC₇₁BM=1:4. Using lower weight ratios of PCBM in blended polymer **PP6DHTBT**: PC₇₁BM (1:1 and 1:3 w/w) led to reductions in the J_{sc} values due to the inefficient charge separation and electron transporting properties, resulting in the lower PCE results.⁹⁸

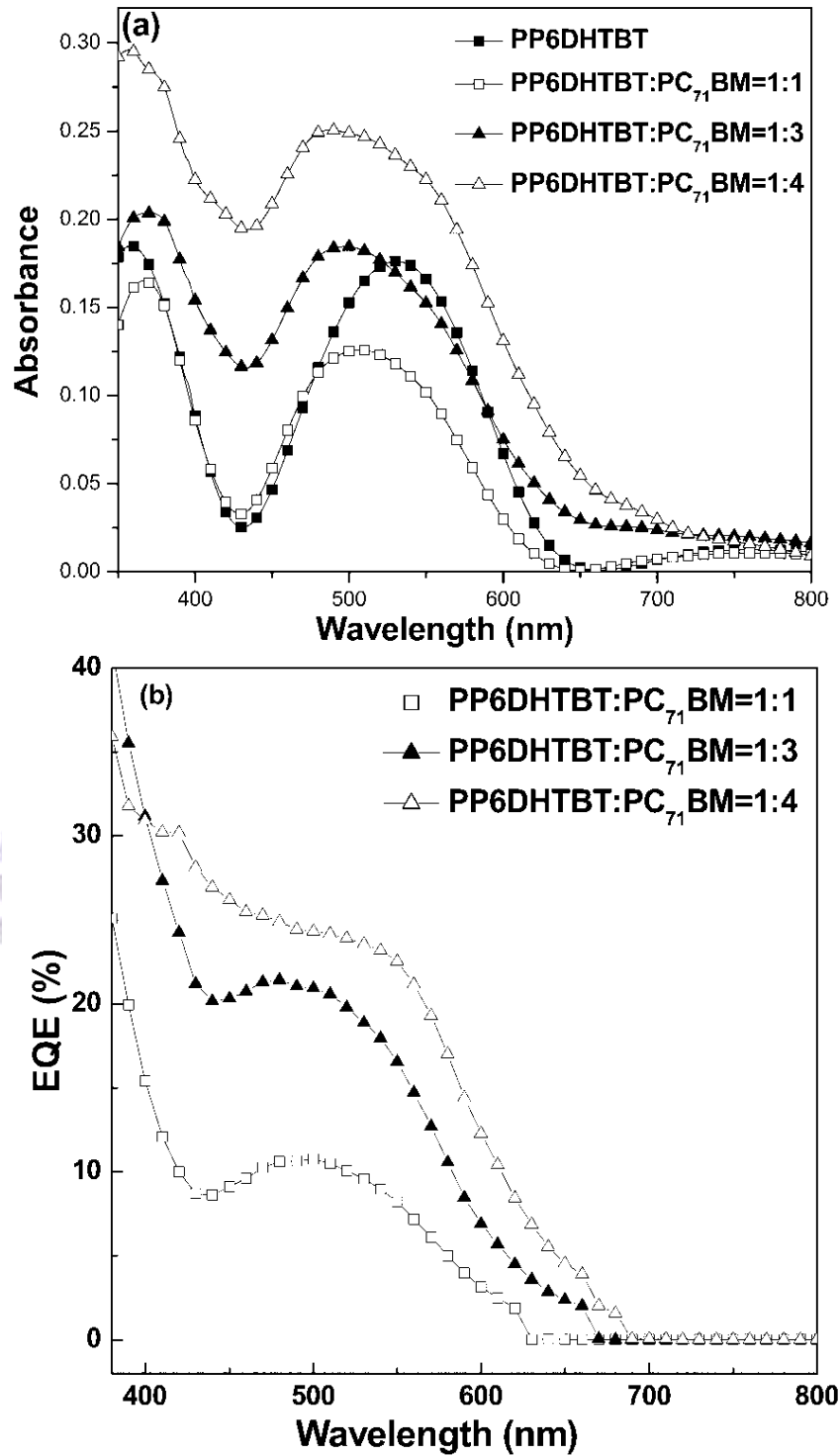


Figure 2.8 (a) Absorbance spectra of **PP6DHTBT:PC₇₁BM** thin films measured from the solar cell devices by using an ITO/PEDOT substrate as a reference. (b) External quantum efficiency (EQE) of **PP6DHTBT:PC₇₁BM** solar cells.

The V_{oc} values observed in **PP6DHTBT**:PC₇₁BM solar cells were fairly stable (0.73-0.75 V) in all polymer blend compositions (1:1 to 1:4 w/w) with PC₇₁BM (see Table 2.4), which are comparable to that of some of donor acceptor polymer:fullerene BHJ solar cells. The EQE curves of the PSC devices are also plotted in Figure 2.8(b) to compare with the absorption spectra of the polymer blends **PP6DHTBT**:PC₇₁BM shown in Figure 2.8(a). It is apparent that the PSC devices exhibited a very broad response range covering from 400 to 700 nm, where the external quantum efficiencies (EQE) were within 30%. The main reason for the low EQE values of the PSC devices are due to the limited absorbances of the active layer as shown in Figure 2.8(a). In BHJ solar cell devices, the absorptions of the long wavelength region are contributed by the polymers, and the absorptions in the short wavelength region are mainly from PC₇₁BM. However, the peak values of the absorbances in the long wavelength region are only 0.17-0.30, so it means that only some portions of light were absorbed in the PSC devices, which might be due to the small thickness of the active layer (~80 nm).

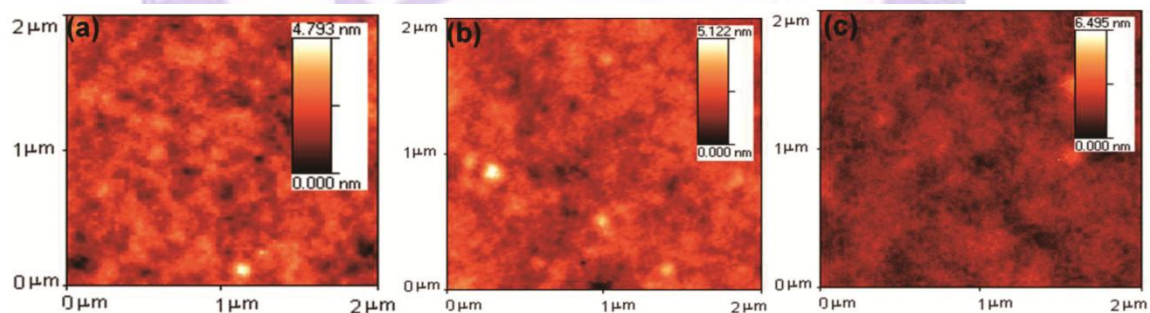


Figure 2.9 AFM images of **PP6DHTBT**: PC₇₁BM blend films. (a) 1:1 (w/w), (b) 1:3 (w/w), and (c) 1:4 (w/w) ratios.

Carrier transport properties, including hole and electron mobilities of **PP6DHTBT**:PC₇₁BM (1:4 wt%) were evaluated by fabricating the hole- and electron-only devices. The devices were prepared following the same procedure as the

fabrication of BHJ devices, except that Ca was replaced with MoO₃ ($\Phi = 5.3$ eV) in the hole-only devices, and the PEDOT:PSS layer was replaced with Cs₂CO₃ ($\Phi = 2.9$ eV) for the electron-only devices. The electron and hole mobilities were determined precisely by fitting the plots of the dark current versus voltage ($J-V$) curves for single carrier devices to the space charge limited current (SCLC) model. The dark current is given by $J = 9\varepsilon_0\varepsilon_r\mu V^2/8L^3$, where $\varepsilon_0\varepsilon_r$ is the permittivity of the polymer, μ is the carrier mobility, and L is the device thickness. The hole and electron mobilities of **PP6DHTBT:PC₇₁BM** (1:4 wt%) are 3.68×10^{-9} cm²/Vs and 1.76×10^{-8} cm²/Vs, respectively. The electron mobility was much higher (i.e., ca. 1 order of magnitude) than the hole mobility, resulting in an imbalance in the hole and electron transport in the blended polymer film. Due to the poor hole mobility and the imbalance of the hole and electron transport in the blended polymer film, the device was limited to have a low FF value, which could be another reason for the lower PCE value.⁹⁹ From the AFM images of **PP6DHTBT:PC₇₁BM** with various weight ratios (Figure 2.9), we observed that the roughness is increased from 0.67 nm (with PCE = 0.74 %) to 1.48 nm (with PCE = 0.88 %) and 2.60 nm (with PCE = 1.20 %) as the weight ratio of **PP6DHTBT:PC₇₁BM** changed from 1:1 to 1:3 and 1:4 w/w ratio, respectively. Therefore, we can summarize that the increased PCE value caused by a higher content of PC₇₁BM in the polymer blend of **PP6DHTBT:PC₇₁BM** = 1:4 w/w was induced by the larger roughness in the polymer blend. Additionally, the optimum PSC device (without annealing, PCE = 1.20 %) containing polymer blend of **PP6DHTBT:PC₇₁BM** = 1:4 (w/w) was further investigated for the thermal annealing effects. As shown in Table 2.5, the PCE values of 1.14, 1.05, and 0.86% were obtained at the thermal annealing (20 min.) of 50, 100, and 150 °C, respectively.

Finally, the thermal annealing effects were proven to have no substantial increase on the solar cell device performance.

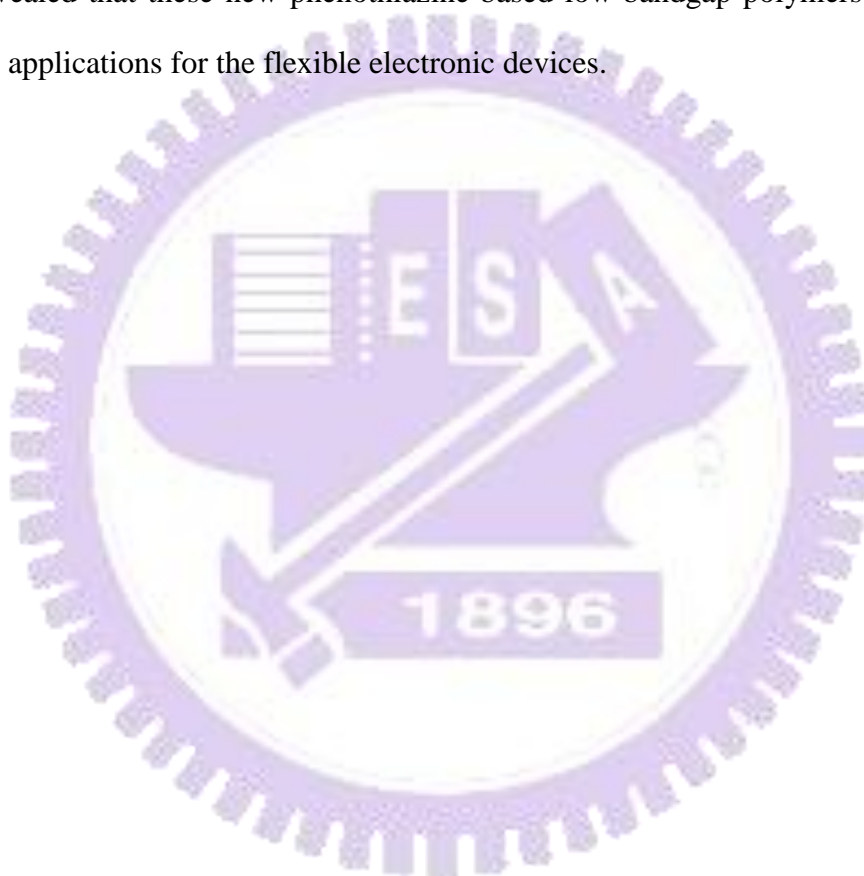
Table 2.5 Annealing Effects on Polymer Solar Cell Device Containing PP6DHTBT:PC₇₁BM (1:4 wt%)

Annealing Temperature (°C)	V_{oc} (V)	J_{sc} (mA/cm ²)	FF (%)	PCE (%)
50	0.73	4.99	31.3	1.14
100	0.74	4.37	32.6	1.05
150	0.67	4.09	31.2	0.86

2.4 Conclusion

A series of new low-bandgap polymers containing the phenothiazine unit as an electron donor conjugated with various benzodiazole acceptors via hexyl-thiophene linkers were synthesized and characterized. These polymers show strong absorptions in the range of 300-700 nm and have ideal ranges of HOMO and LUMO levels (with optical bandgaps of 1.80-1.93 eV). Bulk heterojunction polymer solar cells were fabricated from the polymer blends consisting of these low-bandgap polymers (**PP6DHTBT**, **PP6DHTBSe**, and **PP6DHTBX**) as an electron donor and PC₆₁BM/PC₇₁BM as an electron acceptor. With the similar V_{oc} values and fill factor in the PSC devices containing the polymers blended with PC₆₁BM in a weight ratio of 1:1 (w/w), it was found that due to the major variations of the J_{sc} values (1.92, 1.43, and 1.24 mA/cm²) in polymers **PP6DHTBT**, **PP6DHTBSe**, and **PP6DHTBX**, they are crucially affected to have the power conversion efficiency (PCE) values of 0.41, 0.28, and 0.25, respectively. The PSC device containing a polymer blend of **PP6DHTBT:PC₇₁BM (1:4 wt%)** exhibited the best device performance with a PCE

value of 1.20%, an open-circuit voltage (V_{oc}) of 0.75 V, a short-circuit current (J_{sc}) of 4.60 mA/cm², and a fill factor (FF) of 0.35. The optimization of photovoltaic properties in the PSC devices containing polymer blends **PP6DHTBT**:PC₇₁BM can be adjusted by the morphology variations with different weight ratios of PC₇₁BM, which were observed to have higher roughnesses with larger PC₇₁BM contents, and thus to substantially increase the PCE values of the PSC devices. Finally, the present study revealed that these new phenothiazine-based low-bandgap polymers will have potential applications for the flexible electronic devices.



Chapter 3.

Cyclopentadithiophene- and Dithienosilole-Based Polymers Containing Cyano-Vinylene Groups for Photovoltaic Applications

3.1 Introduction

Till now, polymer solar cells (PSC), composed of bicontinuous intermixing of electron donors and acceptors, have played a leading role in obtaining higher efficiencies as these devices allow the photogenerated electron-hole pairs to be efficiently separated throughout the bulk films and transported to the electrodes.^{9,20,25-26} Though the conventional blends of poly(3-hexylthiophene) (P3HT) and [6,6]-phenyl-C₆₁-butyric acid methyl ester (PC₆₁BM) have reached power conversion efficiency up to 5%,³⁷⁻⁴⁷ further increase is rather difficult due to their limited photocurrent generation and intrinsic absorption properties. Therefore, an alternative approach to have better performance is to use low band gap (LBG) donor-acceptor (D-A) polymeric materials, and higher efficiencies up to 6.0-7.7% were obtained by such polymers.^{61,70-74} Recently, it remains a key challenge to design new ideal LBG polymers with broad absorption ranges, high carrier mobilities, and appropriate molecular energy levels for better solar photon harvesting and improved photovoltaic properties, and thus to have higher efficiencies in PSC applications.

To meet the requirements of good PSC materials, LBG polymers containing electron donating moieties from 2,2'-bithiophene unit covalently bridged with an atom, such as C, N, S, and Si, at 3,3'-position have attracted considerable research attentions. The bridging atoms at 3,3'-position of donor moieties play an important role for LBG polymers in terms of solubility, planarity, band gap, and interchain packing, as well as for the performance of the bulk heterojunction (BHJ) solar cells.⁵⁹

Among these four donor moieties, both dithienopyrrole and dithienothiophene units

(containing N and S atoms, respectively at 3,3'-position) had lower efficiencies in BHJ solar cells due to the lower V_{oc} values arising from their high HOMO levels.¹⁰⁰⁻¹⁰² Thus, the LBG polymers containing the other two electron donor moieties, i.e., cyclopentadithiophene and dithienosilole units (containing C and Si atoms, respectively at 3,3'-position), have emerged as potential materials for field-effect transistors (FETs)¹⁰³⁻¹⁰⁴ and photovoltaic cells^{87,99,105-106} due to their similar ranges of HOMO and LUMO levels as ideal polymers.

To obtain the broad absorption bands with high absorptivities, electron-donating groups and/or electron-withdrawing groups are substituted on the main-chains of the conjugated polymers to raise the HOMO levels and/or to reduce the LUMO levels of the polymers.¹⁰⁷⁻¹⁰⁸ Hence, introduction of electron-withdrawing cyano-vinylene groups to polymer backbones to lower the LUMO levels,¹⁰⁹ tune their electro-optical properties,¹¹⁰ and enhance the electrochemical stabilities of the polymers¹¹¹ are desirable for optoelectronic device applications. Moreover, LBG polymers containing electron-accepting cyano-vinylene groups were proven to possess higher hole mobilities,¹¹² and were applied as photovoltaic materials in BHJ solar cells.¹¹³⁻¹¹⁶ However, the PCE values of these photovoltaic cells are still low at present. All these research results inspire further development in exploring cyclopentadithiophene- and dithienosilole- derivatives with cyano-vinylene cgroups for the better photophysical, electrochemical, and photovoltaic properties. Based on this concept, soluble cyclopentadithiophene- and dithienosilole-based LBG D-A polymers (**CPDT-CN**, **DTS-CN**) containing β -cyano-thiophenevinylene groups are designed and synthesized. The effects of the bridged atoms on the optical, electrochemical, charge transporting and photovoltaic properties of the polymers are compared and reported in this study. A maximum PCE of 2.25% could be reached by a PSC device containing

an active layer of **DTS-CN:PC₇₁BM**. The preliminary study reveals that these LBG polymers may have potential applications in flexible electronic devices in the future.

3.2 Experimental Section

3.2.1 Materials

4,4-Bis(2-ethylhexyl)-cyclopenta[2,1-*b*:3,4-*b'*]dithiophene (1),¹¹⁷
3,3'-di-*n*-hexylsilylene-2,2'-bithiophene (4),¹⁰³ 5-bromo-2-thiopheneacetonitrile (3)¹¹²,
4,4-Bis(2-ethylhexyl)-2,6-bis(trimethylstannanyl)-4H-cyclopenta- [2,1-*b*:3,4-*b'*]
dithiophene (6),¹¹⁷ 5,5'-bis(trimethylstannanyl)-3,3'-di-*n*-hexylsilylene-2,2'-
bithiophene (7)¹⁰⁴ were prepared according to the published methods. All other
chemicals were purchased from Aldrich, ACROS, Fluka, or TCI. Toluene,
tetrahydrofuran (THF), and diethyl ether were distilled over sodium/benzophenone.
Chloroform (CHCl₃) was purified by refluxing with calcium hydride and then
distilled.

3.2.2 Measurements and Characterization

¹H and ¹³C NMR spectra were measured using Varian Unity 300 MHz spectrometer. Elemental analyses were performed on a HERAEUS CHN-OS RAPID elemental analyzer. Thermogravimetric Analyses (TGA) were conducted with a TA Instruments Q500 at a heating rate of 10 °C/min under nitrogen. The molecular weights of polymers were measured by gel permeation chromatography (GPC) using Waters 1515 separation module (concentration: 1 mg/1 mL in THF; flow rate: 1 mL/1min), and polystyrene was used as a standard with THF as an eluant. UV-visible absorptions were recorded in dilute chloroform solutions (10⁻⁶ M) on a HP G1103A. Solid films of UV-vis measurements were spin-coated on a glass substrate from chlorobenzene solutions with a concentration of 10 mg/mL.

Cyclic voltammetry (CV) measurements were performed using a BAS 100 electrochemical analyzer with a standard three-electrode electrochemical cell in a 0.1 M Tetrabutylammonium Hexafluorophosphate ((TBA)PF₆) solution (in acetonitrile) at room temperature with a scanning rate of 100 mV/s. During the CV measurements, the solutions were purged with nitrogen for 30 s. In each case, a carbon working electrode coated with a thin layer of polymers, a platinum wire as the counter electrode, and a silver wire as the quasi-reference electrode were used, and Ag/ AgCl (3 M KCl) electrode was served as a reference electrode for all potentials quoted herein. The redox couple of ferrocene/ ferrocenium ion (Fc/Fc⁺) was used as an external standard. The corresponding highest occupied molecular orbital (HOMO) and lowest unoccupied molecular orbital (LUMO) levels were calculated using $E_{\text{ox/onset}}$ and $E_{\text{red/onset}}$ for experiments in solid films of polymers, which were performed by drop-casting films with the similar thickness from THF solutions (ca. 5 mg/mL). The onset potentials were determined from the intersections of two tangents drawn at the rising currents and background currents of the cyclic voltammetry (CV) measurements.

3.2.3 Fabrication of Polymer Solar Cells

The polymer solar cells in this study were composed of an active layer of blended polymers (CPDT-CN or DTS-CN:PCBM) in solid films, which was sandwiched between a transparent indium tin oxide (ITO) anode and a metal cathode. Prior to the device fabrication, ITO-coated glass substrates (1.5 × 1.5 cm²) were ultrasonically cleaned in detergent, deionized water, acetone, and isopropyl alcohol. After routine solvent cleaning, the substrates were treated with UV ozone for 15 min. Then a modified ITO surface was obtained by spin-coating a layer of poly(ethylene dioxythiophene): polystyrenesulfonate (PEDOT:PSS) (~30 nm).

After baking at 130 °C for one hour, the substrates were transferred to a nitrogen-filled glove-box. Then, on the top of PEDOT:PSS layer, the active layer was prepared by spin coating from blended solutions of polymers **CPDT-CN** or **DTS-CN:PC₆₁BM** (with 1:1 w/w) and **DTS-CN:PC₇₁BM** (with 1:1, 1:2, 1:3, w/w) subsequently with a spin rate ca. 1000 rpm for 60 s, and the thickness of the active layer was typically ca. 80 nm. Initially, the blended solutions were prepared by dissolving both polymers and PCBM in 1,2 dichlorobenzene (20 mg/1 mL), followed by continuous stirring for 12 h at 50 °C. In the slow-growth approach, blended polymers in solid films were kept in the liquid phase after spin-coating by using the solvent with a high boiling point. Finally, a calcium layer (30 nm) and a subsequent aluminum layer (100 nm) were thermally evaporated through a shadow mask at a pressure below 6×10^{-6} Torr. The active area of the device was 0.12 cm². All PSC devices were prepared and measured under ambient conditions. The solar cell measurements were done inside a glove box under simulated AM 1.5G irradiation (100 mW/cm²) using a Xenon lamp based solar simulator (Thermal Oriel 1000W). The light intensity was calibrated by a mono-silicon photodiode with KG-5 color filter (Hamamatsu, Inc.). The external quantum efficiency (EQE) spectra were obtained at short-circuit conditions. The light source was a 450 W Xe lamp (Oriel Instrument, model 6266) equipped with a water-based IR filter (Oriel Instrument, model 6123NS). The light output from the monochromator (Oriel Instrument, model 74100) was focused on the photovoltaic cell under test.

3.2.4 Fabrication of Hole- and Electron-only Devices

The hole- and electron-only devices in this study contain polymers **CPDT-CN** or **DTS-CN:PC₆₁BM** (1:1 w/w) blend films sandwiched between transparent ITO anode and cathode. The devices have been prepared following the same procedure

as the fabrication of BHJ devices, except that in the hole-only devices, Ca was replaced with MoO₃ ($\Phi = 5.3$ eV) and for the electron-only devices, the PEDOT:PSS layer was replaced with Cs₂CO₃ ($\Phi = 2.9$ eV). In hole-only devices, MoO₃ was thermally evaporated with a thickness of 20 nm and then capped with 50 nm of Al on the top of the active layer. On the other hand, Cs₂CO₃ was thermally evaporated in the electron-only devices with a thickness of approximately 2 nm on the top of transparent ITO. For both devices, annealing of the active layer was performed at 130 °C for 20 minutes. The space charge limited current (SCLC) method was used to evaluate the hole and electron mobilities of polymer blend films **CPDT-CN** or **DTS-CN:PC₆₁BM** (1:1 w/w) by fabricating the hole- and electron-only devices. The electron and hole mobilities were determined precisely by fitting the plots of the dark current versus voltage ($J-V$) curves for single carrier devices to the SCLC model. The dark current is given by $J = 9\varepsilon_0\varepsilon_r\mu V^2/8L^3$, where $\varepsilon_0\varepsilon_r$ is the permittivity of the polymer, μ is the carrier mobility, L is the device thickness.

3.2.5 Synthesis of Monomers and Polymers

4,4-Bis(2-ethylhexyl)-4H-cyclopenta[2,1-*b*:3,4-*b'*]dithiophene-2,6-dicarbaldehyde (2). A three-neck round-bottom flask containing 3.8 mL (50 mmol) of anhydrous DMF was cooled in an ice bath. To the solution, 4.7 mL (50 mmol) of phosphoryl chloride was added dropwise over a period of 20 min. 4,4-Bis(2-ethylhexyl)-cyclopenta[2,1-*b*:3,4-*b'*]dithiophene (**1**),¹¹⁷ (4.03g, 10 mmol) in 30 mL of 1,2-dichloroethane was added to the above solution dropwise and heated to ca. 90 °C for 2 days. The solution was cooled to room temperature, poured into ice cold saturated aqueous solution of sodium acetate (200 mL). Then, the mixture was extracted with CH₂Cl₂/water. The organic layer was concentrated under reduced

pressure. Finally, the crude product was purified by column chromatography using mixture of ethyl acetate and hexane (1:4) to get a yellow solid (3.90g, 85%). ¹H NMR (300 MHz, CDCl₃): δ (ppm) 9.88 (s, 2H), 7.61 (s, 2H), 1.94 (m, 4H), 0.96-0.86 (m, 18H), 0.71 (m, 6H), 0.55 (t, *J* = 7.2 Hz, 6H).

3,3'-di-n-hexylsilylene-2,2'-bithiophene-5,5'-dicarbaldehyde (5). Compound **5** was synthesized in a similar synthetic procedure as described for compound **2** by taking 3,3'-di-n-hexylsilylene-2,2'-bithiophene (**4**),¹⁰³ (3.63g, 10 mmol) to get the desired product as a yellow solid (3.53g, 83%). ¹H NMR (300 MHz, CDCl₃): δ (ppm) 0.88-0.98 (m, 10H), 1.28-1.36 (m, 16H), 7.75 (s, 2H), 9.92 (s, 2H). ¹³C NMR (75 MHz, CDCl₃): δ (ppm) 11.69, 14.25, 22.69, 24.23, 31.53, 32.96, 139.07, 146.45, 147.30, 156.53, 183.12

M1. To a mixture of compound **2** (1.15 g, 2.5 mmol) and 5-bromo-2-thiopheneacetonitrile (**3**) (2.02 g, 10 mmol) in methanol (100 mL), a catalytic amount of potassium tert-butoxide was added. The mixture was stirred at room temperature for 24 h. Then, the crude product was filtered and dried. Chromatography on silica gel eluted with CH₂Cl₂/hexane 1:4 afforded **M1** as a dark orange solid (1.71 g). Yield: 82%. ¹H NMR (300 MHz, CDCl₃): δ (ppm) 7.57 (d, *J* = 5.1 Hz, 2H), 7.29 (d, *J* = 11.1 Hz, 2H), 7.09 (d, *J* = 3.6 Hz, 2H), 7.03 (d, *J* = 3.9 Hz, 2H), 1.96 (m, 4H), 0.97-0.90 (m, 16H), 0.79-0.73 (m, 6H), 0.72-0.61 (m, 8H). ¹³C NMR (75 MHz, CDCl₃): δ (ppm) 160.56, 142.20, 140.52, 133.27, 132.50, 127.18, 126.96, 123.14, 118.49, 105.59, 54.47, 43.32, 35.57, 34.35, 28.70, 27.56, 22.99, 14.28, 10.89. MS (FAB): *m/z* [M⁺] 827; calcd *m/z* [M⁺] 826.83. Anal. Calcd for C₃₉H₄₂Br₂N₂S₄: C, 56.65; H, 5.12; N, 3.39. Found: C, 56.91; H, 5.44; N, 3.65.

M2. **M2** was synthesized in a similar synthetic procedure as described for **M1** by taking compound **5** (1.05 g, 2.5 mmol) to get a purple solid (1.45 g). Yield: 73%. ¹H NMR (300 MHz, CDCl₃): δ (ppm) 7.57 (d, *J* = 4.8 Hz, 2H), 7.31 (d, *J* = 9 Hz, 2H), 7.1 (d, *J* = 3.6 Hz, 2H), 7.03 (d, *J* = 3.9 Hz, 2H), 1.10-1.62 (m, 16H), 0.92-0.73 (m, 10H). ¹³C NMR (75 MHz, CDCl₃): δ (ppm) 147.25, 142.01, 138.85, 133.12, 131.41, 129.28, 127.42, 116.48, 113.38, 103.07, 59.17, 33.21, 31.59, 23.18, 22.75, 18.57, 14.28. MS (FAB): *m/z* [M⁺] 786; calcd *m/z* [M⁺] 786.80. Anal. Calcd for C₃₄H₃₄Br₂N₂S₄Si: C, 51.90; H, 4.36; N, 3.56. Found: C, 50.97; H, 4.85; N, 3.46.

4,4-Bis(2-ethylhexyl)-2,6-bis(trimethylstannanyl)-4*H*-cyclopenta-[2,1-*b*:3,4-*b'*]-dithiophene (6). 4,4-Bis(2-ethylhexyl)-cyclopenta[2,1-*b*:3,4-*b'*]dithiophene (1.5 g, 3.72 mmol) was dissolved in dry THF (30 mL). The solution was cooled to -78 °C, and *n*-butyllithium (2.5 M solution in hexane, 5.96 mL, 14.9 mmol) was added dropwise. The reaction mixture was stirred at this temperature for 1 h and allowed to warm to room temperature over 3 h, at that point it was stirred for an additional hour. The reaction was again cooled to -78 °C, and trimethyltin chloride (1 M in hexanes, 18 mL, 18 mmol) was added dropwise. The reaction was allowed to warm up to room temperature and stirred overnight (ca. 20 h). Water was added, and the reaction was extracted with ethyl ether. The organic layer was washed with water and dried over sodium sulfate. Solvent was removed under vacuum, and the residue was dissolved in toluene and quickly passed through a plug of Celite pretreated with triethylamine. Solvent was removed, and the residue was dried under vacuum at 80 °C overnight. The distannyl compound was dissolved in hexanes and filtered through a plug of densely packed Celite. Solvent was removed, and the residue was dried under vacuum overnight. The bis(trimethyltin) monomer was obtained as a light brownish viscous

oil (2.52 g, 93%). ^1H NMR (300 MHz, CDCl_3): δ (ppm) 6.93 (m, 2H), 1.86 (m, 4H), 1.29 (m, 2H), 0.94 (m, 16H), 0.78 (t, $J = 6.8$ Hz, 6H), 0.62 (t, $J = 7.3$ Hz, 6H), 0.37 (m, 18H). ^{13}C NMR (75 MHz, CDCl_3): δ (ppm) 160.12, 143.04, 136.60, 130.52, 52.78, 43.57, 35.56, 34.91, 29.18, 28.07, 23.28, 14.63, 11.26, -7.79. MS (FAB) m/z [M^+] 728.0 calcd m/z [M^+] 728.2. Anal. Calcd for $\text{C}_{31}\text{H}_{54}\text{S}_2\text{Sn}_2$: C, 51.12; H, 7.47. Found: C, 51.47; H, 7.30.

Synthesis of 5,5'-bis(trimethylstannyl)-3,3'-di-n-hexylsilylene-2,2'-bithiophene (7). In a flame-dried 100 mL two-neck round-bottom flask, 5,5'-dibromo-3,3'-di-n-hexylsilylene-2,2'-bithiophene (1.041 g, 2 mmol) was placed in anhydrous THF (20 mL), to which n-butyllithium in hexane (2.5 M, 1.84 mL, 4.6 mmol) was added at -78°C under stirring for 1 h. Thereafter, the mixture was warmed up slowly to room temperature in an ambient environment with stirring. After the reaction mixture was again cooled down to -78°C , trimethyltin chloride in hexane (1 M, 4.6 mL, 4.6 mmol) was added slowly. The mixed solution was then stirred at ambient temperature for 18 h, followed by the addition of ice-water. Finally, the aqueous layer was extracted with ether (3×50 mL) while the combined organic layer was dried with anhydrous sodium sulfate and concentrated under a reduced pressure to give product 7. ^1H NMR (300 MHz, CDCl_3): δ (ppm) 0.36 (s, 18H), 0.83-0.88 (m, 10H), 1.23-1.28 (m, 16H), 7.08 (s, 2H). ^{13}C NMR (75 MHz, CDCl_3): δ (ppm) -7.87, 12.22, 14.33, 22.83, 24.47, 31.65, 33.11, 125.03, 137.89, 143.32, 155.22. Anal. Calcd for $\text{C}_{26}\text{H}_{46}\text{S}_2\text{SiSn}_2$ (%): C, 45.37; H, 6.74. Found (%): C, 46.69; H, 6.82.

General Polymerization Procedure

In a 25 mL flame dried flask, 1.0 mmol of dibromo monomers **M1** or **M2** and 1.0 mmol of distannyl compound **6** or **7** were added in 15 mL of anhydrous toluene and degassed with argon for 30 min. The Pd(0) complex, i.e.,

tetrakis(triphenylphosphine)palladium (1 mol %), was transferred into the mixture in a dry environment. After another flushing with argon for 20 min, the reaction mixture was heated to reflux for 18 h. Then, an excess amount of 2-bromothiophene was added to end-cap the trimethylstannyl groups and reacted for 2 h. The reaction mixture was cooled to 40 °C and added slowly into a vigorously stirred mixture of methanol/acetone (3:1). The polymers were filtered through a Soxhelt thimble and then subjected to Soxhelt extraction with methanol, hexane, acetone, and chloroform. The polymers were recovered as solids from chloroform fraction by rotary evaporation and reprecipitation into methanol solutions. The solids were dried under vacuum for 1 day. The yields, ¹H NMR data, and molecular weights of the polymers are listed as follows:

CPDT-CN. Yield: 66%. ¹H NMR (300 MHz, CDCl₃): δ (ppm) 7.65-7.29 (br, m, 6H), 7.20-6.89 (br, m, 4H), 2.01 (br, m, 8H), 1.02-0.67 (br, m, 60H). Anal. Calcd: C, 71.86; H, 7.54; N, 2.62. Anal. Found: C, 71.46; H, 7.35; N, 2.50. Mn = 16.4 K; Polydispersity Index (PDI) = 1.34.

DTS-CN. Yield: 59%. ¹H NMR (300 MHz, CDCl₃): δ (ppm) 7.75-7.34 (br, m, 6H), 7.10-6.79 (br, m, 4H), 1.26 (br, m, 32H), 0.87 (br, m, 20H). Anal. Calcd: C, 65.54; H, 6.52; N, 2.83. Anal. Found: C, 64.68; H, 6.91; N, 2.39. Mn = 15.6 K; Polydispersity Index (PDI) = 1.86.

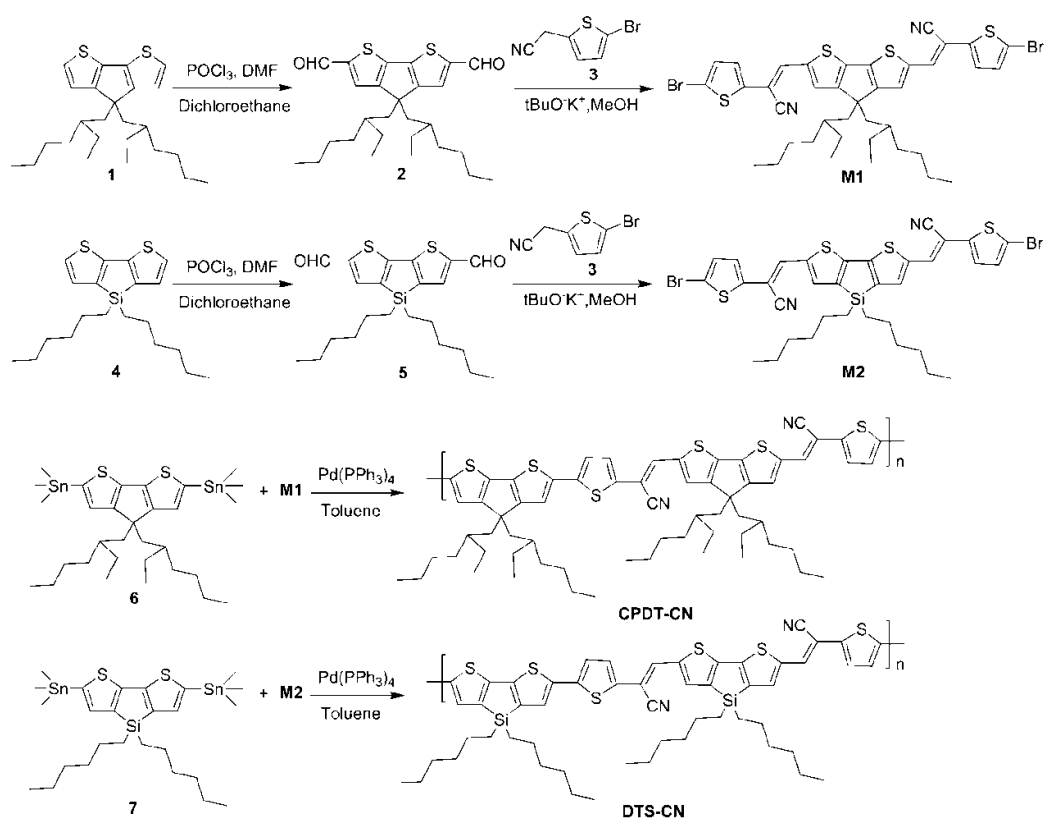


Figure 3.1 Synthetic route for monomers and polymers.

3.3 Results and Discussion

3.3.1 Synthesis and Structural Characterization

The general synthetic procedures for monomers and polymers are outlined in Figure 3.1. Compound **1** or **4** were treated with Vilsmeier reagent to produce the corresponding dicarbaldehyde compounds. Then those compounds (**2** or **5**) were carried out condensation reaction with 5-bromo-2-thiopheneacetonitrile (**3**) in presence of catalytic amounts of potassium-tert-butoxide to form monomers **M1** and **M2**, respectively. Further Stille coupling reaction of corresponding distannyl compounds with **M1** and **M2** in toluene using $\text{Pd}(\text{PPh}_3)_4$ as a catalyst at 110°C for 18 h, polymers **CPDT-CN** and **DTS-CN** were acquired with yields of 66 and 59%, respectively. After purification in the Soxhlet extraction by leaving insoluble

materials with high molecular weights, all polymers are soluble in organic solvents like CHCl_3 , THF, chlorobenzene, and 1,2-dichlorobenzene at room temperature. The molecular weights of polymers were determined by gel permeation chromatography (GPC) against polystyrene standards in THF eluent. Both the polymers have a similar number-average molecular weight (M_n) of 1.6×10^4 with polydispersity index (PDI) ranging 1.34-1.86 (Table 3.1). The thermal stabilities of the polymers were investigated by thermogravimetric analysis (TGA) under nitrogen (Figure 3.2). Compared with **CPDT-CN** (414 °C), **DTS-CN** (430 °C) shows a higher decomposition temperature. Nevertheless, both the polymers have good thermal stabilities, which are important in BHJ solar cell device fabrications and other applications.

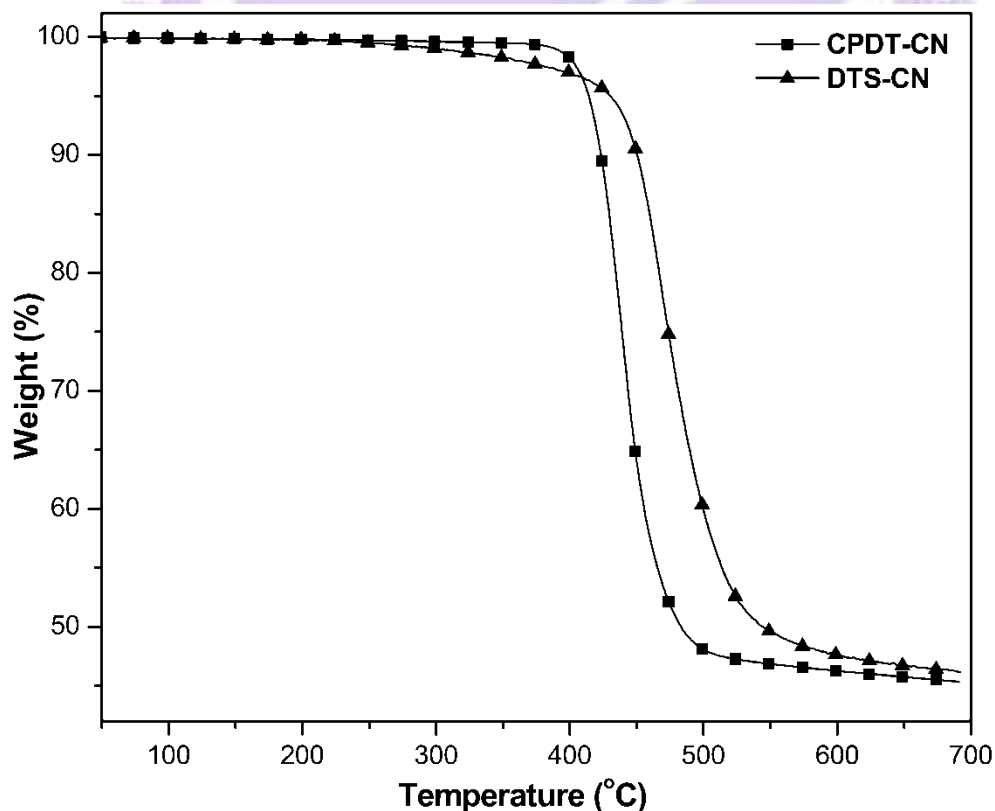


Figure 3.2 TGA measurements of polymers at a heating rate of 10°C/min.

Table 3.1. Molecular Weights and Thermal Properties of Polymers

Polymers	Yield (%)	M_n^a ($\times 10^3$)	M_w^a ($\times 10^3$)	PDI ^a	T_d^b ($^{\circ}\text{C}$)
CPDT-CN	66	16.4	22.0	1.34	414
DTS-CN	59	15.6	29.1	1.86	430

^aMolecular weights (M_n and M_w) and polydispersity index (PDI) values were measured by GPC, using THF as an eluent, polystyrene as a standard. M_n , number average molecular weight. M_w , weight average molecular weight; ^bTemperature ($^{\circ}\text{C}$) at 5% weight loss measured by TGA at a heating rate of $10^{\circ}\text{C}/\text{min}$ under nitrogen.

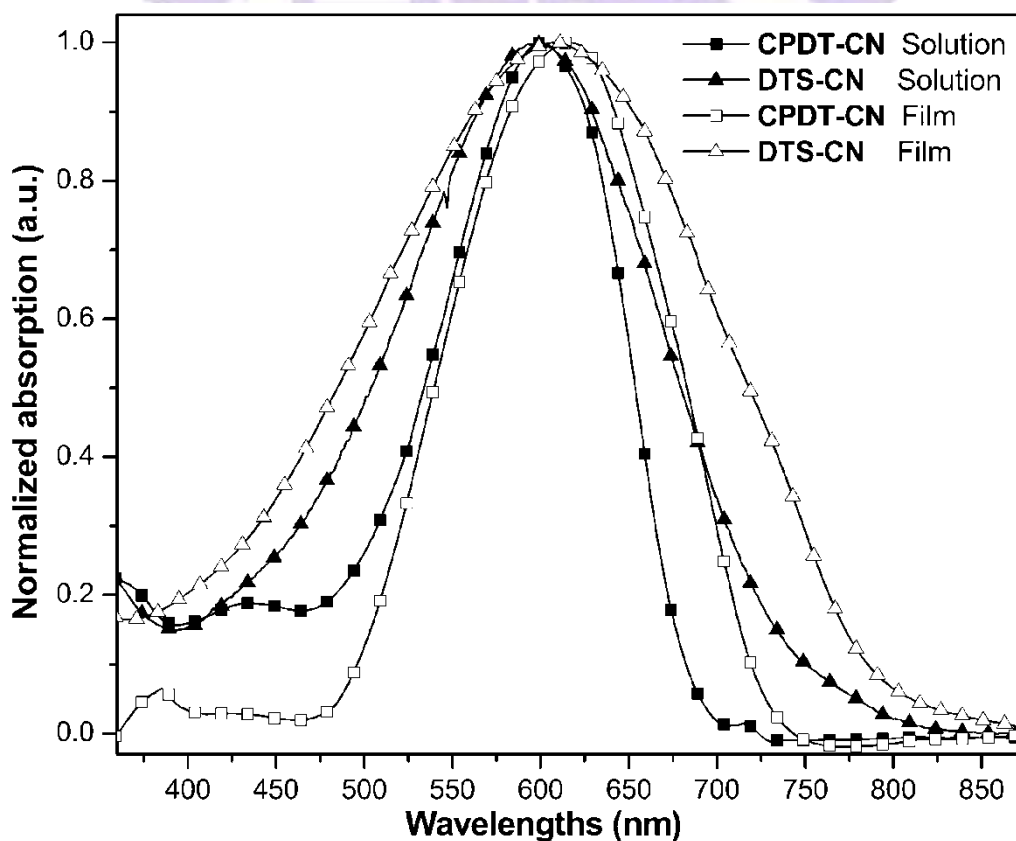


Figure 3.3 Normalized absorption spectra of polymers in dilute chloroform solutions (10^{-6} M) and solid films.

3.3.2 Optical properties

The photophysical characteristics of the polymers were investigated by UV-vis absorption spectroscopy in dilute chloroform solutions (10^{-6} M) and solid films are shown in Figure 3.3, and their optical data are summarized in Table 3.2. All absorption spectra appeared as broad absorption bands from 350 to 800 nm. Reflecting much longer effective conjugation lengths of the extended coplanar CPDT- and DTS-based polymer backbones, the maximum absorption wavelengths ($\lambda_{\text{max,abs}}$) were 604 and 612 nm in solutions and at 621 and 628 nm in solid films for **CPDT-CN** and **DTS-CN**, respectively, which were more red shifted from the corresponding absorption wavelengths of monomers. It is noted that both polymers exhibited maximum absorption wavelengths, longer than those of corresponding homopolymers (565 and 502 nm for polycyclopentadithiophene **PCPDT** and polydithienosilole **PDTs**, respectively),¹¹⁸⁻¹¹⁹ which could be attributed to the strong ICT interactions between donor and acceptor moieties along with the formation of more rigid polymers in the presence of cyano-vinylene groups. Due to the inter-chain associations and π - π stackings of these polymers in solid state, the π - π^* transitions were red shifted (ca. 17 nm) in solid films than those in the corresponding solutions. The optical band gaps (E_g^{opt}) of the polymers determined by the absorption edges of UV-vis spectra in solid films were 1.65 and 1.56 eV for **CPDT-CN** and **DTS-CN**, respectively, which have the similar trends as the maximum absorption wavelengths. In brief, **DTS-CN** possessed the smallest band gap due to the electron-rich dithienosilole donor groups in combination with the cyano-vinylene acceptor groups linked via thiophene units, which promoted an efficient intra-molecular charge transfer and led to an extensive delocalization within the polymer backbones.¹²⁰

Table 3.2 Optical and electrochemical properties of Polymers.

Polymers	Absorption Spectra				Cyclic Voltammetry (vs Ag/Ag ⁺)				
	Solution ^a		Solid film ^b		p-doping		n-doping		
	λ_{\max} (nm)	λ_{\max} (nm)	λ_{edge} (nm)	$E_g^{\text{opt c}}$ (eV)	$E_{\text{ox/onset}}$ (V)	HOMO ^d (eV)	$E_{\text{red/onset}}$ (V)	LUMO ^d (eV)	E_g^{ec} (eV)
CPDT-CN	604	621	751	1.65	0.88	-5.28	-0.78	-3.62	1.66
DTS-CN	612	628	791	1.56	0.90	-5.30	-0.70	-3.70	1.60

^aIn dilute chloroform solution; ^bSpin-coated from chlorobenzene solution; ^cOptical band gap obtained from $E_g = 1240/\lambda_{\text{edge}}$; ^d $E_{\text{HOMO}}/E_{\text{LUMO}} = [-(E_{\text{onset}} - E_{\text{onset}}(\text{FC}/\text{FC}^+ \text{ vs. Ag/Ag}^+)) - 4.8]$ eV where 4.8 eV is the energy level of ferrocene below the vacuum level and $E_{\text{onset}}(\text{FC}/\text{FC}^+ \text{ vs. Ag/Ag}^+) = 0.4$ eV.

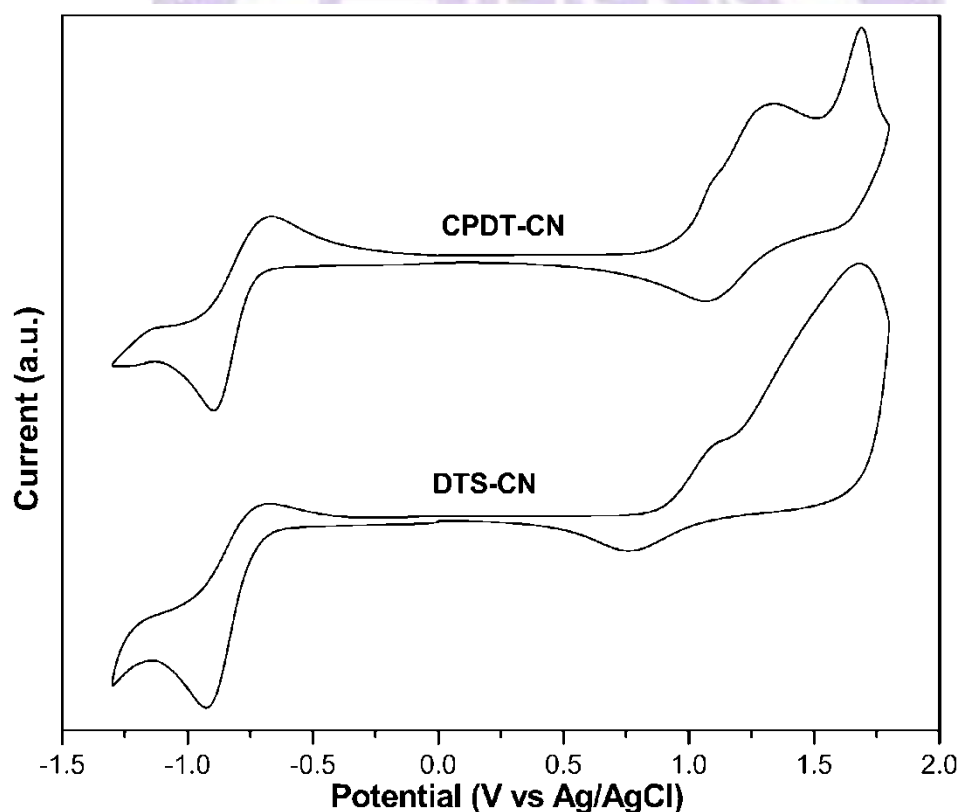


Figure 3.4 Cyclic voltammograms of polymers in solid films at a scan rate of 100 mV/s.

3.3.3 Electrochemical properties

Cyclic voltograms of polymers are illustrated in Figure 3.4 and the related data are summarized in Table 3.2. The HOMO and LUMO energy levels were estimated by the oxidation and reduction potentials from the reference energy level of ferrocene (4.8 eV below the vacuum level) according to the following equation:⁹⁷ $E_{\text{HOMO}}/E_{\text{LUMO}} = [-(E_{\text{onset}} - E_{\text{onset}}(\text{FC/FC}^+ \text{ vs. Ag/Ag}^+)) - 4.8]$ eV where 4.8 eV is the energy level of ferrocene below the vacuum level. It can be seen from Figure 3.4 that both polymers exhibited similar two quasi-reversible or reversible p-doping/dedoping processes at positive potentials (ca. 1.1 and 1.7 V) and one reversible n-doping/dedoping (reduction/reoxidation) process at negative potentials (ca. -0.8 V), which are good signs of high structural stability in the charged state. The onset oxidation potentials ($E_{\text{ox/onset}}$) of polymers **CPDT-CN** and **DTS-CN** were 0.88 and 0.90 V, and the onset reduction potentials ($E_{\text{red/onset}}$) were -0.78 and -0.70 V, respectively. Polymers **CPDT-CN** and **DTS-CN** have the estimated HOMO levels of -5.28 and -5.30 eV and LUMO levels of -3.62 and -3.60 eV, correspondingly. As all HOMO levels were below the air oxidation threshold, the polymers should show good air stabilities.¹²¹ It is also worthy noting that the electrochemical band gaps (E_{g}^{ec} , 1.66 and 1.60 eV for **CPDT-CN** and **DTS-CN**, respectively) calculated from $E_{\text{g}}^{\text{ec}} = (E_{\text{ox/onset}} - E_{\text{red/onset}})$ are in good agreements with the optical band gap values observed from UV-vis spectra ($E_{\text{g}}^{\text{opt}}$, 1.65 and 1.56 eV). All these electrochemical characteristics are within the desirable range for the ideal polymers to be utilized in the organic photovoltaic applications.

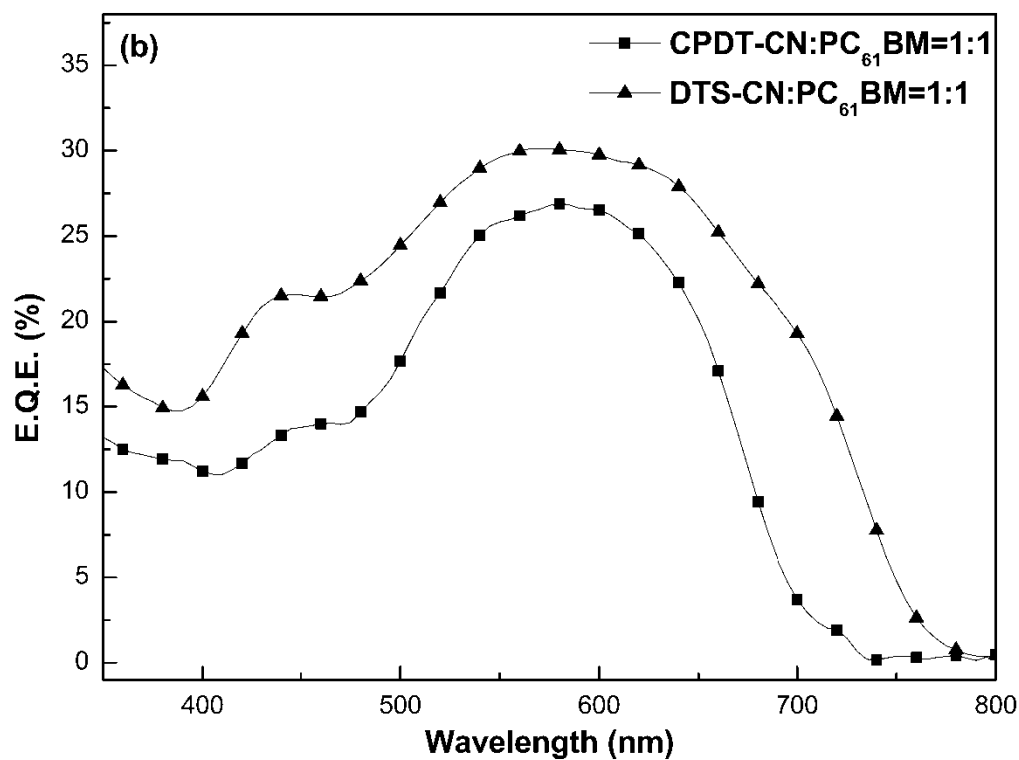
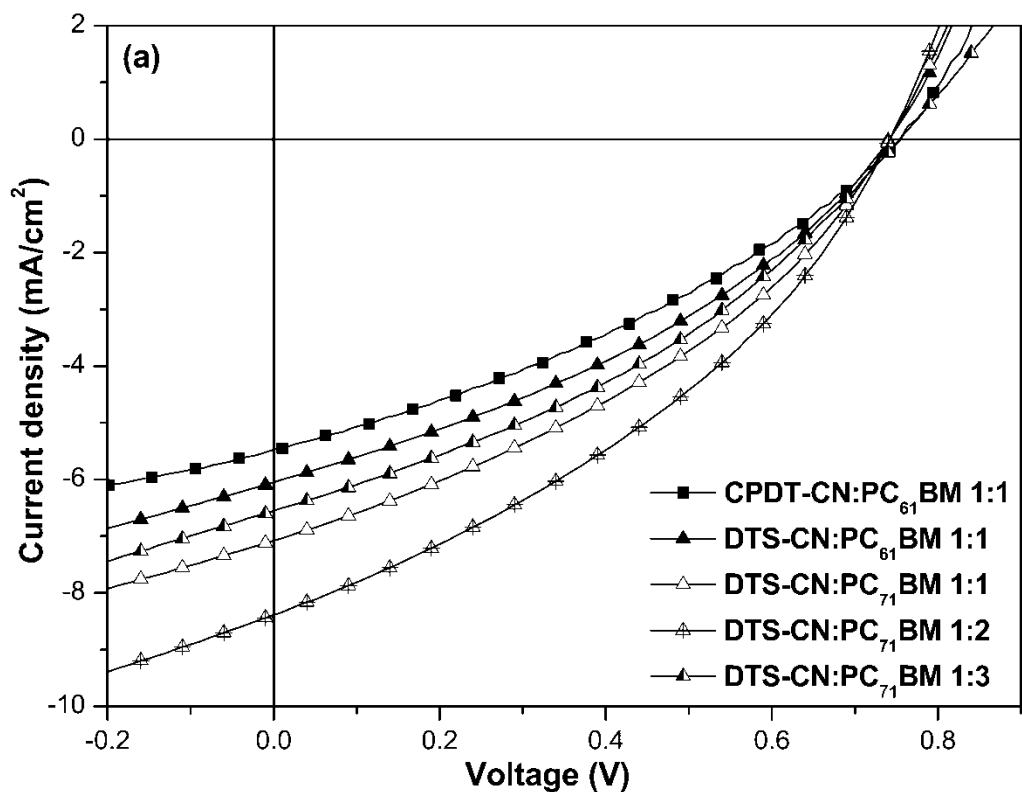


Figure 3.5 (a) Current-voltage curves of polymer solar cells using polymer:PCBM blends under the illumination of AM 1.5G, 100 mW/cm^2 . (b) EQE curves of the PSC devices based on polymers/ PC_{61}BM (1:1, w/w).

3.3.4 Photovoltaic properties

To investigate the potential use of these polymers in polymer solar cell (PSC), the bulk heterojunction PSC devices with a configuration of ITO/PEDOT:PSS/CPDT-CN or DTS-CN:PCBM/Ca/Al were fabricated from an active layer where polymers were blended with PC₆₁BM in a weight ratio of 1:1 w/w initially. Later on, the active layer compositions were modified with various weight ratios for the optimum polymer DTS-CN with PC₇₁BM. Figure 3.5 (a) and 3.5 (b) illustrate the *J-V* curves (current density *J* versus voltage *V*) and external quantum efficiency (EQE) curves as a function of wavelengths, respectively. The photovoltaic properties, i.e., the values of open circuit voltage (V_{oc}), short circuit current density (J_{sc}), fill factor (FF), and power conversion efficiency (PCE) of BHJ solar cell devices are listed in Table 3.3. Due to negligible differences in HOMO levels of both polymers, they exhibited similar V_{oc} values (0.74-0.75 V) in the BHJ solar cell devices containing CPDT-CN or DTS-CN:PC₆₁BM in 1:1 weight ratio. With the similar V_{oc} values and fill factors (33.9-35.7 %), the PCE values of polymers CPDT-CN and DTS-CN were dependent on their J_{sc} values of 5.46 and 6.05 mA/cm², respectively. The PSC device based on the polymer blend of DTS-CN:PC₆₁BM (1:1 wt%) reached a higher PCE value of 1.60% with V_{oc} = 0.74 V, J_{sc} = 6.05 mA/cm², and FF = 35.7%. As reported, the more balanced hole and electron transport properties in the films and the higher hole mobilities are favorable factors for LBG polymers utilized in the BHJ solar cell devices,¹²² so the PCE and J_{sc} values in the PSC device based on DTS-CN were higher than that based on CPDT-CN. This may be due to the higher hole mobility (9.82×10^{-4} cm²/V s) and more balanced charge transport ($\mu_e/\mu_h = 1.6$) in the polymer blend of DTS-CN compared with those properties (5.99×10^{-4} cm²/V and 3.4, respectively)

of the polymer blend of **CPDT-CN**. Furthermore, from the absorption spectra and EQE curves (Figure 3.5 (b)), it is evident that **DTS-CN** exhibited broader absorption bands and higher EQE values between 350 to 800 nm than those of **CPDT-CN**, which may be another reason for the higher J_{sc} value.

Table 3.3 Photovoltaic properties of PSC devices with the configuration of ITO/PEDOT:PSS/Polymer:PCBM/Ca/Al.

Active layer	Hole mobility (cm^2/Vs)	Electron mobility (cm^2/Vs)	V_{oc} (V)	J_{sc} (mA/cm^2)	FF (%)	PCE (%)
CPDT-CN: PC ₆₁ BM=1:1	5.99×10^{-4}	2.01×10^{-3}	0.75	5.46	33.9	1.39
DTS-CN: PC ₆₁ BM=1:1	9.82×10^{-4}	1.65×10^{-3}	0.74	6.05	35.7	1.60
DTS-CN: PC ₇₁ BM=1:1			0.74	7.07	35.9	1.89
DTS-CN: PC ₇₁ BM=1:2			0.74	8.39	36.1	2.25
DTS-CN: PC ₇₁ BM=1:3			0.75	6.55	36.5	1.79

Since the best performance of PSC device was observed in the previous optimum polymer blend of **DTS-CN:PC₆₁BM** (1:1 wt%) as an active layer, the PSC devices as a function of polymer blends **DTS-CN:PC₇₁BM** in various weight compositions were fabricated. Another electron acceptor PC₇₁BM was used to optimize the device properties due to its stronger light absorption in the visible region than that of PC₆₁BM.⁹ The V_{oc} values observed in **DTS-CN:PC₇₁BM** solar cells were fairly stable in all polymer blend compositions (1:1 to 1:3 w/w) with PC₇₁BM, but the J_{sc} , FF, and PCE values are strongly dependent on the donor-to-acceptor weight ratios in the active layers. The PSC device based on **DTS-CN:PC₇₁BM** (1:2,w/w) exhibited the highest PCE= 2.25% with V_{oc} = 0.74 V, J_{sc} =8.39 mA cm⁻², and FF=36.1%. Though these polymers exhibited a higher J_{sc} compared with the other CPDT and DTS- based

polymers, their efficiencies were limited by their low FF and EQE values. Therefore, if the EQE values of the PSC devices can be enhanced by increasing the thickness of the active layer without hampering charge separation and transporting properties, the PSC device performance can be improved significantly. Low EQE values were also observed in some other LBG polymer systems, but this problem can be solved by developing new electron acceptor materials to replace PCBM.¹²³

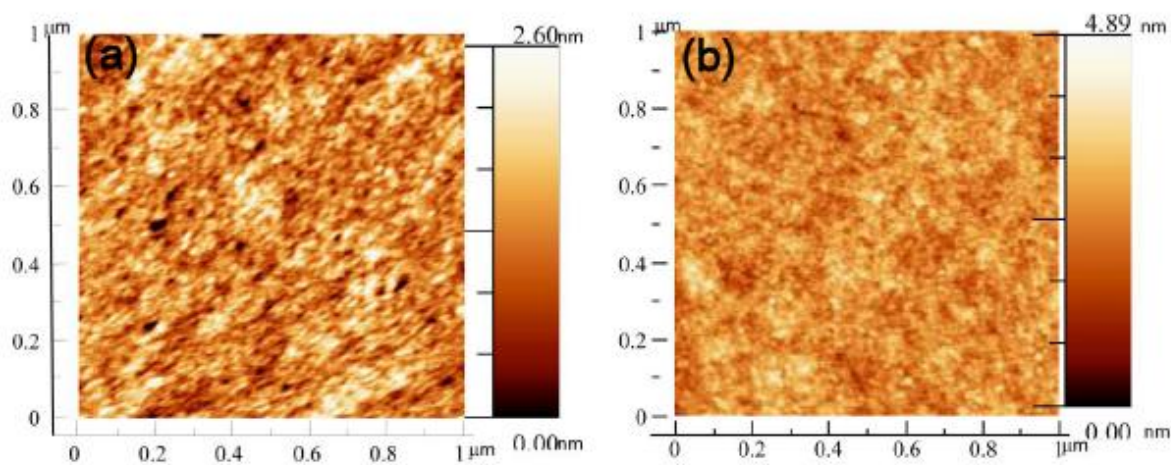
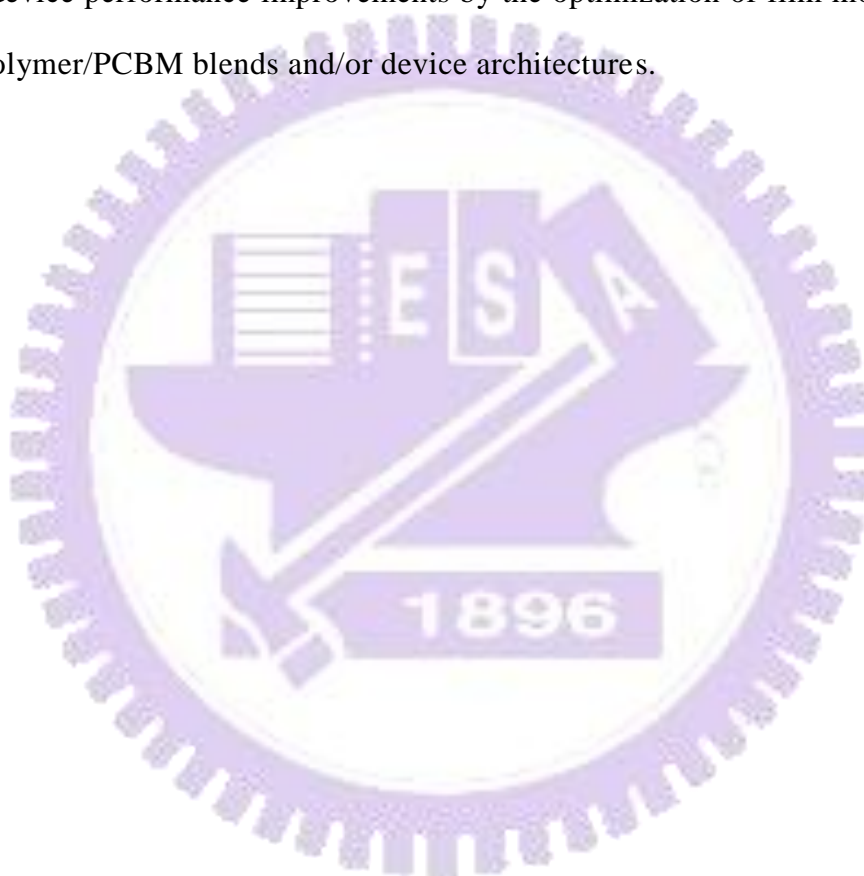


Figure 3.6 AFM images of (a) CPDT-CN: PC₆₁BM 1:1 (w/w) and (b) DTS-CN: PC₆₁BM 1:1 (w/w).

3.4 Conclusion

The concept of incorporation of electron deficient β -cyano-vinylene groups with donor-acceptor polymer architectures was utilized to improve the efficiencies of polymer solar cells. Cyano-vinylene groups were introduced via palladium(0)-catalyzed Stille coupling reactions into electron-rich building blocks, such as cyclopentadithiophene and dithienosilole to yield LBG polymers (CPDT-CN and DTS-CN). These polymers showed excellent charge-transporting properties with high hole mobilities in the range of $(5.99-9.82) \times 10^{-4} \text{ cm}^2\text{V}^{-1}\text{s}^{-1}$ and good processabilities for PSC applications. Due to the lowest band gap and the

highest hole mobility with more balanced charge transport of **DTS-CN** (with Si atom), an optimum PSC device based on the blended polymer **DTS-CN:PC₇₁BM** = 1:2 (w/w) achieved the maximum power conversion efficiency (PCE) value up to 2.25 %, with $V_{oc} = 0.74$ V, $J_{sc} = 8.39$ mA/cm², and FF = 36% (under AM 1.5 G 100 mW/cm²). Regardless of the high open-circuit voltages and the large short-circuit currents of all PSC devices, the low fill factor values indicated the possibility of further device performance improvements by the optimization of film morphology of the polymer/PCBM blends and/or device architectures.



Chapter 4.

Synthesis and Applications of Main-Chain RuII Metallo-Polymers Containing Bis-terpyridyl Ligands with Various Benzodiazole Cores for Solar Cells

4.1 Introduction

In the extensive search of new materials for optoelectronics applications, supramolecular metallo-polymers have gained much interest in last decades.¹²⁴⁻¹²⁷ The self-recognition and self-assembly of functional structures into supramolecular metallo-architectures through the interactions of transition metal ions and appropriate chelating ligands has afforded many intriguing architectures that attains highly attention in modern supramolecular chemistry.¹²⁸⁻¹²⁹ Polypyridyl ligands, especially 2,2':6',2''-terpyridine (terpy) derivatives, which have high binding affinities towards transition-metal ions due to $d\pi-p\pi^*$ back-bonding of metal ions to pyridine rings have been utilized recently for multinuclear supramolecular interactions.¹³⁰⁻¹³² Terpy derivatives bearing π -conjugated substituents at the 4'-position possess fascinating photophysical, electrochemical, catalytic, and magnetic properties with promising applications in the field of self-assembled molecular devices and photoactive molecular wires,¹³³ and their properties can be tuned by varying substituents at 4'-position of terpy moieties.¹³⁴⁻¹³⁵ Furthermore, chemically and thermally stable ditopic bis-terpyridine derivatives, where two terpy units are linked back-to-back with a covalent bond through a spacer, are able to form stable complexes with a large variety of transition-metal ions for the design of functional materials.¹³⁶ Three chelating pyridyl units in terpy ligands offer a higher binding constants and the formation of distorted octahedral 2:1 ligand-metal complexes. In particular, by

proper selections of metal-ligand combinations, it is possible to realize the formation of ligand-metal complexes from kinetically labile to inert but nevertheless thermodynamically stable bonds.

Constable et al. have developed the concept concerning the utilization of ditopic bis-terpyridyl ligands as building blocks for coordination oligomers and polymers.¹³⁷ By coordinating to suitable metal ions, the electronic properties of these materials can be tuned and that highlights their potential in the applications of new functional materials.¹³⁸⁻¹⁴⁰ In the past years, a large number of terpy complexes containing heavy transition metal ions, such as ruthenium(II), iridium(III), or osmium(II), as photoactive species, as well as coordination polymers built up from terpy ligands have been introduced by several research groups.¹³⁶ Zinc(II) ions have also recently attracted much interest as novel templates for the fabrication of structurally well-defined photoluminescent and electroluminescent supramolecular metallo-cycles and metallo-polymers.¹⁴¹⁻¹⁴⁶ In our previous reports,¹⁴⁴⁻¹⁴⁶ a series of terpyridyl Zn(II) metallo-polymers containing polyfluorene backbones as emitters were fabricated into PLED devices with multilayer structures.

Nowadays, some terpyridyl Ru(II) complexes have attracted researchers to use in the applications of photovoltaic cells (PVC).^{62-65,147-150} The insertion of ruthenium metals into conjugated backbones has several advantages, such as to facilitate the charge generation by extending its absorption range due to its characteristic long-lived metal to ligand charge transfer (MLCT) transition¹³⁶ and to exhibit a reversible Ru^{II,III} redox process along with some ligand-centered redox processes. Motivations for examining the potential incorporation of such conjugated polyelectrolytes into solar cell development include the easy

processability, layer-by-layer (LBL) processing capability, and also due to efficiently quenched by electron acceptors. Recently, terpyridyl Ru(II) complexes have been utilized in bulk heterojunction (BHJ) PVC devices by using LBL self-assembled techniques. Chan et. al. reported that the use of a terpyridyl Ru(II) complex containing conjugated polymer (Ru-PPV) and sulfonated polyaniline (SPAN) for the fabrication of different multilayer PVCs by LBL deposition method. The short-circuit currents in the PVC devices were measured ca. 7.5-32.9 $\mu\text{A}/\text{cm}^2$ and the PCE values were in the range of 0.95-4.4 $\times 10^{-3}$ %.⁶⁵ They also synthesized conjugated polymers with pendant Ru^{II} terpyridine trithiocyanato complexes and applied in bulk heterojunction photovoltaic cells with high PCE values ca. 0.12%.⁶² Similarly, Mikroyannidis et al used metallo-polymers in bulk heterojunction photovoltaic cells as a buffer layer along with an active layer of polymer blend P3HT:PCBM (1:1 w/w) and found the maximum power conversion efficiency value of 0.71% among four metallo-polymers.⁶³ In all cases, the PCE values were limited either by the low open-circuit voltage (V_{oc}) or low short circuit current (J_{sc}). Due to relatively high HOMO levels and less sensitization ranges in all reported polymers, there were inefficient photocurrents generated which probably affected their PCE values.

One of the feasible solutions to conquer these problems, i.e. to get a higher V_{oc} value and a more favorable overlap of the absorption spectra from both active layer and solar emission, is to introduce electron donor-acceptor structures to the cores of bis-terpyridyl ligands. By choosing different electron donors and acceptors, their absorption edges can be extended due to the intramolecular charge transfer (ICT) between them and also the energy band structures, i.e., highest occupied molecular orbital (HOMO) and lowest unoccupied molecular orbital

(LUMO) levels, of these materials can be tuned. The incorporation of the thiophene donor units with benzodiazole acceptor units at the cores of bis-terpyridyl ligands in Ru^{II}-containing metallo-polymers to have better photophysical, electrochemical, and photovoltaic properties are very intriguing and thus to motivate this study. Here, we report the design, synthesis, properties, and device applications of Ru^{II}-containing metallo-polymers (**P1-P3**) containing donor-acceptor (D-A) bis-terpyridyl ligands bearing different benzodiazole acceptors, including benzothiadiazole, benzoselenodiazole, and benzoxadiazole cores sandwiched between symmetrical thiophene and terpyridyl units. By introducing such D-A structures, broad absorption ranges ca. 300-750 nm and ideal HOMO/LUMO levels of the metallo-polymers were obtained. The effects of their donor-acceptor strengths on the electronic and optoelectronic properties were also investigated. In addition, the PVC devices fabricated by these bis-terpyridyl ligands (**M1-M3**) and metallo-polymers (**P1-P3**) with [6,6]-phenyl-C₆₁-butyric acid methyl ester (PCBM) inserted between a transparent anode (ITO/PEDOT:PSS) and a cathode (Ca) were explored, and all photovoltaic parameters obtained are also comparable with the BHJ solar cells fabricated from ionic polythiophene and C₆₀.⁶⁶⁻⁶⁷

4.2 Experimental Section

4.2.1 Materials

All chemicals and solvents were reagent grades and purchased from Aldrich, ACROS, Fluka, TCI, TEDIA, and Lancaster Chemical Co. Toluene, tetrahydrofuran, and diethyl ether were distilled over sodium/benzophenone to keep anhydrous before use. Chloroform (CHCl₃) was purified by refluxing with

calcium hydride and then distilled. If not otherwise specified, the other solvents were degassed by nitrogen 1 h prior to use.

4.2.2 Measurements and Characterization

¹H NMR spectra were recorded on a Varian Unity 300 MHz spectrometer using CDCl₃ and DMSO-*d*₆ solvents. Elemental analyses were performed on a HERAEUS CHN-OS RAPID elemental analyzer. Thermogravimetric analyses (TGA) were conducted with a TA Instruments Q500 at a heating rate of 10°C/min under nitrogen. Viscosity measurements were proceeded by 10% weight of metallo-polymer solutions (in NMP) in contrast to that proceeded by bis-terpyridyl ligand solutions under the same condition (with viscosity $\eta = 6$ cp) on a BROOKFILEL DV-III+ RHEOMETER system at 25°C (100 RPM, Spindle number 4). UV-visible absorption were recorded in dilute chloroform (for **M1-M3**) and DMF (for **P1-P3**) solutions (10^{-6} M) on a HP G1103A spectrophotometer. Solid films of UV-vis measurements were spin-coated on quartz substrates from chloroform and DMF solutions with a concentration of 10 mg/mL for bis-terpyridyl ligands (**M1-M3**) and polymers (**P1-P3**), respectively. UV-vis titrations were performed by taking 10^{-5} M of bis-terpyridyl ligands (**M1-M3**) in the co-solvent of chloroform: acetonitrile (8:2 v/v), and titrated with 50 μ l aliquots of 3.9×10^{-4} M solutions containing metal salts Zn(OAc)₂ in the EtOH. Cyclic voltammetry (CV) measurements were performed using a BAS 100 electrochemical analyzer with a standard three-electrode electrochemical cell in a 0.1 M tetrabutylammonium hexafluorophosphate (Bu₄NPF₆) solution (in acetonitrile) at room temperature with a scanning rate of 100 mV/s. During the CV measurements, the solutions were purged with nitrogen for 30 s. In each case, a carbon working electrode coated with a thin layer of monomers or polymers, a

platinum wire as the counter electrode, and a silver wire as the quasi-reference electrode were used, and Ag/AgCl (3 M KCl) electrode was served as a reference electrode for all potentials quoted herein. The redox couple of ferrocene/ferrocenium ion (Fc/Fc⁺) was used as an external standard. The corresponding HOMO and LUMO levels were calculated using $E_{\text{ox/onset}}$ and $E_{\text{red/onset}}$ for experiments in solid films, which were performed by drop-casting films with the similar thicknesses from THF or DMF solutions (ca. 5 mg/mL).

4.2.3 Device fabrication of polymer solar cells

The photovoltaic (PV) cells in this study were composed of an active layer of blended bis-terpyridyl ligands (**M1-M3**) or metallo-polymers (**P1-P3**) with [6,6]-phenyl-C₆₁-butyric acid methyl ester (PCBM) in solid films, which was sandwiched between a transparent indium tin oxide (ITO) anode and a metal cathode. Prior to the device fabrication, ITO-coated glass substrates (1.5×1.5 cm²) were ultrasonically cleaned in detergent, deionized water, acetone, and isopropyl alcohol sequentially. After routine solvent cleaning, the substrates were treated with UV ozone for 15 min. Then, a modified ITO surface was obtained by spin-coating a layer of poly(ethylene dioxythiophene): polystyrenesulfonate (PEDOT:PSS) (~30 nm). After baking at 130°C for one hour, the substrates were transferred to a nitrogen-filled glove box. The PVC devices were fabricated by spin-coating solutions of blended bis-terpyridyl ligands (**M1-M3**) or metallo-polymers (**P1-P3**):PCBM (1:1 w/w) onto the PEDOT:PSS modified substrates at 1500 rpm for 60 s (ca. 100 nm), and placed in a covered glass Petri dish. Initially, the blended solutions were prepared by dissolving both bis-terpyridyl ligands (**M1-M3**) and PCBM (1:1 w/w) in chloroform (20 mg/1 mL) and both metallo-polymers (**P1-P3**) and PCBM (1:1 w/w) in DMF (20 mg/1 mL),

and followed by continuous stirring for 12 h at 50°C. Finally, a calcium layer (30 nm) and a subsequent aluminum layer (100 nm) were thermally evaporated through a shadow mask at a pressure below 6×10^{-6} Torr, where the active area of the device was 0.12 cm^2 . All PVC devices were prepared and measured under ambient conditions. The solar cell testing was done inside a glove box under simulated AM 1.5G irradiation (100 mW/cm^2) using a Xenon lamp based solar simulator (Thermal Oriel 1000W). The light source was a 450 W Xe lamp (Oriel Instrument, model 6266) equipped with a water-based IR filter (Oriel Instrument, model 6123NS). The light output from the monochromator (Oriel Instrument, model 74100) was focused onto the photovoltaic cell under test.

4.2.4 Synthesis of Monomers and Polymers

4'-(2-Bromo-5-thienyl)-2,2',6',2''-terpyridine (1). Aqueous potassium hydroxide (8.4 g, 150 mmol in 40 mL water) was added to a solution of 2-Acetylpyridine in 400 mL of methanol. The reaction mixture was stirred for 30 min and then 9.55 g (50 mmol) of 2-bromothiophene carboxaldehyde in 50 mL of methanol was added dropwise. The solution was stirred overnight at room temperature. The solvent was then evaporated off under vacuum and extracted with dichloromethane. Then the crude was taken for the next step without further purifications. To the above crude an excess amount (50 gm) ammonium acetate in 200 mL of ethanol/acetic acid (2/1) was added. The mixture was heated to reflux for 6 h. The reaction mixture was cooled to room temperature, poured onto ice and water (1 liter) to give a pale yellow precipitate that was recrystallized with ethanol to yield the title compound as a white solid. (9.25 g, 47%). $^1\text{H NMR}$ (CDCl_3 , 300 MHz, δ): 8.72 (d, $J = 3.2 \text{ Hz}$, 2H), 8.61 (d, $J = 7.8 \text{ Hz}$, 2H), 8.58 (s, 2H), 7.88 (ddd, $J = 1.8 \text{ Hz}$, $J = 7.5 \text{ Hz}$, $J = 7.5 \text{ Hz}$, 2H), 7.51 (d, $J = 4.2 \text{ Hz}$, 1H), 7.35 (ddd, $J = 1 \text{ Hz}$, $J = 4.8 \text{ Hz}$, J

=7.8 Hz, 2H), 7.11 (d, $J = 3.9$ Hz, 1H). ^{13}C NMR (CDCl_3 , 75 MHz, δ): 156.5, 156.1, 149.5, 143.6, 142.8, 137.3, 131.6, 126.3, 124.4, 121.7, 116.6, 114.6.

4'-(5-Tributylstannanyl-thiophen-2-yl)-[2,2';6',2'']terpyridine (2). To a solution of 4'-(2-Bromo-5-thienyl)-2,2',6',2''-terpyridine (4.00 g, 10.15 mmol) in toluene (20 mL), bis(tributyltin) (13 mL, 25 mmol, 2.5 equiv) was added in one portion, and the mixture was degassed with argon. $(\text{PPh}_3)_4\text{Pd}(0)$ (400 mg, 0.34 mmol) was added, and the mixture was refluxed overnight. The reaction mixture was cooled to room temperature, filtered and solvents were removed by reduced pressure. The residue was purified by column chromatography on alumina with 3:1 hexane/ ethyl acetate to give product as slightly yellowish oil, (3.2 g, 52%). ^1H NMR (CDCl_3 , 300 MHz, δ): 8.74 (d, $J = 3.2$ Hz, 2H), 8.69 (s, 2H), 8.63 (d, $J = 7.8$ Hz, 2H), 7.88 (ddd, $J = 1.8$ Hz, $J = 7.5$ Hz, $J = 7.5$ Hz, 2H), 7.81 (d, $J = 4.2$ Hz, 1H), 7.36 (ddd, $J = 1$ Hz, $J = 4.8$ Hz, $J = 7.8$ Hz, 2H), 7.21 (d, $J = 3.9$ Hz, 1H), 1.55–1.63 (m, 6H), 1.30–1.44 (m, 6H), 1.09–1.15 (m, 6H), 0.92 (t, $J = 7.3$ Hz, 9H). ^{13}C NMR (CDCl_3 , 75 MHz, δ): 157.5, 155.1, 149.5, 147.6, 141.8, 137.3, 131.6, 127.3, 124.4, 121.7, 117.6, 114.6, 29.8, 28.0, 14.4, 10.4.

General Synthetic Procedure for Bis-terpyridyl Ligands (M1-M3)

M1-M3 were prepared via Stille coupling reaction using tetrakis(triphenylphosphine)palladium as a catalyst. In a flame dried two-neck flask, 1.00 eq of dibromo compounds (**5a-5c**) and 2.50 eq of compound **2** in toluene were degassed with Argon. Then, 0.03 eq $\text{Pd}(\text{PPh}_3)_4$ were added and refluxed for 2 days. The reaction mixtures were cooled to room temperature, and solvents were removed by reduced pressure. After removal of the solvents, the product was precipitated from methanol. Further purification was achieved by

column chromatography on alumina with chloroform as an eluant to give the products.

M1. According to the above-mentioned general procedure, **M1** was obtained as a purple solid (yield: 68%). ^1H NMR (CDCl_3 , 300 MHz, δ): 8.77 (d, $J=4.2$ Hz, 4H), 8.63 (m, 8H), 7.91 (s, 2H), 7.85 (dd, $J=7.8$ Hz, $J=1.8$ Hz, 4H), 7.72 (s, 2H), 7.69 (d, $J=3.9$ Hz, 2H), 7.35 (dd, $J=7.8$ Hz, $J=1.8$ Hz, 4H), 7.22 (d, $J=3.9$ Hz, 2H), 2.87(t, $J=6.9$ Hz, 4H), 1.75 (m, 4H), 1.40-1.29 (m, 12H), 0.93(t, $J=5.4$ Hz, 6H). ^{13}C NMR (CDCl_3 , 75 MHz, δ): 156.29, 149.43, 149.35, 143.29, 141.28, 138.26, 137.10, 132.95, 132.09, 130.91, 129.51, 128.83, 126.60, 125.47, 124.16, 121.54, 117.84, 116.94, 31.96, 30.69, 29.98, 29.55, 22.90, 14.36. MS (FAB): m/z [M^+] 1096; calcd m/z [M^+] 1095.49. Element Anal. Calcd for $\text{C}_{64}\text{H}_{54}\text{N}_8\text{S}_5$: C, 70.17; H, 4.97; N, 10.23; Found: C, 69.51; H, 5.26; N, 10.15.

M2. According to the above-mentioned general procedure, **M2** was obtained as a black solid (yield: 63%). ^1H NMR (CDCl_3 , 300 MHz, δ): 8.74 (d, $J=4.2$ Hz, 4H), 8.61 (m, 8H), 7.85 (dd, $J=7.8$ Hz, $J=1.8$ Hz, 4H), 7.78 (s, 2H), 7.67 (d, $J=3.9$ Hz, 2H), 7.62 (s, 2H), 7.35 (dd, $J=7.8$ Hz, $J=1.8$ Hz, 4H), 7.19 (d, $J=3.6$ Hz, 2H), 2.84 (t, $J=6.9$ Hz, 4H), 1.74 (m, 4H), 1.40-1.29 (m, 12H), 0.93(t, $J=5.4$ Hz, 6H). ^{13}C NMR (CDCl_3 , 75 MHz, δ): 158.41, 156.22, 149.31, 143.22, 141.15, 140.79, 138.44, 137.83, 137.05, 132.93, 130.51, 127.98, 126.54, 125.44, 124.11, 121.67, 117.84, 116.88, 31.99, 30.63, 29.98, 29.61, 22.93, 14.39. MS (FAB): m/z [M^+] 1143; calcd m/z [M^+] 1142.39. Element Anal. Calcd for $\text{C}_{64}\text{H}_{54}\text{N}_8\text{S}_4\text{Se}$: C, 67.29; H, 4.76; N, 9.81. Found: C, 66.77; H, 5.30; N, 9.63.

M3. According to the above-mentioned general procedure, **M3** was obtained as a dark purple solid (yield: 76%). ^1H NMR (CDCl_3 , 300 MHz, δ): 8.75 (d, $J=4.2$ Hz, 4H), 8.69 (m, 8H), 7.96 (s, 2H), 7.87 (dd, $J=7.2$ Hz, $J=1.8$ Hz, 4H), 7.73 (d,

$J = 3.6$ Hz, 2H), 7.50 (s, 2H), 7.37 (dd, $J = 6.9$ Hz, $J = 1.2$ Hz, 4H), 7.25 (d, $J = 3.9$ Hz, 2H), 2.88 (t, $J = 7.2$ Hz, 4H), 1.78 (m, 4H), 1.40-1.29 (m, 12H), 0.93 (t, $J = 6.9$ Hz, 6H), ^{13}C NMR (CDCl_3 , 75 MHz, δ): 155.72, 148.96, 148.35, 143.10, 141.16, 138.10, 137.36, 133.05, 132.09, 130.68, 129.41, 128.63, 126.85, 125.28, 122.94, 121.61, 117.69, 116.97, 31.98, 30.60, 30.03, 29.60, 22.94, 14.38. MS (FAB): m/z [M⁺] 1078; calcd m/z [M⁺] 1078.33. Element Anal. Calcd for $\text{C}_{64}\text{H}_{54}\text{N}_8\text{S}_4\text{O}$: C, 71.21; H, 5.04; N, 10.38. Found: C, 70.75; H, 5.21; N, 10.11.

General Procedure for Metallo-Polymers (P1-P3)

In a flame dried flask, a mixture of $\text{RuCl}_3 \cdot 3\text{H}_2\text{O}$ (0.11 mmol) and AgBF_4 (0.38 mmol) was refluxed for 2 h in acetone (15 mL). After cooling to room temperature, the precipitated AgCl was filtered off, and the obtained solution is evaporated to dryness. The remaining solid was redissolved in *n*-butanol (15 mL), and to this solution, bis-terpyridyl ligand **M1**, **M2**, or **M3** (0.1 mmol) was added, and the resulting solution is refluxed for 5 days. As soon as the precipitation of the formed polymer was observed, a small portion of DMA was added to the mixture ($\Sigma \approx 20$ mL) to redissolve the product. Finally, an excess of NH_4PF_6 (50 mg in 20 mL DMA) was added to the hot solution and stirring was continued for 1 h. The resulting solution is dropwise poured into methanol (200 mL). The precipitated metallo-polymer product was filtered off, washed with methanol (200 mL). Further purification was achieved by repetitively dissolving the metallo-polymer in NMP (2 mL) and precipitating from diethyl ether. Finally, the products were dried under vacuum at 40 °C for 24 h.

P1. According to the above-mentioned procedure, metallo-polymer **P1** was obtained as a dark solid (yield: 66%). ^1H NMR (DMSO-d_6 , 300 MHz, δ): 9.36 (br, 4H), 9.12 (br, 4H), 8.52 (br, 2H), 8.24 (br, 8H), 7.67 (br, 6H), 7.31 (br, 4H), 3.05

(br, 4H), 1.86 (br, 4H), 1.25-1.40 (br, 12H), 0.92 (br, 6H).

P2. According to the above-mentioned procedure, metallo-polymer **P2** was obtained as a dark solid (yield: 58%). ^1H NMR (DMSO- d_6 , 300 MHz, δ): 9.36 (br, 4H), 9.12 (br, 4H), 8.48 (br, 2H), 8.14 (br, 8H), 7.68 (br, 6H), 7.30 (br, 4H), 3.08 (br, 4H), 1.83 (br, 4H), 1.20-1.53 (br, 12H), 0.91 (br, 6H).

P3. According to the above-mentioned procedure, metallo-polymer **P3** was obtained as a dark solid (yield: 77%). ^1H NMR (DMSO- d_6 , 300 MHz, δ): 9.39 (br, 4H), 9.13 (br, 4H), 8.54 (br, 2H), 8.10 (br, 8H), 7.65 (br, 6H), 7.33 (br, 4H), 2.94 (br, 4H), 1.83 (br, 4H), 1.20-1.53 (br, 12H), 0.89 (br, 6H).

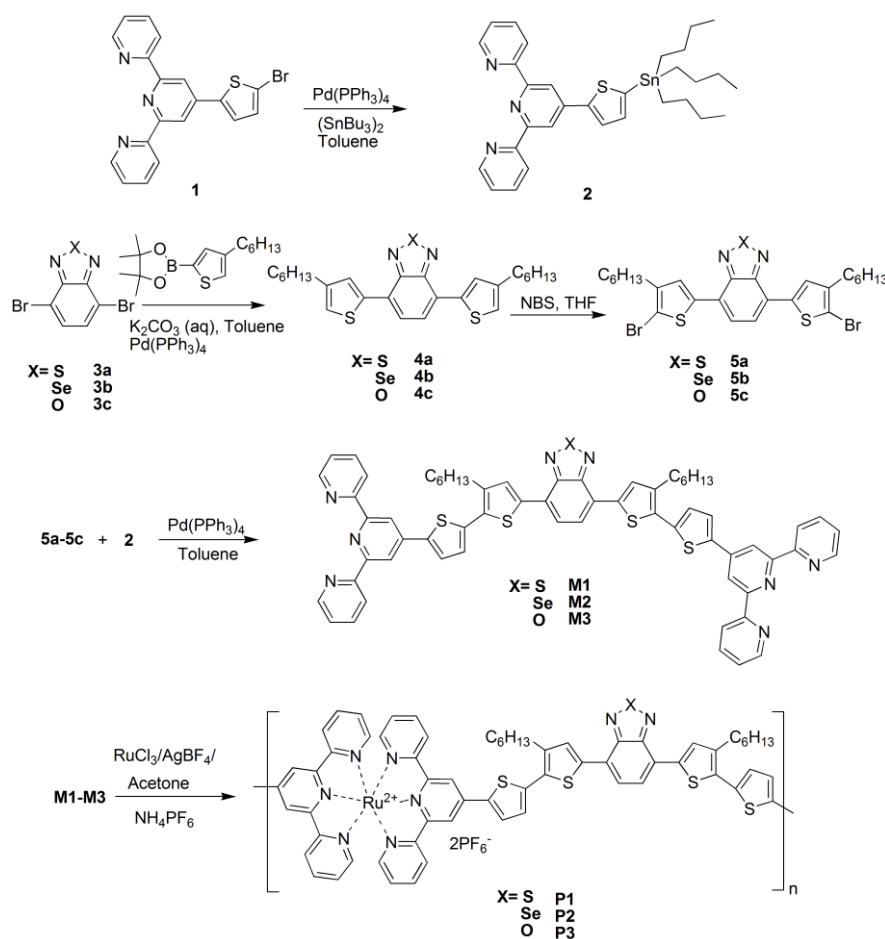


Figure 4.1 Synthetic Route for Bis-terpyridyl Ligands (**M1-M3**) and Ru^{II} -containing Metallo-Polymers (**P1-P3**)

4.3 Results and Discussion

4.3.1 Synthesis and Structural Characterization

The general synthetic routes of ditopic bis-terpyridyl ligands (**M1-M3**) and metallo-polymers (**P1-P3**) are shown in Figure 4.1. The ditopic bis-terpyridyl monomers in which, acceptor spacer units sandwiched in between two hexyl thiophene units were synthesized in multistep procedures. 4'-(2-Bromo-5-thienyl)-2,2',6',2''-terpyridine (**1**) was prepared by the modified method described in the literature,¹⁵¹ then tributyltin group was introduced by a palladium(0) catalyzed reaction of compound **1** with excess bis-(tributyltin). Synthesis of **5a-5c** were described in Chapter 2.¹⁵² The aromatic dibromides **5a-5c** were reacted with two equivalents of 4'-(5-Tributylstannanyl-thiophen-2-yl)-[2,2';6',2'']terpyridine (**2**) under Pd⁰-catalyzed Stille cross-coupling conditions to form ditopic bis-terpyridyl ligands (**M1-M3**). After precipitation from methanol and column chromatographic purification, the bis-terpyridyl ligands (**M1-M3**) were obtained in moderate to good yields and fully characterized by ¹H NMR, ¹³C NMR, MS spectroscopy, and elemental analysis.

The synthesis of Ru^{II}-based metallo-polymers (**P1-P3**) is also depicted in Figure 4.1. The metallo-polymerization by self-assembly was carried out according to the methods described in the literature.¹⁵³ In a typical polymerization process, an appropriate quantity of ruthenium trichloride was activated by de-chlorinating with AgBF₄ in acetone. The resulting hexa-acetone Ru^{III} complex was reacted with exactly 1 equiv of bis-terpyridyl ligands **M1-M3** in n-butanol/DMA for 5 days, which involved a reduction of Ru^{III} to Ru^{II} with the chain growth process using n-butanol solvent itself as a reducing agent. The

resulting metallo-polymers (**P1-P3**) were purified by repetitive precipitation from NMP in diethyl ether and dried in vacuum, leading to homopolymers **P1-P3** (yield: 58-78%). The resulting highly linear-rigid polymer containing charged metal ions exhibited less solubility in common organic solvents as compared with terpyridyl ligands **M1-M3**, but were soluble in highly polar aprotic solvents, e.g., DMSO, DMF, NMP, or DMA.

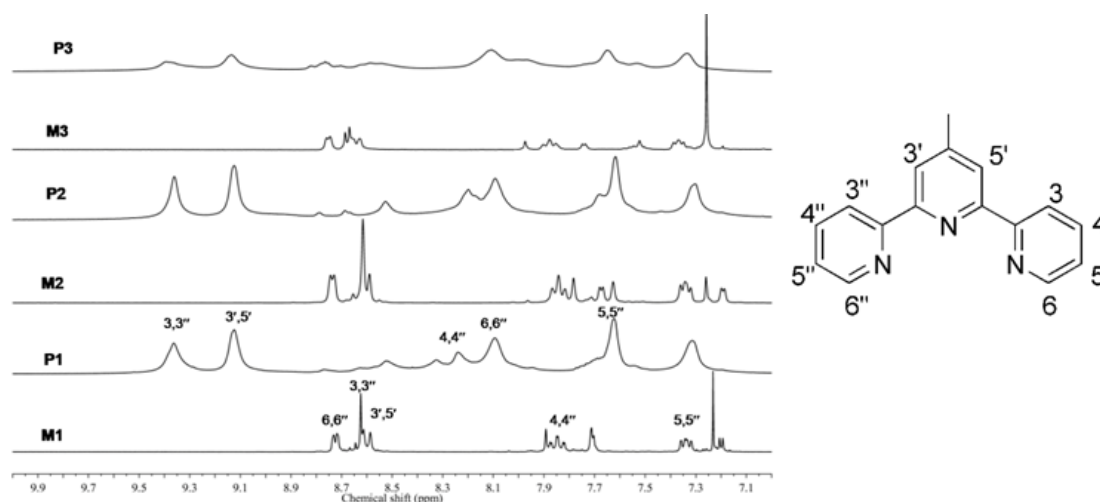


Figure 4.2 ^1H NMR spectra (aromatic region) of bis-terpyridyl ligands **M1-M3** (in CDCl_3) and metallo-polymers **P1-P3** (in DMSO-d_6).

Figure 4.2 shows ^1H NMR spectra in aromatic regions of ligands and metallo-polymers. As a result of metallo-polymerization, broadened signals of bis-terpyridyl ligands, as well as the absence of the signals from the uncomplexed terpyridyl units were observed. Furthermore, clear and dramatic downfield shifts of (5,5''), (4,4''), (3,3''), and (3',5')-terpyridyl signals and upfield shifts of the (6,6'')- signals were observed upon polymerization, which are consistent with the reported literature.¹⁵⁴ The assignments of terpyridyl signals are shown in Figure 4.2 based on those reported for Ru^{II} model complexes. Due to the lack of end

group-signals in ^1H NMR spectra and also considering the limit of NMR spectroscopy, the formation of cyclic oligomers can be discarded and the synthesized metallo-polymers should consist of more than 30 repeating units.¹⁵³ Hence, the molar masses of **P1–P3** were estimated to be higher than 30000 g/mol. To further confirm the formation of supramolecular metallo-polymers, the relative viscosity measurements of polymers to bis-terpyridyl ligands were evaluated. For this purpose, solutions of bis-terpyridyl ligands **M1–M3** (10 wt%) in NMP with viscosities $\eta = 6\text{--}7$ cp at 25°C were taken as references to determine the viscosities of metallo-polymers (**P1–P3**). As shown in Table 2.1, **P1–P3** (with $\eta = 9\text{--}11$ cp) exhibited viscosity 1.50-1.66 times larger than their corresponding bis-terpyridyl ligands **M1–M3**, which are in good agreements with similar reports known from literature.^{144-146,155}

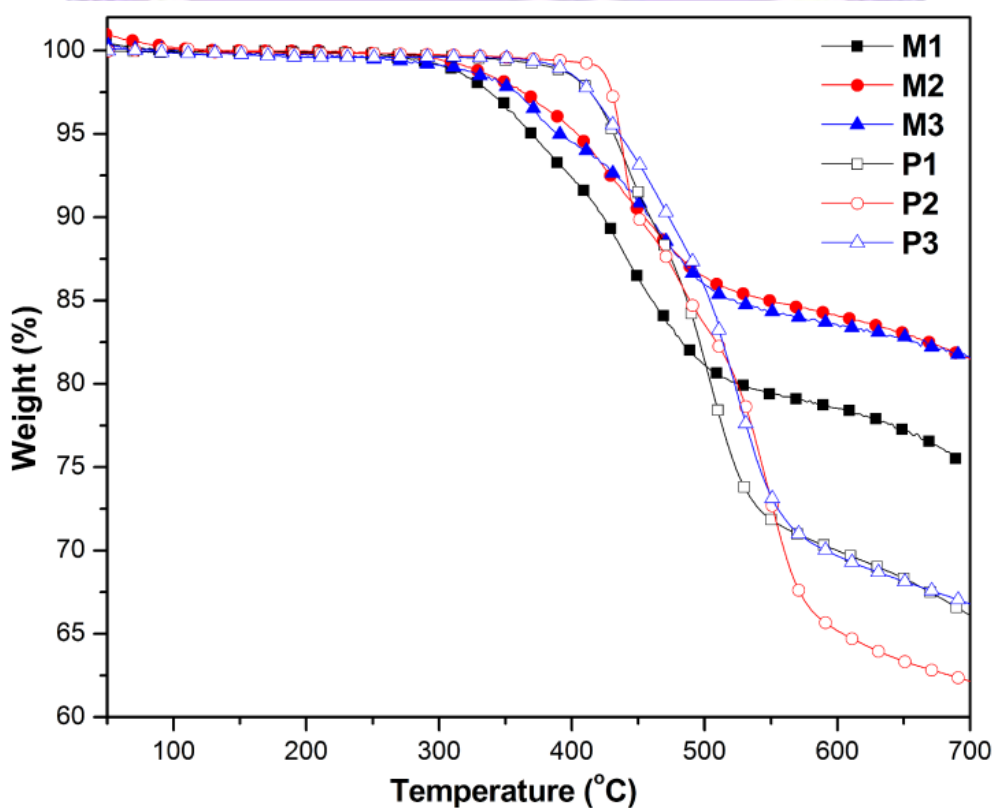


Figure 4.3 TGA thermograms of bis-terpyridyl ligands (**M1–M3**) and metallo-polymers (**P1–P3**) at a heating rate of $10^\circ\text{C}/\text{min}$ under nitrogen.

The thermal properties of bis-terpyridyl ligands **M1-M3** and metallo-polymers **P1-P3** were determined by thermogravimetric analysis (TGA) at a heating rate of 10°C/min under nitrogen and are shown in Figure 4.3 and summarized in Table 2.1. The TGA thermograms revealed decomposition temperatures (Td) (5% weight loss) of the bis-terpyridyl ligands and polymers were in the range of 369-404 and 431-438 °C, respectively. All bis-terpyridyl ligands and polymers demonstrated the same appearance of two degradation temperatures. In contrast to bis-terpyridyl ligands, polymers exhibited slightly enhanced thermal stability due to the increased rigidity of main-chain structures in metallo-polymers.

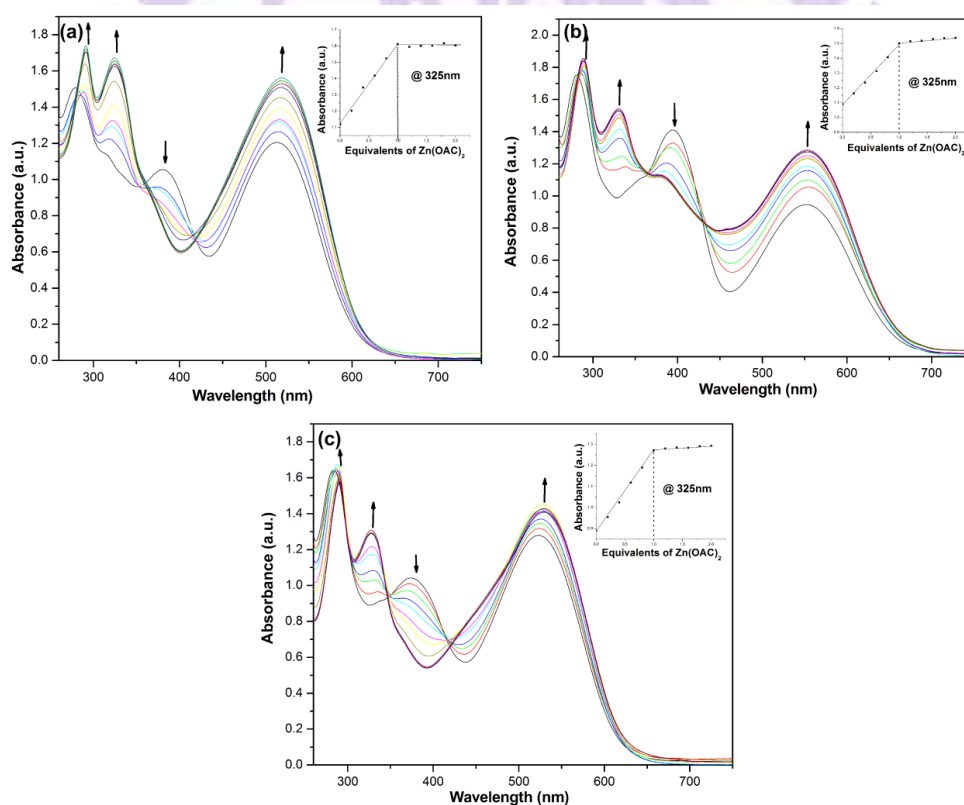


Figure 4.4 UV-vis absorption spectra acquired upon the titration of (a) **M1**, (b) **M2**, and (c) **M3** (in 2:8 v/v CH₃CN:CHCl₃) with Zn(OAc)₂ (in EtOH). The insets show the normalized absorption at 325 nm as a function of Zn²⁺:**M1-M3**, respectively.

4.3.2 UV-Visible Titration

UV-vis titration experiments were carried out to verify the formation of metallo-polymers from bis-terpyridyl ligands (**M1-M3**). As the kinetic studies by titration are too slow to detect Ru^{II}-containing metallo-polymers, which require heat and relatively long reaction time, these techniques could not be applied to the development of **P1-P3**. In our previous reports, ¹H-NMR and UV-vis absorption titration experiments were proceeded to characterize Zn^{II}-based metallo-polymers,¹⁴⁴⁻¹⁴⁶ where the formation of linear metallo-polymers were controlled by the exact stoichiometric ratios of the metal ions (Zn²⁺) and bis-terpyridyl ligands. Therefore, the same technique is chosen to gain a further insight into the self-assembly mechanism of **M1-M3** towards metallo-polymers, and the related titration data are depicted in Figure 4.4. Upon stepwise addition of Zn²⁺ to a solution of bis-terpyridyl ligand **M1** (Figure 4.4 (a)), the absorption spectra revealed the gradual emergence of an absorption band at 325 nm along with the disappearance of an absorption band at 380 nm. Furthermore, a red-shifted absorption band ca. 280 nm along with two isosbestic points (ca. 351 and 416 nm) were observed, which suggests that equilibrium occurred among a finite number of spectroscopically distinct species. The titration curve (Figure 4.4, inset) showed a linear increase and a sharp end point reaching a ratio of 1:1 (Zn²⁺:**M1**), indicating the formation of Zn^{II}-based metallo-polymers. New absorption peak observed at 325 nm could be attributed to the intra-ligand charge transfer (ILCT) in Zn^{II}-based metallo-polymers.¹⁵⁶⁻¹⁵⁷ The same trends were observed in bis-terpyridyl ligands **M2** and **M3** (Figure 4.4 (b) and (c)). Thus, the results of all titration experiments performed for bis-terpyridyl ligands (**M1-M3**) with Zn²⁺ ions are consistent with the fact that, at 1:1 ratio of Zn²⁺ ions and the

ditopic ligands, supramolecular assemblies of metallo-polymers have formed, where each Zn^{2+} ion is complexed with two bis-terpyridyl ligands, and the resulting repeating unit of bis-terpyridyl- Zn^{2+} in metallo-polymers can be considered as the origin of the observed electronic transitions.

Table 4.1 Optical, Thermal, and Viscosity Properties of Bis-terpyridyl Ligands (M1-M3) and Metallo-Polymers (P1-P3)

Compound	η (cp) ^a	T_d (°C) ^b	$\lambda_{abs,sol}$ (nm) ^c	$\lambda_{abs,film}$ (nm) ^d	λ_{onset} (nm)	E_g^{opt} (eV) ^e
M1	7	369	280, 381, 514	285, 415, 566	698	1.77
M2	6	404	281, 396, 553	286, 428, 602	744	1.66
M3	6	401	280, 378, 520	287, 422, 572	702	1.76
P1	11	431	278, 318, 335, 550, 576	282, 320, 335, 554, 605	710	1.74
P2	9	438	278, 318, 335, 551, 596	280, 321, 335, 554, 638	761	1.63
P3	10	432	278, 318, 335, 549, 572	282, 321, 335, 554, 606	713	1.73

^a The viscosities of polymers (10% in weight) in NMP solutions at 25°C (100 rpm, Spindle number 4) were determined by rheometer system. Solutions of bis-terpyridyl ligands **M1-M3** (10% in weight) in NMP were used as references to determine the viscosities of corresponding metallo-polymers. ^b The decomposition temperatures (T_d) (5% weight loss) were determined by TGA with a heating rate of 10°C/min under N_2 atmosphere. ^c Concentration of 10^{-6} M in chloroform for **M1-M3** and 10^{-6} M in DMF for **P1-P3**. ^d Spin coated from solutions on quartz substrates. ^e Optical band gaps were estimated from the absorption spectra in films by using the equation of $E_g = 1240/\lambda_{edge}$.

4.3.3 Optical Properties

The photophysical characteristics of the bis-terpyridyl ligands (**M1-M3**) and metallo-polymers (**P1-P3**) were investigated by ultraviolet-visible (UV-vis) absorption spectroscopy in dilute solutions (10^{-6} M) and spin-coated films on quartz substrates. Figure 4.5 shows the absorption spectra of **M1-M3** and **P1-P3** in solutions as well as in solid films, and their optical data, including the absorption wavelengths (λ_{abs}) and optical band gaps (E_g^{opt}), are also summarized in Table 4.1.

The absorption spectra of ditopic ligands **M1-M3** showed three intense band regions, where the band ca. 280 nm was associated with the characteristic π - π^* transitions of the terpyridine moieties¹⁵⁸ and the low energy peaks ca. 380 nm and 514-553 nm (with tailing around 700 nm) were due to the π - π^* transitions and intramolecular charge transfer (ICT) occurred inside the overall π -conjugated systems. Compared with solutions, these two longer bands in solid films were red-shifted (ca. 34 nm and 52 nm, respectively), which could be attributed to the strong interchain associations and aggregations in solids. Due to the larger size and less electronegativity of Selenium (Se) atom than those of both S and O atoms in benzodiazole acceptors, bis-terpyridyl ligand **M2** showed the most pronounced bathochromic shift of the absorption maximum and, thereby, the smallest optical energy bandgap (1.66 eV) than the other bis-terpyridyl ligands (1.77 and 1.76 eV for **M1** and **M3**, respectively). In all bis-terpyridyl ligands, as the acceptor moieties are sandwiched between thiophene units, resulting in more planar structures to facilitate inter-chain associations and strong ICT interactions between thiophene donors and benzodiazole acceptors,⁵⁶ so their absorption spectra covered a broad range. In contrast to the recently published bis-terpyridyl monomers containing acceptor moieties,¹⁴¹ our terpyridyl ligands (**M1-M3**) showed stronger red shifts in the absorption spectra with smaller optical band gaps due to the stronger ICT interactions, which are highly essential for the PVC devices to increase the photo-current generations.

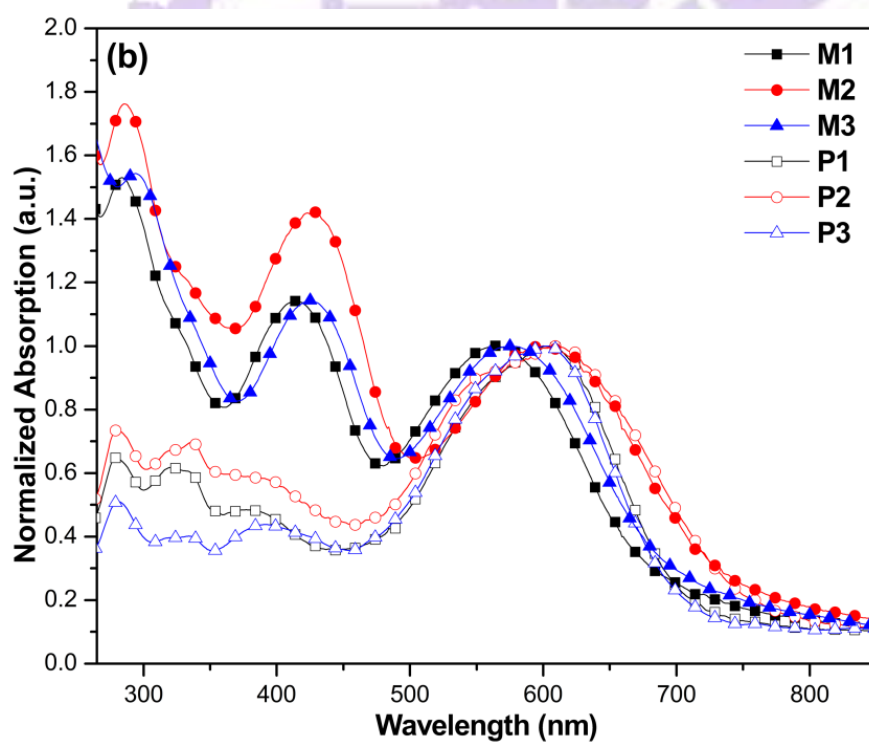
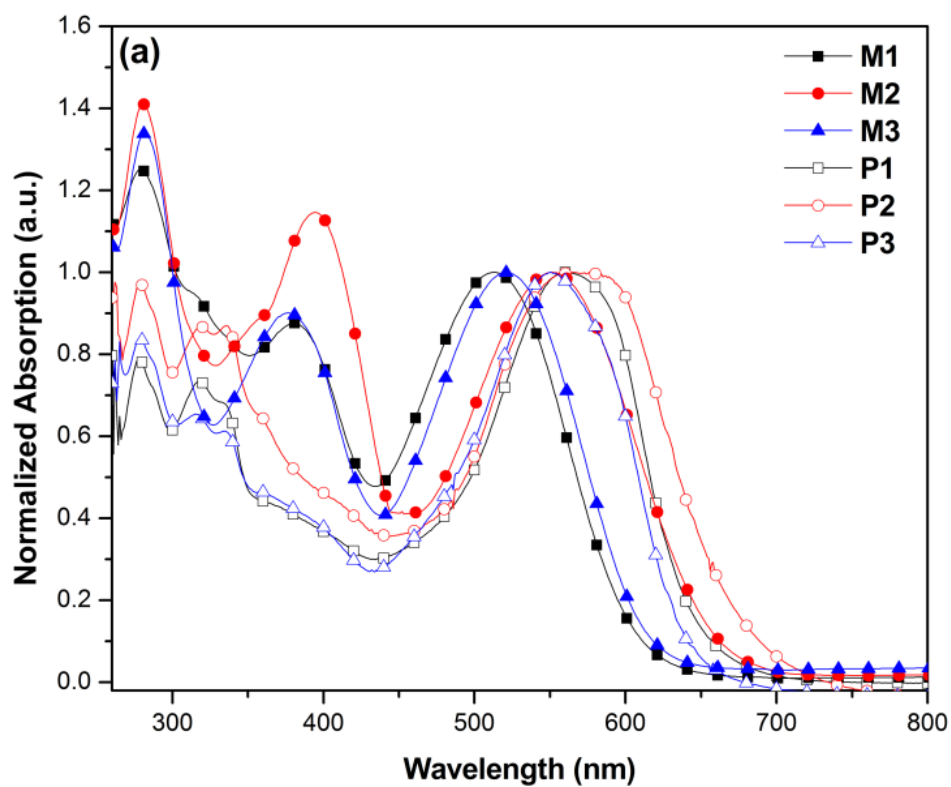


Figure 4.5 Normalized UV-vis spectra of bis-terpyridyl ligands (**M1-M3**) and metallo-polymers (**P1-P3**). In (a) dilute (10^{-6} M) solutions and (b) solid films, respectively.

Metal–ligand coordination, i.e., formation of metallo-polymers (**P1-P3**), can also be easily confirmed through UV-vis absorption spectroscopy. In ruthenium-containing metallo-polymers, self-assembly induced by metal ions is readily observed by the occurrence of an additional absorption band (metal-to-ligand charge-transfer, i.e., MLCT) at 490-560 nm,^{136,159-160} which were derived from the promotion of an electron from the metal (Ru^{II})-centered d-orbital to unfilled ligand-centered π^* orbitals. For all metallo-polymers **P1-P3**, they showed the ligand-centered $\pi-\pi^*$ transitions between terpy moieties and central chromophores situated ca. $\lambda_{\text{abs}} < 350$ nm. The metal-to-ligand charge transfer (MLCT) bands were in the range of 550-554 nm in these coordination polymers (**P1-P3**), and a strong bathochromic effect in MLCT was observed due to the presence of benzodiazole acceptors inserted between thiophene units as the central cores.¹⁴⁸ The absorption peaks beyond 550 nm were attributed to the stronger ICT interactions inside the bis-terpyridyl ligands. It is worth noting that compared with the other Ru^{II}-containing metallo-polymers,¹³⁶ our metallo-polymers showed extended absorption beyond MLCT. Due to the long absorption range of these metallo-polymers, they possessed small optical band gaps in the range of 1.63-1.74 eV. Similar to bis-terpyridyl ligands, low energy absorption wavelengths (λ_{abs}) in solid films (ca. 605-638 nm) of metallo-polymers **P1-P3** were red shifted (29-42 nm) in comparison with those in solutions (572-596 nm), which could be also attributed to the strong interchain associations and aggregations in solids. Compared with bis-terpyridyl ligands (**M1-M3**) in both solutions and solid films, the maximum absorption wavelengths (λ_{abs}) of metallo-polymers (**P1-P3**) exhibited stronger bathochromic shifts due to the formation of linear and rigid metallo-polymers.

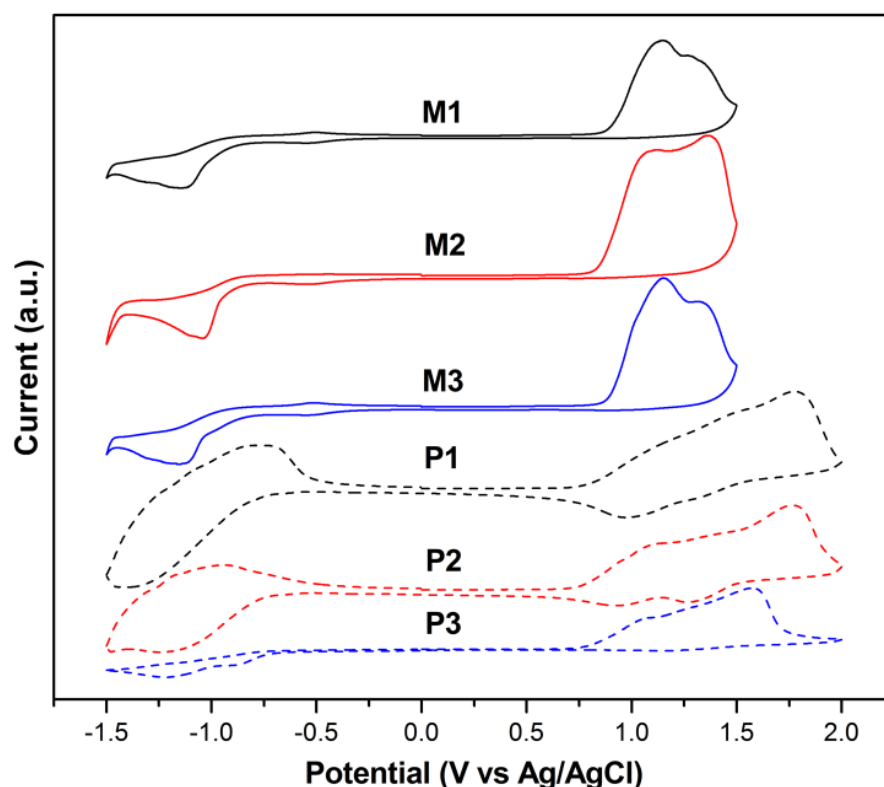


Figure 4.6 Cyclic voltammograms of bis-terpyridyl ligands (**M1-M3**) and metallo-polymers (**P1-P3**) at a scan rate of 100 mV/s.

Table 4.2 Electrochemical Properties of Bis-terpyridyl Ligands (M1-M3) and Metallo-Polymers (P1-P3)^a

Compound	Oxidation potential (V vs. Ag/Ag ⁺)		Reduction Potential (V vs. Ag/Ag ⁺)		Energy Level ^d (eV)		Band Gap (eV)	
	E _{ox/onset} ^b	E _{ox/o} ^c	E _{red/onset} ^b	E _{red/o} ^c	HOMO	LUMO	E _g ^{ec}	E _g ^{opt}
M1	0.89	1.15, 1.28	-0.93	-1.12	-5.24	-3.42	1.82	1.77
M2	0.88	1.05, 1.34	-0.85	-1.03	-5.23	-3.50	1.73	1.66
M3	0.89	1.13, 1.31	-0.92	-1.15	-5.24	-3.43	1.81	1.76
P1	0.77	1.01, 1.57	-0.79	-1.08	-5.12	-3.56	1.56	1.74
P2	0.76	1.00, 1.51	-0.73	-1.06	-5.11	-3.62	1.49	1.63
P3	0.77	1.02, 1.57	-0.77	-1.12	-5.12	-3.58	1.54	1.73

^a Reduction and oxidation potentials measured by cyclic voltammetry in solid films. ^b

Onset oxidation and reduction potentials. ^c Formal oxidation and reduction potentials.

^d E_{HOMO}/E_{LUMO} = [-(E_{onset} - 0.45) - 4.8] eV, where 0.45 V is the value for ferrocene vs. Ag/Ag⁺ and 4.8 eV is the energy level of ferrocene below the vacuum.

4.3.4 Electrochemical Properties

The redox behavior and electronic states, i.e., HOMO and LUMO levels, of the bis-terpyridyl ligands (**M1-M3**) and their corresponding Ru^{II}-containing metallo-polymers (**P1-P3**) were investigated by cyclic voltammetry (CV) measurements to understand the energy band structures of associated materials used in the PVC devices. The cyclic voltammograms of bis-terpyridyl ligands **M1-M3** and metallo-polymers **P1-P3** in solid films are displayed in Figure 4.6 and the related CV data (formal potentials, onset potentials, HOMO and LUMO levels, and band gaps) are summarized in Table 2.2. Ag/AgCl was served as a reference electrode and it was calibrated by ferrocene ($E_{1/2(FC/FC^+)} = 0.45$ eV versus Ag/AgCl). The HOMO and LUMO levels were estimated by the oxidation and reduction potentials from the reference energy level of ferrocene (4.8 eV below the vacuum level) according to the following equation:⁹⁷ $E_{\text{HOMO}}/E_{\text{LUMO}} = [-(E_{\text{onset}} - E_{\text{onset}(FC/FC^+ \text{ vs. Ag/Ag}^+)}) - 4.8]$ eV where 4.8 eV is the energy level of ferrocene below the vacuum level and $E_{\text{onset}(FC/FC^+ \text{ vs. Ag/Ag}^+)} = 0.45$ eV. All bis-terpyridyl ligands (**M1-M3**) exhibited two p-doping/dedoping (oxidation/reduction) process at positive potentials and one n-doping/dedoping (reduction/reoxidation) process at negative potentials. The onset oxidation potentials ($E_{\text{ox/onset}}$) were the same for **M1-M3** ca. 0.88 V, and two of their formal oxidation potentials were in the range of 1.05-1.15 V and 1.28-1.34 V, respectively. In addition, the onset reduction potentials ($E_{\text{red/onset}}$) of **M1-M3** were in the range of (-0.85)-(-0.93) V and their formal oxidation potentials were in the range of (-1.03)-(-1.15) V. From the onset oxidation potentials ($E_{\text{ox/onset}}$) and onset reduction potentials ($E_{\text{red/onset}}$) of bis-terpyridyl ligands **M1-M3**, the estimated HOMO levels were at ca. -5.24 eV and LUMO levels were in the range of

(-3.42)-(-3.50) eV. The similar values in the HOMO levels of these ligands suggest that different electron-deficient center units have almost no effect on their oxidation potentials, but the reduction potentials of these ligands behave quite differently. The LUMO levels are clearly affected by the electron-deficient centers of the ligand cores, a stronger electron-deficient unit resulting in a lower LUMO energy level.⁵⁶

All Ru^{II}-containing metallo-polymers (**P1-P3**) exhibited two reversible or quasi-reversible oxidation peaks in the range of 1.00-1.02 V and 1.51-1.57 V, respectively. In agreement with the literature, these waves were attributed to the metal localized oxidation (corresponding to the II/III redox transition) and redox transitions across the bridging ligands, respectively.¹⁵⁹⁻¹⁶¹ These polymers also showed one reduction process at ca. 1.08 V, which was assigned to the ligand-based reduction.¹⁴⁴⁻¹⁴⁶ From the onset oxidation potentials ($E_{\text{ox/onset}}$, ca. 0.77 V) and onset reduction potentials ($E_{\text{red/onset}}$, between 0.73 and 0.79 V) of metallo-polymers, the estimated HOMO levels were at ca. -5.11 eV and LUMO levels were between -3.56 and -3.62 eV. Apparently, the HOMO levels in these metallo-polymers stayed relatively constant while the LUMO levels were tuned by varying the electron withdrawing aromatic substituents on the bis-terpyridyl ligands.¹⁶² Again, compared with the bis-terpyridyl ligands, the HOMO levels of metallo-polymers were enhanced by ca. 0.12 eV. As a result, their band gaps decreased to give narrow-band-gap metallo-polymers. The electrochemical band gaps (E_g^{ec}) calculated from $E_g^{\text{ec}} = e(E_{\text{ox/onset}} - E_{\text{red/onset}})$ were 1.56, 1.49, and 1.54 eV for **P1-P3**, respectively. All these electrochemical characteristics are within the desirable range of ideal materials to be utilized in the organic photovoltaic applications.

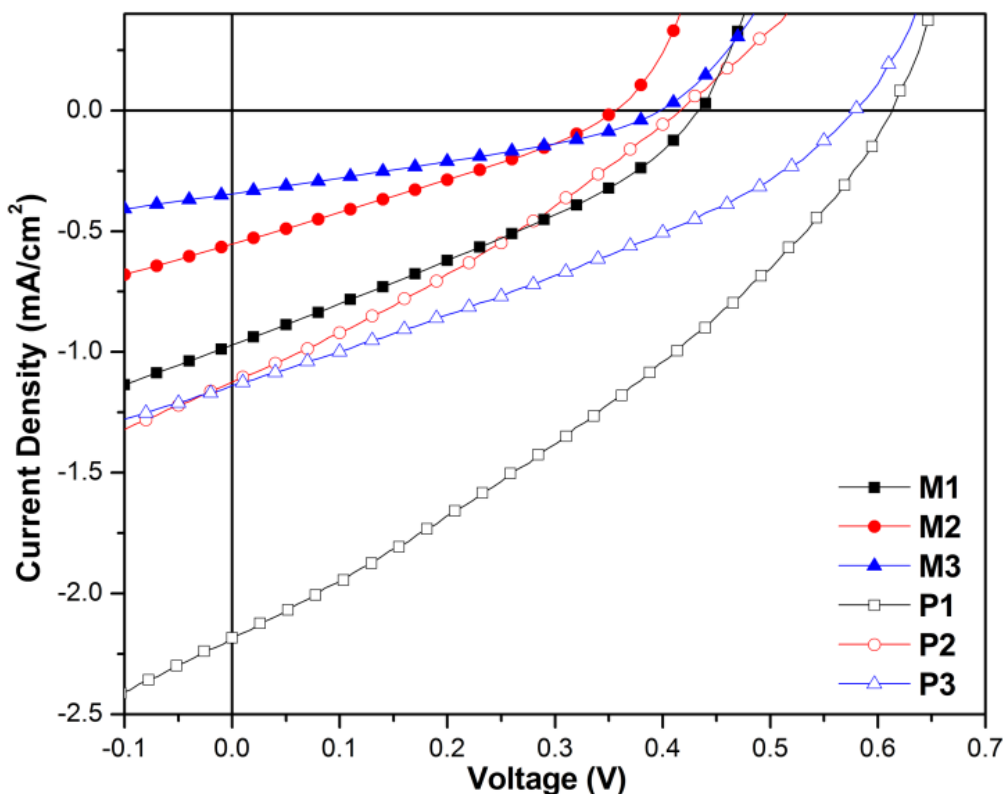


Figure 4.7 Current-voltage curves of BHJ solar cells using blended films of **M1-M3** or **P1-P3:PCBM** (1:1 w/w) under the illumination of AM 1.5G, 100 mW/cm².

Table 4.3 Photovoltaic Properties of BHJ Solar Cell Device with a Configuration of ITO/PEDOT:PSS/Compound:PCBM/Ca/Al^a

Active Layer ^b (Compound:PCBM)	V_{oc} (V)	J_{sc} (mA/cm ²)	FF (%)	PCE (%)
M1	0.43	0.97	31.8	0.13
M2	0.36	0.55	28.8	0.06
M3	0.40	0.34	32.0	0.04
P1	0.61	2.18	34.1	0.45
P2	0.42	1.14	30.2	0.14
P3	0.58	1.14	33.3	0.22

^a Measured under AM 1.5 irradiation, 100 mW/cm²; ^b Active layer with the weight ratio of **Compound:PCBM**=1:1.

4.3.5 Photovoltaic Properties

To investigate the potential use of bis-terpyridyl ligands **M1-M3** and their Ru^{II}-containing metallo-polymers **P1-P3** in PVCs, the bulk hetero-junction (BHJ) solar cell devices comprising blends of these compounds as electron donors and [6,6]-phenyl-C₆₁-butyric acid methyl ester (PCBM) as an electron acceptor in their active layer were fabricated with a configuration of ITO/PEDOT:PSS(30 nm)/**M1-M3** or **P1-P3**:PCBM blend (~80 nm)/Ca(30 nm)/Al(100 nm) and measured under AM 1.5 stimulated solar light. The blended solutions were prepared from compounds and PCBM in a weight ratio of 1:1 (w/w) from chloroform solutions of **M1-M3** and from DMF solutions of **P1-P3**. The current density (J) versus voltage (V) curves of the PVCs are shown in Figure 4.7, where the open circuit voltage (V_{oc}), short circuit current density (J_{sc}), fill factor (FF), and the PCE values are summarized in Table 4.3. In all PVC devices, the thickness of the active layer was kept at ca. 80 nm, which has the optimum performance due to the balance in optical absorption and serial resistance of the blended film.

Among bis-terpyridyl ligands **M1-M3**, the highest PCE value of 0.13% was obtained from the device containing an active layer of **M1**:PCBM (1:1 w/w) with $V_{oc} = 0.43$ V, $J_{sc} = 0.97$ mA/cm², and FF = 31.8 %. It can be seen from Figure 4.7 and Table 4.3 that the devices made from ligands **M1-M3** were limited by low J_{sc} values, which may be due to less creation and dissociation of excitons at the BHJ interfaces followed by transport of free charge carriers towards the collecting electrodes.⁷⁷ However, higher J_{sc} values were obtained when the active layers were fabricated from metallo-polymers **P1-P3**. With the similar values of V_{oc} (0.42-0.61 V) and FF (30.2-34.1 %) in the devices containing metallo-polymers **P1-P3**:PCBM (1:1 w/w), it is evident that their variations of PCE values (0.45, 0.14, and 0.22, respectively) were

mainly dependent on the J_{sc} values (2.18, 1.14, and 1.14 mA/cm², respectively). Among PVC devices containing metallo-polymers **P1-P3**, the device containing **P1** exhibited the highest PCE value of 0.45% with J_{sc} (2.18 mA/cm²), V_{oc} (0.61 V), and FF (34.1%).

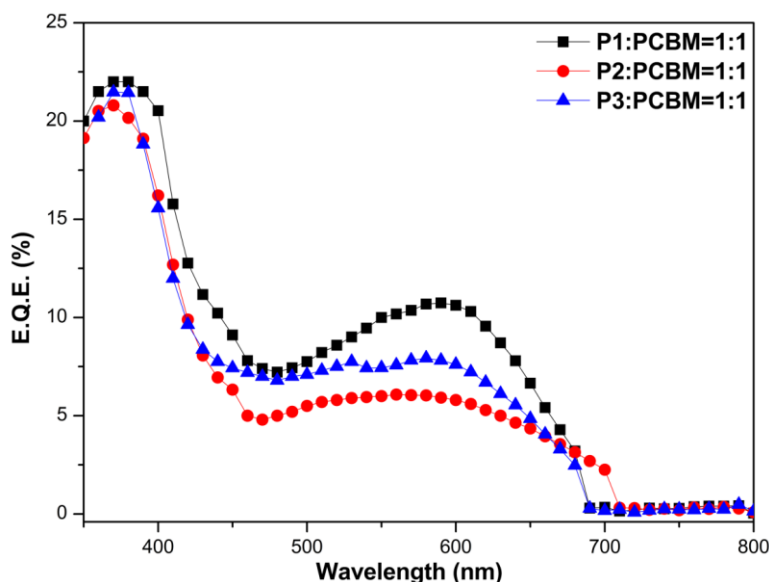


Figure 4.8 EQE curves of the PSC devices based on polymers **P1-P3**: PCBM (1:1 wt%).

Among the PVC devices containing metallo-polymers **P1-P3**:PCBM (1:1 w/w), **P1** demonstrated a higher J_{sc} values compared to **P2** and **P3**, this could be explained by their EQE curves (Figure 4.8). It is evident from the EQE curves that, though all devices exhibited similar EQE values in the short wavelength (ca. 400 nm) region but **P1** exhibited higher EQE value at the long wavelength (ca. 600 nm) region, this could be the main reason for the higher J_{sc} value of the PVC cell containing **P1**. In BHJ solar cell devices, the absorptions of the long wavelength region are contributed from polymers, and the absorptions in the short wavelength region are mainly from PCBM. The low EQE values in the low-energy absorption bands as well as the high-energy absorption bands in these polymer blends may be due to their poor dissociations of

excitons. Therefore, if the EQE values of the devices can be enhanced by increasing the thickness of the active layer without hampering charge separation and transport properties, then the device performances can be improved significantly. Low EQE values can also be observed in some other LBG polymer systems and this problem can be solved by developing new electron acceptor materials.

To the best of our knowledge, compared with all reported heterojunction PVC devices fabricated from terpyridine-containing Ru^{II}-metallo-polymers as the active layer,^{62-65,147-150} our device containing metallo-polymer **P1** demonstrated the highest PCE value (0.45%), which probably due to the presence of electron donor and acceptor moieties at the core of bis-terpyridyl units in **P1** with the stronger ICT and the broadening of the sensitization range. The reported devices with lower PCE values were because their low V_{oc} values arose from the relatively high HOMO levels, which caused losses due to the limited numbers of photo-generated charges induced by incomplete quasi-Fermi level splittings.¹⁶³ To conquer these problems, layer-by-layer (LBL) deposition techniques of Ru^{II}-containing polymers with sulfonated polyaniline (SPAN) were utilized, but these techniques were limited by photocurrents.^{65,110} With polymers as solid polyelectrolytes, Maura et al. also fabricated LBL devices by incorporating 50 bilayers of poly(phenylene ethynylene)-based polyanions with cationic C₆₀-NH₃⁺ with a total thickness of 50 nm to obtain a maximum PCE value only up to 0.04%.¹⁶⁴ In our case, all metallo-polymers were in the ideal ranges of HOMO and LUMO to be utilized for BHJ solar cells, so BHJs with **P1-P3** were used to obtain high photocurrents.¹⁶⁵ Compared with the BHJ solar cells fabricated from ionic polythiophene and C₆₀,⁶⁶⁻⁶⁷ our PVC device made from **P1** exhibited a higher J_{sc} value (2.18 vs. 0.97 mA/cm²) with a similar V_{oc} value (0.61 vs. 0.67 V), but a similar or little higher PCE value (0.45 vs. 0.43) was obtained due to the limited FF

value (34.1 vs. 53%). No significant improvements of PCE values in the device performance were observed by changing the PCBM ratio (due to the less solubility of metallo-polymers **P1-P3** in PCBM by DMF). Finally, the device efficiencies of these metallo-polymers are lower than those of neutral polymer-based solar cells, such as P3HT-PCBM, but the highest PCE value of our PVC device containing **P1** is reported among all ionic conjugated polymer-based solar cells so far.

4.4 Conclusions

A series of π -conjugated bis-terpyridyl ligands bearing donor-acceptor units and their corresponding Ru^{II}-containing main-chain metallo-polymers were developed and synthesized. The formation of the metallo-polymers were confirmed from the broadened ¹H NMR signals, relative viscosity measurements, and UV-vis titration experiments. Apparently, the electro-optical properties of the bis-terpyridyl ligands as well as the metallo-polymers were strongly influenced by the nature of the attached π -conjugated donor-acceptor units and some distinct differences in electro-optical properties were observed between ligands and their analogous metallo-polymers. Because of the broader sensitization of donor-acceptor design in **M1-M3** and **P1-P3**, they exhibited higher J_{sc} values. In addition, owing to the strong intramolecular charge transfers inside the bis-terpyridyl units of **M1-M3** and **P1-P3**, their HOMO levels were tuned to get higher V_{oc} values. An optimum PVC device based on the blended polymer **P1**:PCBM = 1:1 (w/w) achieved the PCE value up to 0.45 %, with $V_{oc} = 0.61$ V, $J_{sc} = 2.18$ mA/cm², and FF = 34.1 % (under AM 1.5 G 100 mW/cm²), and those values are comparable with BHJ solar cells fabricated from ionic polythiophene and C₆₀. These metallo-polymers demonstrate a novel family of conjugated polyelectrolytes with the highest PCE value towards potential PVC applications.

Chapter 5.

Conclusion

A series of new low-bandgap polymers containing the phenothiazine unit as an electron donor conjugated with various benzodiazole acceptors via hexyl-thiophene linkers were synthesized and characterized. These polymers show strong absorptions in the range of 300-700 nm and have ideal ranges of HOMO and LUMO levels. Bulk heterojunction polymer solar cells were fabricated from the polymer blends consisting of these low-bandgap polymers as an electron donor and PC₆₁BM/PC₇₁BM as an electron acceptor. With the similar V_{oc} values and fill factor in the PSC devices containing the polymers blended with PC₆₁BM in a weight ratio of 1:1 (w/w), it was found that due to the major variations of the J_{sc} values in polymers they are crucially affected to have the major difference in power conversion efficiency. The PSC device containing a polymer blend of **PP6DHTBT**:PC₇₁BM (1:4 wt%) exhibited the best device performance with a PCE of 1.20%, an V_{oc} of 0.75 V, a J_{sc} of 4.60 mA/cm², and a FF of 0.35. The optimization of photovoltaic properties in the PSC devices containing polymer blends **PP6DHTBT**:PC₇₁BM can be adjusted by the morphology variations with different weight ratios of PC₇₁BM, which were observed to have higher roughnesses with larger PC₇₁BM contents, and thus to substantially increase the PCE values of the PSC devices.

The concept of incorporation of electron deficient β -cyano-vinylene groups with donor-acceptor polymer architectures was utilized to improve the efficiencies of polymer solar cells. Cyano-vinylene groups were introduced into electron-rich building blocks, such as cyclopentadithiophene and dithienosilole to yield LBG polymers (**CPDT-CN** and **DTS-CN**). These polymers showed excellent charge-transporting properties with high hole mobilities in the range of (5.99-9.82)

$\times 10^{-4} \text{ cm}^2\text{V}^{-1}\text{s}^{-1}$ and good processabilities for PSC applications. Due to the lowest band gap and the highest hole mobility with more balanced charge transport of **DTS-CN**, an optimum PSC device based on the blended polymer **DTS-CN:PC₇₁BM** = 1:2 (w/w) achieved the maximum power conversion efficiency (PCE) value up to 2.25 %, with $V_{oc} = 0.74 \text{ V}$, $J_{sc} = 8.39 \text{ mA/cm}^2$, and FF = 36%. Regardless of the high open-circuit voltages and the large short-circuit currents of all PSC devices, the low fill factor indicated the possibility of further device performance improvements by the optimization of film morphology of the polymer blends and/or device architectures.

A series of π -conjugated bis-terpyridyl ligands bearing donor-acceptor units and their corresponding Ru^{II}-containing main-chain metallo-polymers were developed and synthesized. The formation of the metallo-polymers were confirmed from the broadened ¹H NMR signals, relative viscosity measurements, and UV-vis titration experiments. Apparently, the electro-optical properties of the bis-terpyridyl ligands as well as the metallo-polymers were strongly influenced by the nature of the attached π -conjugated donor-acceptor units and some distinct differences in electro-optical properties were observed between ligands and their analogous metallo-polymers. Owing to the strong intramolecular charge transfers inside the bis-terpyridyl units of **M1-M3** and **P1-P3**, their HOMO levels were tuned to get higher V_{oc} values. An optimum PVC device based on the blended polymer **P1:PCBM** = 1:1 (w/w) achieved the PCE value up to 0.45 %, with $V_{oc} = 0.61 \text{ V}$, $J_{sc} = 2.18 \text{ mA/cm}^2$, and FF = 34.1 %, and those values are comparable with BHJ solar cells fabricated from ionic polythiophene and C₆₀. These metallo-polymers demonstrate a novel family of conjugated polyelectrolytes with the highest PCE value towards potential PVC applications.

References

1. Becquerel, A. E. *Compt. Rend. Acad. Sci.* **1839**, 9, 561.
2. Pulfrey, D. L. *Photovoltaic Power Generation*, Van Nostrand Reinhold, New York **1978**.
3. Chapin, D. M.; Fuller, C. S.; Pearson, G. L. *J. Appl. Phys.* **1954**, 25, 676.
4. Gustafsson, G.; Cao, Y.; Treacy, G. M.; Klavetter, F.; Colaneri, N.; Heeger, A. *J. Nature* **1992**, 357, 477.
5. Green, M. A.; Emery, K.; Hishikawa, Y.; Warta, W. *Prog. Photovolt. Res. Appl.* **2010**, 18, 346.
6. Tang, C. W. *Appl. Phys. Lett.* **1986**, 48, 183.
7. Yu, G.; Gao, J.; Hummelen, J. C.; Wudl, F. A.; Heeger, J. *Science* **1995**, 270, 1789.
8. Po, R.; Maggini, M.; Camaioni, N. *J. Phys. Chem. C* **2010**, 114, 695.
9. Thompson, B. C.; Fréchet, J. M. J. *Angew. Chem. Int. Ed.* **2008**, 47, 58.
10. Brabec, C. J.; Sariciftci, N. S.; Hummelen, J. C. *Adv. Funct. Mater.* **2001**, 11, 15.
11. Kietzke, T.; *Adv. in OptoElectronics* **2007**, Article ID 40285, 1.
12. Coakley, K. M.; McGehee, M. D. *Chem. Mater.* **2004**, 16, 4533.
13. Parker, I. D. *J. Appl. Phys.* **1994**, 75, 1656.
14. Marks, R. N.; Halls, J. J. M.; Bradley, D. D. C.; Friend, R. H.; Homes, A. B. *J. Phys.: Condens. Matter* **1994**, 6, 1379.
15. Sariciftci, N. D.; Braun, D.; Zhang, C.; Srdanov, V. I.; Heeger, A. J.; Stucky, G.; Wudl, F. *Appl. Phys. Lett.* **1993**, 62, 585.
16. Pettersson, L. A. A.; Roman, L. S.; Inganas, O. *J. Appl. Phys.* **1999**, 86, 487.
17. Yu, G.; Heeger, A. J. *J. Appl. Phys.* **1995**, 78, 4510.

18. Halls, J. J. M.; Walsh, C. A.; Greenham, N. C.; Marseglia, E. A.; Friend, R. H.; Moratti, S. C.; Holmes, A. B. *Nature* **1995**, *376*, 498.
19. Kannan, B.; Castelino, K.; Majumdar, A. *Nano Lett.* **2003**, *3*, 1729.
20. Li, Y.; Zou, Y. *Adv. Mater.* **2008**, *20*, 2952.
21. Günes, S.; Neugebauer, H.; Sariciftci, N. S. *Chem. Rev.* **2007**, *107*, 1324.
22. Winder, C.; Sariciftci, N. S. *J. Mater. Chem.* **2004**, *14*, 1077.
23. Kitamura, C.; Tanaka, S.; Yamashita, Y., *Chem. Mater.* **1996**, *8*, 570.
24. Ajayaghosh, A. *Chem. Soc. Rev.* **2003**, *32*, 181.
25. Bundgaard, E.; Krebs, F. C. *Sol. Energy Mater. Sol. Cells* **2007**, *91*, 954.
26. Mühlbacher, D.; Scharber, M.; Morana, M.; Zhu, Z.; Waller, D.; Gaudiana, R.; Brabec, C. J. *Adv. Mater.* **2006**, *18*, 2884.
27. Chen, J. W.; Cao, Y. *Acc. Chem. Res.* **2009**, *42*, 1709.
28. Kim, Y.; Cook, S.; Tuladhar, S. M.; Choulis, S. A.; Nelson, J.; Durrant, J. R.; Bradley, D. D. C.; Giles, M.; McCulloch, I.; Ha, C.; Ree, M. *Nat. Mater.* **2006**, *5*, 197.
29. Gadisa, A.; Oosterbaan, W. D.; Vandewal, K.; Bolsee, J.C.; Bertho, S.; D'Haen, J.; Lutsen, L.; Vanderzande, D.; Manca, J. V. *Adv. Funct. Mater.* **2009**, *19*, 3300.
30. Lenes, M.; Wetzelaer, G. A. H.; Kooistra, F. B.; Veenstra, S. C.; Hummelen, J. C.; Blom, P. W. M. *Adv. Mater.* **2008**, *20*, 2116.
31. Dennler, G.; Scharber, M.; Brabec, C. J. *Adv. Mater.* **2009**, *21*, 1323.
32. Brédas, J. L.; Beljonne, D.; Coropceanu, V.; Cornil, J. *Chem. Rev.* **2004**, *104*, 4971.
33. Cai, W.; Gong, X.; Cao, Y. *Sol. Energy Mater. Sol. Cells* **2007**, *94*, 114.

34. Singh, T. B.; Marjanovic, N.; Matt, G. J.; Günes, S.; Sariciftci, N. S.; Ramil, A. M.; Andreev, A.; Sitter, H.; Schwödiauer R.; Bauer, S. *Org. Electron.* **2005**, *6*, 1199.
35. Hoppe, H.; Sariciftci, N. S. *J. Mater. Chem.* **2006**, *16*, 45.
36. Shaheen, S.; Brabec, C. J.; Sariciftci, N. S.; Padinger, F.; Fromherz, T.; Hummelen, J. C. *Appl. Phys. Lett.* **2001**, *78*, 841.
37. Schilinsky, P.; Waldauf, C.; Brabec, C. J. *Appl. Phys. Lett.* **2002**, *81*, 3885.
38. Padinger, F.; Rittberger, R. S.; Sariciftci, N. S.; *Adv. Funct. Mater.* **2003**, *13*, 85.
39. Yang, X.; Loos, J.; Veenstra, S. C.; Verhees, W. J. H.; Wienk, M. M.; Kroon, J. M.; Michels, M. A. J.; Janssen, R. A. J. *Nano Lett.* **2005**, *5*, 579.
40. Kim, Y.; Choulis, S. A.; Nelson, J.; Bradley, D. D. C.; Cook, S.; Durrant, J. R. *Appl. Phys. Lett.* **2005**, *86*, 063502.
41. Li, G.; Shrotriya, V.; Yao, Y.; Yang, Y. *J. Appl. Phys.* **2005**, *94*, 043704.
42. Li, G.; Shrotriya, V.; Huang, J.; Mariarty, T.; Emery, K.; Yang, Y. *Nat. Mater.* **2005**, *4*, 864.
43. Reyes-Reyes, M.; Kim, K.; Carroll, D. L.; *Appl. Phys. Lett.* **2005**, *87*, 083506.
44. Ma, W.; Yang, C.; Gong, X.; Lee, K.; Heeger, A. J. *Adv. Funct. Mater.* **2005**, *15*, 1617.
45. Kim, Y.; Cook, S.; Tuladhar, M.; Choulis, S. A.; Nelson, J.; Durrant, J. R.; Bradley, D. D. C.; Giles, M.; McCulloch, I.; Ha, C.-S.; Ree, M. *Nat. Mater.* **2006**, *5*, 197.
46. White, M. S.; Olson, D. C.; Shaheen, S. E.; Kopidakis, N.; Ginley, D. S. *Appl. Phys. Lett.* **2006**, *89*, 143517.

47. Irwin, M. D.; Buchholz, D. B.; Hains, A. W.; Chang, R. P. H.; Marks, T. J. *PNAS*, **2008**, *105*, 2783.
48. Perzon, E.; Wang, X.; Admassie, S.; Inganäs, O.; Andersson, M. R. *Polymer* **2006**, *47*, 4261.
49. Slooff, L. H.; Veenstra, S. C.; Kroon, J. M.; Moet, D. J. D.; Sweelssen, J. S.; Koetse, M. M. *Appl. Phys. Lett.* **2007**, *90*, 143506.
50. Ashraf, R. S.; Hoppe, H.; Shahid, M.; Gobsch, G.; Sensfuss, S.; Klemm, E. J. *Polym. Sci. Part A-Polym. Chem.* **2006**, *44*, 6952.
51. Wang, F.; Luo, J.; Yang, K.; Chen, J.; Huang, F.; Cao, Y. *Macromolecules* **2005**, *38*, 2253.
52. Tang, W. H.; Kietzke, T.; Vemulamada, P.; Chen, Z. K. *J Polym Sci Part A: Polym Chem* **2007**, *45*, 5266.
53. Sang, G. Y.; Zou, Y. P.; Li, Y. F. *J Phys Chem C* **2008**, *112*, 12058.
54. Li, Y. W.; Xue, L. L.; Li, H.; Li, Z. F.; Xu, B.; Wen, S. P.; Tian, W. J. *Macromolecules* **2009**, *42*, 4491.
55. Li, K. C.; Hsu, Y. C.; Lin, J. T.; Yang, C. C.; Wei, K. H.; Lin, H. C. *J Polym Sci Part A: Polym Chem* **2008**, *46*, 4285.
56. Blouin, N.; Michaud, A.; Gendron, D.; Wakim, S.; Blair, E.; Neagu-Plesu, R.; Belletête, M.; Durocher, G.; Tao, Y.; Leclerc, M. *J. Am. Chem. Soc.* **2008**, *130*, 732.
57. Wienk, M. M.; Turbiez, M.; Gilot, J.; Janssen, R. A. J. *Adv. Mater.* **2008**, *20*, 2556.
58. Zou, Y.; Gendron, D.; Neagu-Plesu, R.; Leclerc, M. *Macromolecules* **2009**, *42*, 6361.

59. Chen, H. Y.; Hou, J. H.; Hayden, A. E.; Yang, H.; Houk, K. N.; Yang, Y. *Adv. Mater.* **2010**, *22*, 371.
60. Cheng, Y. J.; Yang, S. H.; Hsu, C. S. *Chem. Rev.* **2009**, *109*, 5868.
61. Chen, H.-Y.; Hou, J.; Zhang, S.; Liang, Y.; Yang, G.; Yang, Y.; Yu, Li.; Wu, Li.; Li, G. *Nat Photonics* **2009**, *3*, 649.
62. Cheng, K. W.; Mak, C. S. C.; Chan, W. K.; Ng, A. M. C.; Djurii, A. B. *J. Polym. Sci. Part A: Polym. Chem.* **2008**, *46*, 1305.
63. Vellis, P. D.; Mikroyannidis, J. A.; Lo, C. N.; Hsu, C. S. *J. Polym. Sci. Part A: Polym. Chem.* **2008**, *46*, 7702.
64. Duprez, V.; Biancardo, M.; Spanggaard, H.; Krebs, F. C. *Macromolecules* **2005**, *38*, 10436.
65. Man, K. K. Y.; Wong, H. L.; Chan, W. K.; Djuricic, A. B.; Beach, E.; Rozeveld, S.; *Langmuir* **2006**, *22*, 3368.
66. Yang, J., Garcia, A.; Nguyen, T. Q. *Appl. Phys. Lett.* **2007**, *90*, 103514.
67. Hoven, C. V.; Garcia, A.; Bazan, G. C.; Nguyen, T. Q. *Adv. Mater.* **2008**, *20*, 3793.
68. Po, R.; Maggini, M.; Camaioni, N. *J. Phys. Chem. C* **2010**, *114*, 695.
69. Kroon, R.; Lenes, M.; Hummelen, J. C. *Polym Rev* **2008**, *48*, 531.
70. Liang, Y. Y.; Wu, Y.; Feng, D. Q.; Tsai, S. T.; Son, H. J.; Li, G.; Yu, L. P. *J. Am. Chem. Soc.* **2009**, *131*, 56.
71. Liang, Y. Y.; Feng, D. Q.; Wu, Y.; Tsai, S. T.; Li, G.; Ray, C.; Yu, L. P. *J. Am. Chem. Soc.* **2009**, *131*, 7792.

72. Park, S. H.; Roy, A.; Beaupre, S.; Cho, S.; Coates, N.; Moon, J. S.; Moses, D.; Leclerc, M.; Lee, K.; Heeger, A. J. *Nat Photonics* **2009**, *3*, 297.
73. Hou, J. H.; Chen, H. Y.; Zhang, S. Q.; Chen, R. I.; Yang, Y.; Wu, Y.; Li, G. *J. Am. Chem. Soc.* **2009**, *131*, 15586.
74. Peet, J.; Kim, J. Y.; Coates, N. E.; Ma, W. L.; Moses, D.; Heeger, A. J.; Bazan, G. C. *Nature Mater.* **2007**, *6*, 497.
75. Brédas, J. L. *J. Chem. Phys.* **1985**, *82*, 3808.
76. Roncali, J. *Chem. Rev.* **1997**, *97*, 173.
77. Blom, P. W. M.; Mihailetschi, V. D.; Koster, L. J. A.; Markov, D. E. *Adv. Mater.* **2007**, *19*, 1551.
78. Scharber, M. C.; Mühlbacher, D.; Koppe, M.; Denk, P.; Waldauf, C.; Heeger A. J.; Brabec, C. J. *Adv. Mater.* **2006**, *18*, 789.
79. Jenekhe, S. A.; Lu, L.; Alam, M. M. *Macromolecules* **2001**, *34*, 7315.
80. Park, M. J.; Lee, J.; Jung, I. H.; Park J. H.; Hwang, D. H.; Shim, H. K. *Macromolecules* **2008**, *41*, 9643.
81. Cho, N. S.; Park, J. H.; Lee, S. K.; Lee, J.-H.; Shim, H.-K.; Park, M.-J.; Hwang, D.-H.; Jung, B.-J. *Macromolecules* **2006**, *39*, 177.
82. Lai, R. Y.; Kong, X.; Jenekhe, S. A.; Bard, A. J. *J. Am. Chem. Soc.* **2003**, *125*, 12631.
83. Sun, D.; Rosokha, S. V.; Koich, J. K. *J. Am. Chem. Soc.* **2004**, *126*, 1388
84. Zou, Y.; Wu, W.; Sang, G.; Yang, Y.; Liu, Y.; Li, Y. *Macromolecules* **2007**, *40*, 7231.
85. Kong, X.; Kulkarni, A. P.; Jenekhe, S. A. *Macromolecules* **2003**, *36*, 8992.

86. Wang, E. G.; Wang, L.; Lan, L. F.; Luo, C.; Zhuang, W. L.; Peng, J. B.; Cao, Y. *Appl. Phys. Lett.* **2008**, *92*, 033307.
87. Hou, J. H.; Chen, H. Y.; Zhang, S. Q.; Li, G.; Yang, Y. *J. Am. Chem. Soc.* **2008**, *130*, 16144.
88. Yue, W.; Zhao, Y.; Shao, S.; Tian, H.; Xie, Z.; Geng, Y.; Wang, F. *J. Mater. Chem.* **2009**, *19*, 2199.
89. Svensson, M.; Zhang, F. L.; Veenstra, S. C.; Verhees, W. J. H.; Hummelen, J. C.; Kroon, J. M.; Inganäs, O.; Andersson, M. R. *Adv. Mater.* **2003**, *15*, 988.
90. Shi, C.; Yao, Y.; Yang, Y.; Pei, Q. *J. Am. Chem. Soc.* **2006**, *128*, 8980.
91. Wang, E. G.; Wang, M.; Wang, L.; Duan, C. H.; Zhang, J.; Cai, W. Z.; He, C.; Wu, H. B.; Cao, Y. *Macromolecules* **2009**, *42*, 4410.
92. Gautrot, J. E.; Hodge, P.; Cupertino, D.; Helliwell, M. *New J. Chem.* **2007**, *31*, 1585.
93. Hwang, D.-H.; Kim, S.-K.; Park, M.-J.; Lee, J.-H.; Koo, B.-W.; Kang, I.-N.; Kim, S.-H.; Zyung, T. *Chem. Mater.* **2004**, *16*, 1298.
94. McNeill, C. R.; Halls, J. J. M.; Wilson, R.; Whiting, G. L.; Berkebile, S.; Ramsey, M. G.; Friend, R. H.; Greenham, N. C. *Adv. Funct. Mater.* **2008**, *18*, 2309.
95. Iuo, J.; Hou, Q.; Chen, J.; Cao, Y. *Synth. Met.* **2006**, *156*, 470.
96. Jung, I. H.; Kim, H.; Park, M. J.; Kim, B.; Park, J. H.; Jeong, E.; Woo, H. Y.; Yoo, S.; Shim, H. K. *J. Polym. Sci. Part A: Polym. Chem.* **2010**, *48*, 1423.
97. Li, K. C.; Hsu, Y. C.; Lin, J. T.; Yang, C.; Wei, K. H.; Lin, H. C. *J. Polym. Sci. Part A: Polym. Chem.* **2009**, *47*, 2073.
98. Baek, N. S.; Hau, S. K.; Yip, H. L.; Acton, O.; Chen, K. S.; Jen, A. K. Y. *Chem. Mater.* **2008**, *20*, 5734.

99. Hou, J.; Chen, T. L.; Zhang, S.; Chen, H.-Y.; Yang, Y. *J. Phys. Chem. C* **2009**, *113*, 1601.
100. Zhang, X.; Steckler, T. T.; Dasari, R. R.; Ohira, S.; Potscavage, W. J.; Tiwari, S. P.; Coppee, S.; Ellinger, S.; Barlow, S.; Bredas, J. L.; Kippelen, B.; Reynolds, J. R.; Marder, S. R. *J. Mater. Chem.* **2010**, *20*, 123.
101. Zhang, S. M.; Fan, H. J.; Liu, Y.; Zhao, G. J.; Li, Q. K.; Li, Y. F.; Zhan, X. W. *J. Polym. Sci. Part A: Polym. Chem.* **2009**, *47*, 2843.
102. Zhan, X.; Tan, Z. A.; Zhou, E.; Li, Y.; Misra, R.; Grant, A.; Domercq, B., Zhang, X. -H.; An, Z.; Zhang, X.; Barlow, S.; Kippelen B.; Marder, S. R. *J. Mater. Chem.* **2009**, *19*, 5794.
103. Usta, H.; Lu, G.; Facchetti, A.; Marks, T. J. *J. Am. Chem. Soc.* **2006**, *128*, 9034.
104. Lu, G.; Usta, H.; Risko, C.; Wang, L.; Facchetti, A.; Ratner, M. A.; Marks, T. J. *J. Am. Chem. Soc.* **2008**, *130*, 7670.
105. Beaujuge, P. M., Pisula, W., Tsao, H. N., Ellinger, S., Muellen, K. and Reynolds, J. R. *J. Am. Chem. Soc.* **2009**, *131*, 7514.
106. Moul, A. J.; Tsami, A.; Bnnagel, T. W.; Forster, M.; Kronenberg, N. M.; Scharber, M.; Koppe, M.; Morana, M.; Brabec, C. J.; Meerholz, K.; Scherf, U. *Chem. Mater.* **2008**, *20*, 4045.
107. Shi, W.; Fan, S. Q.; Huang, F.; W. Yang, W.; Liu, R. S.; Cao, Y. *J. Mater. Chem.* **2006**, *16*, 2387.
108. Hou, J. H.; Huo, L. J.; He, C.; Yang, C. H.; Li, Y. F. *Macromolecules* **2006**, *39*, 594.
109. Halls, J. J. M.; Walsh, C. A.; Greenham, N. C.; Marseglla, E. A.; Friend, R. H.; Moratti, S. C.; Holmes, A. B. *Nature* **1995**, *376*, 498.

110. Greenham, N. C.; Moratti, S. C.; Bradley, D. D. C.; Friend, R. H.; Holmes, A. B. *Nature* **1993**, *365*, 628.
111. Liu, M. S.; Jiang, X. Z.; Liu, S.; Herguth, P.; Jen, A. K.-Y. *Macromolecules* **2002**, *35*, 3532.
112. Wan, M. X.; Wu, W. P.; Sang, G. Y.; Zou, Y. P.; Liu, Y. Q.; Li, Y. F. *J. Polym. Sci. Part A: Polym. Chem.*, **2009**, *47*, 4028.
113. Sang, G.; Zhou, E.; Huang, Y.; Zou, Y.; Zhao, G.; Li, Y. *J. Phys. Chem. C* **2009**, *113*, 5879.
114. Zou, Y. P.; Sang, G. Y.; Zhou, E. J.; Li, Y. F. *Macromol. Chem. Phys.* **2008**, *209*, 431.
115. Shen, P.; Sang, G. Y.; Lu, J. J.; Zhao, B.; Wan, M. X.; Zou, Y. P.; Li, Y. F.; Tan, S. T. *Macromolecules* **2008**, *41*, 5716.
116. Mikroyannidis, J. A.; Stylianakis, M. M.; Cheung, K. Y.; Fung, M. K.; Djurisic, A. B. *Synth. Met.* **2009**, *159*, 142.
117. Li, K. C.; Huang, J. H.; Hsu, Y. C.; Huang, P. J.; Chu, C. W.; Lin, J. T.; Ho, K. C.; Wei, K. H.; Lin, H. C. *Macromolecules* **2009**, *42*, 3681.
118. Liao, L.; Dai, L.; Smith, A.; Durstock, M.; Lu, J.; Ding, J.; Tao, Y. *Macromolecules* **2007**, *40*, 9406.
119. Asawapirom, U.; Scherf, U. *Macromol. Rapid Commun.* **2001**, *22*, 746.
120. Kim, J. Y.; Qin, Y.; Stevens, D. A.; Ugurlu, O.; Kalihari, V.; Hillmyer, M. A.; Frisbie, C. D. *J. Phys. Chem. C* **2009**, *113*, 10790.
121. de Leeuw, D. M.; Simenon, M. M. J.; Brown, A. R.; Einhard, R. E. F. *Synth. Met.* **1997**, *87*, 53.
122. Huang, J. H.; Ho, Z. Y.; Kekuda, D.; Chang, Y.; Chu, C. W.; Ho, K. C. *Nanotechnology* **2009**, *20*, 025202.

123. Wang, X. J.; Perzon, E.; Delgado, J. L.; de la Cruz, P.; Zhang, F. L.; Langa, F.; Andersson, M.; Ingans, O. *Appl. Phys. Lett.* **2004**, *85*, 5081.
124. Lehn, J.-M. *Supramolecular Chemistry: Concepts and Perspectives*; VCH: Weinheim, 1995.
125. Constable, E. C. In *Comprehensive Supramolecular Chemistry*; Lehn, J.-M., Ed.; Pergamon: Elmsford, NY, 1996; Vol. 9, pp 213-252.
126. Jones, C. J. *Chem. Soc. Rev.* **1998**, *27*, 289.
127. Elhabiri, M.; Elbrecht-Gary, A.-M. *Coord. Chem. Rev.* **2008**, *252*, 1079.
128. Mamula, O.; von Zelewsky, A. *Coord. Chem. Rev.* **2003**, *242*, 87.
129. Maier, A.; Rabindranath, A. R.; Tieke, B. *Chem. Mater.* **2009**, *21*, 3668.
130. Schubert, U. S.; Hofmeier, H.; Newkome, G. R. *Modern Terpyridine Chemistry*; Wiley-VCH: Weinheim, 2006.
131. Constable, E. C. *Chem. Soc. Rev.* **2007**, *36*, 246.
132. Medlycott, E.; Hanan, G. S.; *Chem. Soc. Rev.* **2005**, *34*, 133.
133. Cooke, M. W.; Hanan, G. S. *Chem. Soc. Rev.* **2007**, *36*, 1466.
134. Benniston, A.; Harriman, A.; Li, P.; Patel, P. V.; Sams, C. A.; *J. Org. Chem.* **2006**, *71*, 3481.
135. Cooke, M. W.; Hanan, G. S.; Loiseau, F.; Campagna, S.; Watanabe, M.; Tanaka, Y. *J. Am. Chem. Soc.* **2007**, *129*, 10479.
136. Sauvage, J. P.; Collin, J. P.; Chambron, J. C.; Guillerez, S.; Coudret, C.; Balzani, V.; Barigelletti, F.; Decola, L.; Flamigni, L. *Chem. Rev.* **1994**, *94*, 993.
137. Constable, E. C.; Thompson, A. M. W. C. *J. Chem. Soc., Chem. Commun.* **1992**, 617.
138. Newkome, G. R.; He, E.; Moorefield, C. N. *Chem. Rev.* **1999**, 1689.
139. Hofmeier, H.; Schubert, U. S. *Chem. Soc. Rev.* **2004**, *33*, 373.

140. Lainé, P. P.; Bedioui, F.; Louiseau, F.; Chiorboli, C.; Campagna, S. *J. Am. Chem. Soc.* **2006**, *128*, 7510.
141. Schlutter, F.; Wild, A.; Winter, A.; Hager, M. D.; Baumgaertel, A.; Friebe, C.; Schubert, U. S. *Macromolecules* **2010**, *43*, 2759.
142. Dobrawa, R.; Lysetska, M.; Ballester, P.; Grne, M.; Wrthner, F. *Macromolecules* **2005**, *38*, 1315.
143. Winter, A.; Friebe, C.; Chiper, M.; Schubert, U. S.; Presselt, M.; Dietzek, B.; Schmitt, M.; Popp, J. *Chem Phys Chem* **2009**, *10*, 787.
144. Chen, Y. Y.; Lin, H. C. *J. Polym. Sci. Part A: Polym. Chem.* **2007**, *45*, 3243.
145. Chen, Y. Y.; Tao, Y. T.; Lin, H. C. *Macromolecules* **2006**, *39*, 8559
146. Chen, Y. Y.; Lin, H. C. *Polymer* **2007**, *48*, 5268-5278.
147. Man, K. K. Y.; Wong, H. L.; Chan, W. K.; Kwong, C. Y.; Djuricic, A. B. *Chem. Mater.* **2004**, *16*, 365.
148. Hagemann, O.; Jørgensen, M.; Krebs, F. C. *J. Org. Chem.* **2006**, *71*, 5546.
149. Pan, Y.; Tong, B.; Shi, J.; Zhao, W.; Shen, J.; Zhi, J.; Dong, Y. *J. Phys. Chem. C* **2010**, *114*, 8040.
150. Stepanenko, V.; Stocker, M.; Müller, P.; Büchner, M.; Würthner, F. *J. Mater. Chem.* **2009**, *19*, 6816.
151. E. C. Constable, E. Figgemeier, C. E. Housecroft, S. L. Kokatam, E. A. Medlycott, M. Neuburger, S. Schaffner and A. Zampese, *Dalton. Trans.*, 2008, 6752.
152. Padhy, H.; Huang, J. H.; Sahu, D.; Patra, D.; Kekuda, D.; Chu C. W.; Lin, H. C. *J. Polym. Sci. Part A: Polym. Chem.*, 2010, **48**, 4823.
153. Kelch S.; Rehahn, M. *Macromolecules*, **1999**, *32*, 5818.
154. Schmelz, O.; Rehahn, M. *e-Polym.* **2002**, *47*, 1.

155. Hu, B.; Fuchs, A.; Huseyi, S.; Gordaninejad, F. *J. Appl. Polym. Sci.* **2006**, *100*, 2464.
156. Wang, X. Y.; Guerso, A. D.; Schmehl, R. H.; *Chem. Commun.* **2002**, 2344.
157. Hofmeier, H.; El-ghayoury, A.; Shenning, A. P. H. J.; Schubert, U. S. *Chem. Commun.* **2004**, 318.
158. Schlutter, F.; Wild, A.; Winter, A.; Hager, M. D.; Baumgaertel, A.; Friebe, C.; Schubert, U. S. *Macromolecules* **2010**, *43*, 2759.
159. Oyama, D.; Kido, M.; Orita, A.; Takase, T. *Polyhedron* **2010**, *29*, 1337.
160. Zhou, Q. X.; Lei, W. H.; Li, C.; Hou, Y. J.; Wang X. S.; Zhang, B. W. *New J. Chem.* **2010**, *34*, 137.
161. Flores-Torres, S.; Hutchison, G. R.; Soltzberg, L. J.; Abruna, H. D. *J. Am. Chem. Soc.* **2006**, *128*, 1513.
162. Schulze, B.; Friebe, C.; Hager, M. D.; Winter, A.; Hoogenboom, R.; Gorls, H.; Schubert, U. S. *Dalton Trans.* **2009**, 787.
163. Koster, L. J. A.; Mihailetchi, V. D.; Ramaker, R.; Blom, P. W. M. *Appl. Phys. Lett.* **2005**, *86*, 123509.
164. Mwaura, J. K.; Pinto, M. R.; Witker, D.; Ananthakrishnan, N.; Schanze, K. S.; Reynolds, J. R. *Langmuir* **2005**, *21*, 10119.
165. Hiramoto, M.; Fujiwara, H.; Yokoyama, M. *J. Appl. Phys.* **1992**, *72*, 3781.

Curriculum Vitae

Personal Details:

Name: Harihara Padhy

Date of Birth: 10th August, 1978

Nationality: Indian

E.mail: hariharapadhy@rediffmail.com

Contact no: +886-911-582-459 (Taiwan), +91-943-781-2310 (India)

Permanent address: At/Po: Jayantipur, Dist: Ganjam, Orissa, 761006. (INDIA)

Education:

2005-2010 **National Chiao Tung University, Hsinchu, Taiwan.**

Ph.D studies at Department of Materials Science and Engineering

1998-2000 **Berhampur University, Orissa, India**

M.Sc studies at Department of Chemistry

1995-1998 **Berhampur University, Orissa, India**

B.Sc studies at S.K.C.G. College, Parlakhemundi

Work experience

2000-2005 **National Institute of Science and Technology, Orissa, India**

Faculty at Department of Chemistry.

Publications:

1. **Harihara Padhy**, Jen-Hsien Huang, Duryodhan Sahu, Dhananjaya Patra, Dhananjay Kekuda, Chih-Wei Chu and Hong-Cheu Lin*, “Synthesis and applications of low-bandgap conjugated polymers containing phenothiazine donor and various benzodiazole acceptors for polymer solar cells” *Journal of Polymer Science: Part A: Polymer Chemistry*, **2010**, 48, 4823–4834. (SCI IF=3.971, N/M=9/76=11.8%)
2. **Harihara Padhy**, Duryodhan Sahu, I-Hung Chiang, Dhananjaya Patra, Dhananjay Kekuda, Chih-Wei Chu and Hong-Cheu Lin*, “Synthesis and Applications of Main-Chain Ru^{II} Metallo-Polymers Containing Bis-terpyridyl Ligands with Various Benzodiazole Cores for Solar Cells” *J. Mater. Chem.* 2010 (Accepted) (SCI IF= 4.795, N/M=18/212=8.5%)
3. **Harihara Padhy**, Duryodhan Sahu, Jen-Hsien Huang, Dhananjaya Patra, Murali Krishna Pola, Chih-Wei Chu, Kung-Hwa Wei, Hong-Cheu Lin*, “Cyclopentadithiophene- and Dithienosilole-Based Polymers Containing Cyano-Vinylene Groups for Photovoltaic Applications” *Macromol. Rapid Commun.* (submitted).
4. Jen-Hsien Huang, Kuang-Chieh Li, Dhananjay Kekuda, **Harihara Padhy**, Hong-Cheu Lin, Kuo-Chuan Ho, Chih-Wei Chu “Efficient bilayer polymer solar cells possessing planar mixed-heterojunction structures” *J. Mater. Chem.*, 2010, 20, 3295-3300.
5. Dhananjaya Patra, Duryodhan Sahu, **Harihara Padhy**, Dhananjay Kekuda, Chih-Wei Chu, Hong-Cheu Lin*, “Synthesis and Applications of 2,7-Carbazole-Based Conjugated Main-Chain Copolymers Containing Electron Deficient Bithiazole Units for Organic Solar Cells” *Journal of Polymer Science: Part A: Polymer Chemistry*, **2010**, 48, 5479–5489.
6. Duryodhan Sahu, **Harihara Padhy**, Dhananjaya Patra, Jen-Hsien Huang, Chih-Wei Chu, Hong-Cheu Lin*, “Synthesis and Characterization of Novel Low-bandgap Triphenylamine Based Conjugated Polymers with Main-chain

Donors and Pendant Acceptors for Organic Photovoltaics” *Journal of Polymer Science: Part A: Polymer Chemistry*, 2010 (ASAP), DOI: 10.1002/pola.24389.

7. Duryodhan Sahu, **Harihara Padhy**, Dhananjaya Patra, Dhananjay Kekuda, Chih-Wei Chu, I-Hung Chiang, Hong-Cheu Lin* “Synthesis and Application of H-Bonded Cross-Linking Polymers Containing a Conjugated Pyridyl H-Acceptor Side-Chain Polymer and Various Carbazole-Based H-Donor Dyes Bearing Symmetrical Cyanoacrylic Acids for Organic Solar Cells” *Polymer*, **2010**, Accepted.

